Development and Use of Ultra-High-Performance Concrete (UHPC) as a High Friction Surface Treatment (HFST) on Pavements and Bridges

FINAL REPORT

Prepared by:

Prasad Rangaraju
Kyle Maeger
Adam Biehl
Glenn Department of Civil Engineering
School of Civil and Environmental Engineering and Earth Sciences
Clemson University
CLEMSON, SC, 29634

FHWA-SC-25-02

July 2025

Sponsoring Agencies:

South Carolina Department of Transportation
Office of Materials and Research
1406 Shop Road
Columbia, SC 29201

Federal Highway Administration
South Carolina Division
Strom Thurmond Federal Building
1835 Assembly Street, Suite 1270
Columbia, SC 29201

Technical Report Documentation Page

1. Report No FHWA-SC-25-02	2. Government Accession No.	3. Recipient's Catalog No.
4. Title and Subtitle		5. Report Date 6. Performing Organization Code
7. Author/s Rangaraju, P.R., Maeger, K. and Biehl, A.R.		8. Performing Organization Report No.
9. Performing Organization Name and Address Clemson University, 306 S. Palmetto Blvd., Clemson, SC, 29634-0911		10. Work Unit No. (TRAIS) 11. Contract or Grant No. SPR No. 762
12. Sponsoring Organization Name and Address South Carolina Department of Transportation Office of Materials and Research 1406 Shop Road Columbia, SC 29201		13. Type of Report and Period Covered Final Report 14. Sponsoring Agency Code
15. Supplementary Notes		

16. Abstract

High Friction Surface Treatments (HFST) are proven crash reduction technology. However, their high cost necessitates exploring the use of alternative materials. This study assessed the design and application of Ultra-High-Performance Concrete (UHPC) as an alternative to traditional epoxy resin-based binder for HFST. In addition, the use of local alternative aggregates with low abrasion loss was explored as an alternative to the traditional calcined bauxite as an HFST component. Various methods for applying UHPC-based HFST were also evaluated, including the use of intermixing HFST aggregate and exposing aggregate texture with surface retarders or broadcasting HFST aggregate in a similar fashion to traditional HFST methods with and without vibration. The Mean Profile Depth (MPD) and friction (British Pendulum Test and Dynamic Friction Tester) produced from UHPC-based HFST and the performance of the surfaces under polishing by the Three Wheel Polishing Device (TWPD) were also evaluated. While the traditional make-up of epoxy resin with calcined bauxite aggregate exhibited the best performance in testing, both with concrete and asphalt substrates, UHPC based HFST samples were also able to produce adequate friction and texture and maintain performance under polishing such that they could be considered feasible alternatives to traditional resin based HFST surfaces, particularly on concrete substrates. The use of local alternative aggregates as HFST aggregate failed to perform at the same level as calcined bauxite and is not recommended for long-term frictional performance. UHPC, using surface retarders to expose calcined bauxite HFST aggregate, is a viable alternative to traditional resin-based HFST materials. Field evaluation of UHPC-based HFST is recommended for future implementation.

17. Key Words	18. Distribution Statement		
UHPC, HFST, Calcined Bauxite, Friction	No restrictions. This document is available to the public through the National Technical Information Service, Springfield, VA 22161.		
19. Security Classification (of this report) Unclassified	20. Security Classification (of this page) Unclassified	21. No. Of Pages	22. Price

Form DOT F 1700.7 (8-72) Reproduction of form and completed page is authorized

DISCLAIMER

The contents of this report reflect the views of the author who is responsible for the facts and the accuracy of the data presented herein. The contents do not necessarily reflect the official views or policies of the South Carolina Department of Transportation or the Federal Highway Administration. This report does not constitute a standard, specification, or regulation.

The State of South Carolina and the United States Government do not endorse products or manufacturers. Trade or manufacturer's names appear herein solely because they are considered essential to the object of this report.

ACKNOWLEDGMENTS

The research conducted for this report was funded by the South Carolina Department of Transportation (SCDOT) under SPR Project No. 762. We express thanks to the steering committee members, including Ms. Temple Short (Chair), Mr. Merrill Zwanka, Mr. Caleb Gunter, Mr. Eric Carroll, Mr. Luke Gibson, Mr. Jon Greer, Mr. Josh Quattlebaum, Mr. Eugene Taylor, and Mr. Blake Gerken (FHWA). Furthermore, support for analytical testing provided by the National Brick Research Center is appreciated. Also, aggregate suppliers for the study, including Martin Marietta Materials, The Sunrock Group, FX Minerals, and Charleston Mill Services, as well as cement and admixtures provided by Argos USA and Sika USA, respectively, is deeply appreciated.

EXECUTIVE SUMMARY

This report details the research conducted to determine the feasibility of creating a High-Friction Surface Treatment (HFST) utilizing an Ultra-High-Performance Concrete (UHPC) bonding layer. HFSTs are a proven technology to reduce crashes on roadways by increasing the coefficient of friction between vehicle tires and the pavement in both wet and dry conditions. The further implementation of HFSTs is a measure that follows SCDOT's Strategic Plan vision to provide an adequate, safe, and efficient transportation service in the Palmetto State by reducing the number and severity of crashes in South Carolina. However, current HFSTs are a relatively expensive solution due to the high cost of the two default constituent materials: calcined bauxite aggregate and epoxy resin binders. This study evaluates viable alternatives for both constituent materials and related application methods to provide more economical options for the next generation of HFSTs.

To evaluate the quality of local alternatives aggregates to calcined bauxite aggregate, this study quantified the abrasion resistance of four alternative HFST aggregates to calcined bauxite using Los Angeles (LA) Abrasion and Micro-Deval Abrasion tests and studied the surface texture utilizing a high-resolution laser scanner and friction utilizing the British Pendulum Test. The experiments revealed that while two alternative aggregates among the four aggregates could provide seemingly good abrasion resistance and initially high levels of friction with adequate texture, the friction significantly reduced under polishing. Therefore, none of the alternative aggregates tested were found to be suitable for a long service life of an HFST. Calcined bauxite aggregate remains the premier, reliable aggregate choice for long-term HFST application.

To assess the quality of a non-proprietary Ultra High-Performance Concrete (UHPC) as an alternative to epoxy resins, a series of tests were conducted to assess the fresh properties, mechanical strength, and durability performance. The initial non-proprietary UHPCs were compared to a qualified HFST epoxy-resin and existing evaluation criteria. Additionally, the effects of intermixing calcined bauxite aggregate in UHPC at varying contents on the performance of UHPC were evaluated. These tests demonstrated that a UHPC could provide adequate bond strength, compressive strength and flow for use as an HFST binder on concrete substrates. However, for asphalt substrates, the difference in coefficient of thermal expansion and the lesser bond strength compared to resin binders leaves additional questions for the application of UHPC-based HFSTs for asphalt substrates that would require field trials and supplemental testing for evaluation. Secondly, the inclusion of intermixed calcined bauxite in UHPC demonstrated an increase in mechanical strength, especially in mixtures with calcined bauxite to cementitious material ratios between 1.5 and 2.0 by mass. This finding demonstrated that the use of calcined aggregate content resulted in increased mechanical performance while having significantly reduced shrinkage. However, the observed shrinkage was found to be still above the normally accepted limit for UHPC, and the potential for some cracking exists, particularly when in a fully restrained condition. It is therefore necessary to utilize secondary shrinkage mitigation techniques such as shrinkage-reducing admixtures and/or internal curing techniques to decrease the shrinkage of UHPC further and use field trials to determine threshold shrinkage levels that are acceptable for HFST applications.

Lastly, this study developed and evaluated various alternative application methodologies suitable for UHPC-based HFST surfaces and the impact of aggregate moisture content. These methods included broadcasting aggregate onto the UHPC layer and embedding under self-weight, broadcasting aggregate onto the UHPC layer and embedding under vibration and using UHPC with intermixed aggregate with application of surface retarders to expose the aggregate at a later age. The performance of UHPC-based surfaces was evaluated by the British Pendulum Test and the Dynamic Friction Tester for friction, a high-resolution laser scanner for texture, and an outflow meter for drainage. Polishing was conducted using a Three-Wheel Polishing Device, and the effects of polishing on friction and texture across selected surface types were evaluated.

UHPC-based HFSTs with calcined bauxite aggregate were able to produce acceptable levels of friction and texture and maintain the performance under polishing, such that they can be categorized as HFST. However, resin-based surfaces with calcined bauxite were superior across testing and provided a more consistent surface. Additionally, the use of aggregates with varying moisture content in UHPC mixture formulations resulted in larger variability in the properties of UHPC (despite accounting for absorption in aggregates), and it is therefore recommended that only oven-dry aggregates be used in UHPC for HFST applications for consistent performance.

Overall, UHPC-based HFST appears to be a viable alternative to epoxy resins for use as an HFST binder with calcined bauxite aggregate on Portland cement concrete substrates, as it meets the existing HFST frictional and mechanical strength criteria while achieving performance at a significantly reduced cost per square foot. The performance of UHPC-based HFSTs was found to be inferior to that of epoxy-resin-based HFSTs on asphalt concrete substrate, particularly in terms of the bond between the HFST and the substrate. However, it is recommended that a field-scale evaluation be conducted with both concrete and asphalt substrates to verify the findings from this lab study and improve on threshold specifications for performance assessment.

The steering committee of the project included Ms. Temple Short (Chair), Mr. Merrill Zwanka, Mr. Caleb Gunter, Mr. Eric Carroll, Mr. Luke Gibson, Mr. Jon Greer, Mr. Josh Quattlebaum, Mr. Eugene Taylor, and Mr. Blake Gerken (FHWA).

TABLE OF CONTENTS

Chapter 1: Introduction 1

1.1. Problem Statement 1

1.2. Project Objectives 2

Chapter 2: Literature Review 4

2.1. Ultra-High-Performance Concrete (UHPC) 4

2.2. Tire-Pavement Interactions 4

2.3. Pavement Friction Components 5

2.4. Friction Treatment Options 6

2.5. High Friction Surface Treatment (HFST) 6

2.5.1. South Carolina HFST 7

Chapter 3: Experimental Program 9

3.1. Material Selection 9

3.1.1. Aggregates 9

3.1.2. Cement 9

3.1.3. HRWR/Superplasticizer 10

3.1.4. Supplementary Cementitious Materials (SCMs) 10

3.1.5. Fine Aggregate 11

3.2. Aggregate Testing 12

3.3. UHPC Mixture Design 12

3.4. UHPC Surface Evaluation 12

3.5. Analysis 13

Chapter 4: Microtexture Characterization of Bulk-Aggregate Samples for Application in High-Friction Surface Treatments 14

4.1. Objective 14

4.2. Methods and Materials 14
4.2.1. Aggregate Selection 14
4.2.2. Laser Scanning Process 15
4.2.3. Aggregate Abrasion Testing 17
4.2.4. Friction Sample Testing 18
4.3 Results and Discussion 20
4.3.1 Effects of Aggregate Gradation on Microtexture 20
4.3.2 Repeatability 22
4.3.3 Effects of Abrasion on Microtexture 23
4.3.3.1 Micro-Deval 23
4.3.3.2 Los Angeles Abrasion 24
4.3.3.3 Other Abrasion Observation 24
4.3.4 Friction Testing 25
4.4 Conclusions 27
Chapter 5: UHPC-Based HFST Mixture Proportions Optimization 29
5.1. Problem Statement 29
5.2. Objective 29
5.3. Methods 29
5.3.1. Mixing Procedure 29
5.3.2. Flowability 30
5.3.4. Pull-Off Bond Strength (Pull-off Method) 31
5.4 Phase 1: Continuous Packing of UHPC (MA&A Method) 38
5.4.1. Background and Mixture Proportions 38
5.4.2. Results and Discussion 41
5.4.2.1. Flowability 41

5.4.2.2. Setting Time 43
5.4.2.3. Pull-Off Bond Strength 44
5.4.2.4. Slant Shear Bond Strength 46
5.4.2.5. Abrasion Resistance 48
5.4.2.6. Compressive Strength 50
5.4.2.7. Drying Shrinkage 52
5.4.3. Conclusions 55
5.5. Phase 2: Discrete Particle Packing of Intermixed Calcined Bauxite UHPC 56
5.5.1. Background and Mixture Proportions 56
5.5.2. Results and Discussion 58
5.5.2.1. Flowability 58
5.5.2.3. Dry Density 60
5.5.2.4. Pull-Off Bond Strength 61
5.5.2.5. Slant Shear Bond Strength 62
5.5.3. Conclusions 69
5.6. Phase 3: Influence of Steel and Glass Fibers 69
5.6.1. Background and Mixture Proportions 69
5.6.2 Results and Discussion 70
5.6.2.1. Flowability 70
5.6.2.2. Compressive Strength 71
5.6.2.3. Drying Shrinkage 72
5.6.2.4. Thin-Layer Shrinkage 73
5.6.3. Conclusions 75
5.7. Overarching Conclusions 75
Chapter 6: UHPC-Based HFST Surface Application Methods and Evaluation 77

6.1. Problem Statement 77
6.2. Objective 77
6.3. Methods and Materials 77
6.3.1. Phase 1: Evaluation of Application Methods 77
6.3.1.1. UHPC Mix Design Materials 77
6.3.1.2. Surface Retarders 78
6.3.1.3. Sample Construction 78
6.3.1.4. LTS Methods 79
6.3.1.5. BPT Methods 79
6.3.2. Phase 2: Performance of UHPC-Based HFST 79
6.3.2.1. Aggregates 79
6.3.2.2. Substrate casting and preparation 80
6.3.2.3. Surface Retarders 80
6.3.2.4. Mix Design 80
6.3.2.5. Surface casting procedures 81
6.3.2.6. Polishing with the TWPD 82
6.3.2.7. LTS Macrotexture 82
6.3.2.8. Hydrotimer 83
6.3.2.9. Dynamic Friction Tester (DFT) 83
6.4. Results and Discussion 84
6.4.1. Phase 1: Evaluation of Application Methods 84
6.4.1.1. Aggregate Moisture Content 84
6.4.1.2. Results of Friction Testing (BPT) 84
6.4.1.3. Macrotexture and Effect of Retarder Grade 85
6.4.2. Phase 2: Performance of UHPC-Based HFST 88

6.4.2.1. Initial Surface Performance 88
6.4.2.2. Comparison of Methods and Aggregate 93
6.4.2.3. Effects of Water 98
6.4.2.4. Top Performers 99
6.4.2.5. Error and Variability 101
6.5. Conclusions 101
6.5.1. Phase 1: Evaluation of Application Methods 101
6.5.2. Phase 2: Performance of UHPC-Based HFST 102
Chapter 7: Conclusions and Recommendations 103
7.1. Introduction 103
7.2. Experimental Findings 103
7.2.1. Aggregate Conclusions 103
7.2.2. UHPC Mix Design Conclusions 103
7.2.3. UHPC-Based HFST Performance Conclusions 104
7.3. Future Research Recommendations 105
Chapter 8: References 106
APPENDIX A: Other Pavement Surface Treatments ..... A
A.1.1 Chip Seal with and without Fog Seal ..... A
A.1.2 Fog Seal ..... A
A.1.3 Rejuvenating Seal ..... B
A.1.4 Slurry Seal ..... B
A.1.5 Cape Seal ..... B
A.1.6 Scrub Seal ..... B
A.1.7 Microsurfacing ..... B
A.1.8 Ultra-thin Bonded Wearing Course (UTBWC) C

A.1.9 Thin Asphalt Overlays C
A.1.10 Open Graded Friction Course (OGFC) ..... D
A.1.11 Profile Milling ..... D
A.1.12 Shotblasting ..... E
A.1.13 Diamond Grinding (PCC) ..... E
A.1.14 Grooving (PCC) ..... E
A.1.15 Next Generation Concrete Surface (NGCS) ..... F
A.1.16 (Ultra) Thin White Topping ..... F
A.1.17 UHPC Overlay ..... F
A.1.18 Exposed Aggregate Concrete Pavement ..... F
A.2 Summary of Surface Treatments ..... G
APPENDIX B: Supporting Tables and Figures ..... K

LIST OF FIGURES

Figure 2.1: SC Crashes Before and After HFST 8

Figure 3.1: Experimental Flow Chart 9

Figure 3.2: XRD Pattern of Tested SFs 11

Figure 3.3: The PSD of UHPC Constituent Materials 11

Figure 4.1: Aggregates as Received (Scale in millimeters) 15

Figure 4.2: Aggregate Gradation as Received 15

Figure 4.3: Abrasion Testing Schematic 18

Figure 4.4: Sample HFST Surfaces (Scale in mm) 19

Figure 4.5: Box Plots of Aggregate and Gradation Effect on Microtexture, (a) Micro-MPD, (b) Micro-Rsk, (c) PSD Slope 21

Figure 4.6: Abrasion Effect on Micro-MPD for (a) Micro-Deval (b) Los Angeles Abrasion 24

Figure 4.7: Distribution of micro-Rku data by (a) Histogram and Normal Quantiles (b) Data sorted by Aggregate 25

Figure 4.8: Micro-MPD vs Cumulative Mass Loss 27

Figure 5.1: Mix Procedure for UHPC Samples 30

Figure 5.2: Mix Procedure for UHPC and Intermixed Vacuum Mixing 30

Figure 5.3: Failure Modes of the Pull-Off Bond Strength Test 32

Figure 5.4: Failure Modes of the Slant-Shear Test 33

Figure 5.5: Abrasion Resistance Setup 34

Figure 5.6: Thin-Layer Measurement System 38

Figure 5.7: MA&A Curves of (a) SF1 Mixes (b) SF2 Mixes (c) SF3 Mixes (d) Trad. UHPC 39

Figure 5.8: Flowability of Selected Mixes using the Modified Flow Table Test 42

Figure 5.9: Flowability of Intermixed Calcined Bauxite by the Flow Table Test 43

Figure 5.10: Setting Time of Continuously Packed UHPC Mixes 43

Figure 5.11: Compressive Strength of UHPC Samples 51
Figure 5.12: Compressive Strength of Intermixed Calcined Bauxite Samples 52
Figure 5.13: Drying Shrinkage of UHPC Samples 53
Figure 5.14: Autogenous Shrinkage of UHPC Samples 54
Figure 5.15: COTE Results of UHPC Samples Full Scale 55
Figure 5.16: COTE Results of UHPC Samples Reduced Scale 55
Figure 5.17: The MA&A Packing with Calcined Bauxite for (a, c) q = 0.25 and (b, d) q = 0.9 .. 57
Figure 5.18: Influence of CB/CM Ratio on Flowability 58
Figure 5.19: Influence of CB Content on Wet (a) Solids Concentration, (b) Voids Ratio, (c) Wet Density, and (d) Air Content 60
Figure 5.20: Influence of CB Content on Dry (a) Solids Concentration (b) Voids Content (c) Density (d) Air Content 61
Figure 5.21: Influence of CB Content on Pull-Off Bond Strength 62
Figure 5.22: Influence of CB Content on Slant shear bond strength 64
Figure 5.23: Compressive Strength as a Function of Calcined Bauxite Content 65
Figure 5.24: Abrasion Resistance as a Function of CB Content 66
Figure 5.25: Drying Shrinkage as a Function of CB Content 67
Figure 5.26: Unrestrained Thin-Layer Shrinkage at Varying CB Contents 68
Figure 5.27: Restrained Thin-Layer Shrinkage as a Function of CB Content 68
Figure 5.28: Workability of Fiber Reinforced Samples 71
Figure 5.29: Compressive Strength of Fiber Reinforced Samples 71
Figure 5.30: Drying Shrinkage of Fiber Reinforced Samples 73
Figure 5.31: Thin-Layer Shrinkage of Unrestrained Fiber Reinforced Samples 74
Figure 5.32: Thin-Layer Shrinkage of Restrained Fiber Reinforced Samples 75
Figure 6.1: Three Wheel Polishing Device 82

Figure 6.2: Hydrotimer on a HFST Sample Slab 83

Figure 6.3: BPN of Sample Surfaces 85

Figure 6.4: Retarder Grade Effect on Exposure Depth..... 86

Figure 6.5: MPD of Surface Samples..... 87

Figure 6.6: Aggregate embedment and loss on Broadcast Calcined Bauxite Lo-w/c sample (a) after brushing, (b) after conditioning, (c) after DFT testing 90

Figure 6.7: Average DFT 60 of Samples..... 91

Figure 6.8: Average MPD of Samples 92

Figure 6.9: MPD by Application Method and Aggregate..... 93

Figure 6.10: Hydrotimer Outflow Time by Application Method and Aggregate 94

Figure 6.11: DFT20 by Application Method and Aggregate 94

Figure 6.12: DFT40 by Application Method and Aggregate 95

Figure 6.13: DFT60 by Application Method and Aggregate 95

Figure 6.14: MPD effect on Outflow Time (a) linear regression, (b) normal quantile plot..... 96

Figure 6.15: MPD Effect on Friction (a) DFT20 regression, (b) DFT40 regression, (c) DFT60 regression, (d) DFT20 Normal Quantile Plot, (e) DFT40 Normal Quantile Plot, (f) DFT60 Normal Quantile Plot..... 97

Figure 6.16: Vibration Induced Texture on Vibrate Trap Rock Sample (a) whole slab, (b) zoomed into selected area (c) LTS scan profiles (scales in mm)..... 97

Figure 6.17: DFT60 of Calcined Bauxite Surfaces 99

Figure 6.18: MPD of Calcined Bauxite Surfaces..... 99

Figure 6.19: TWPD Cycles Effect on DFT60..... 100

Figure 6.20: TWPD Cycles Effect on MPD 101

LIST OF TABLES

Table 2.1: Pavement Texture Wavelengths (adapted from [19-21]) 5

Table 3.1: The Chemical Composition of the Type III Portland Cement 10

Table 3.2: The Crystal Composition of Tested SFs 10

Table 5.1: Pull-Off Bond Strength of Substrates 32

Table 5.2: Mixture Proportions for UHPC Mixes 40

Table 5.3: Mixture Proportions for Intermixed Calcined Bauxite Mixes 40

Table 5.4: Pull-Off Bond Strength Results of UHPC Samples 45

Table 5.5: Pull-Off Bond Strength Results of Intermixed Samples 46

Table 5.6: Slant Shear Bond Strength Results for UHPC Samples 47

Table 5.7: Slant Shear Bond Strength Results for Intermixed Samples 48

Table 5.8: Abrasion Resistance of UHPC Samples 49

Table 5.9: Abrasion Resistance of Intermixed Calcined Bauxite Samples 50

Table 5.10: Mixture Proportions for Discrete Packing Testing 57

Table 5.11: Mixture Proportions of UHPC Samples Including Fibers 70

Table 6.1: Conditioned Samples Tukey's HSD of MPD 88

Table A.1: Summary of Friction and Safety of Pavement Surface Treatments ..... H

Table B.1 Chemical and Mineralogical Composition of Aggregates ..... K

Table B.2: Effects of Gradation ANOVA Results ..... M

Table B.3: Comparison Surface and Bulk Sample Rank order and Connecting Letters ..... P

Table B.4: Effects of Abrasion ANOVA Results 1

Table B.5: Effect of Abrasion on Aggregate Friction 3

Table B.6: Regression of Texture Parameters Effect on BPN 5

CHAPTER 1: INTRODUCTION

1.1. Problem Statement

Maintaining safety on roadways is a crucial task for transportation agencies. Breaking down the root causes of vehicle crashes can be difficult as they result from the confluence of multiple factors, including drivers' behaviors, weather and visibility conditions, condition of the pavement, and roadway geometry. A recent report from Forbes rated the roads in South Carolina as the second most dangerous in the United States, second only to Montana, based on crash and fatality data from the National Highway Traffic Safety Administration (NHTSA) [1].

Depending on the circumstances, some mitigation strategies may prove more useful than others. For example, law enforcement policy may be a tool to address driver behaviors. However, the infrastructure side of the issue is worthy of serious consideration. Often, a particular crash-prone area will have some geometric issues, such as a tight turn radius or insufficient superelevation. When this is combined with low friction on the surface and high traffic speeds (for example, interstate ramps), the risks of run-off-the-road or other types of accidents increase. Other roadway design problems may include intersections with visibility issues or improper signaling and signage.

In many of these cases, road realignment or reconstruction may be the most thorough solution. However, it is also the most cost-prohibitive and not a realistically achievable solution to the problem in many cases. When assessing an accident-prone area, it is helpful to look at what factors can be controlled or adjusted by engineers. It is often the case that the best option available that is achievable within time and budget constraints is some type of surface treatment. These can be used to restore the surface condition at a much lower cost than reconstruction. Some surface treatments can improve the texture and friction of the pavement, which can help improve safety and reduce roadway crashes.

One method to increase the texture and friction of a pavement that has been proven as an effective crash reduction strategy is the application of high friction surface treatments (HFST). Where these have been employed, they have dramatically reduced accidents. Estimates from recent Federal Highway Administration (FHWA) studies indicate that HFSTs reduced wet crashes by 83 percent and total crashes by 57 percent [2,3]. In South Carolina, data from 2003 to 2016 showed a 73.8% reduction in crashes on a per-vehicle-traveled basis where HFSTs were applied.

While HFSTs are proven to reduce crashes, they come at a high-cost relative to other pavement rehabilitation methods. The typical unit cost of HFST installation is 25 to 35 dollars per square yard [4]. In Florida, the bid costs have ranged from 26 to 40 dollars per square yard, with total costs inclusive of traffic-control, striping and repairs ranging from 36 to 113 dollars per square yard [5]. For comparison, a 2015 FHWA report states that "the total cost of milling and overlay (including milling, tack, overlay placement, and traffic control) for a 1.5-inch-thick overlay is approximately $8.00 per square yard and between $11 and $12 per square yard for a 2-inch or 2.5-inch-thick overlay [6]."

The high cost of HFST is largely due to the materials associated with its construction. The typical make-up of an HFST is a fine gradation (maximum size of three to four millimeters) of calcined bauxite aggregate that is embedded in a thin layer of epoxy applied to the pavement surface [7,8]. This results in about 50% embedment with the rest of the aggregate's surface being exposed, which provides high macrotexture and microtexture, which are the key components of pavement friction [8,9]. Both the calcined bauxite and epoxy resins are specialty materials that are expensive.

Aggregate costs for calcined bauxite are around $750 per ton, not inclusive of the shipping. Part of this cost is because many of the materials are imported to the United States, with some of the largest distributors sourcing materials from China. Additionally, the production of calcined bauxite from the raw material is energy-intensive. In contrast, locally produced aggregates have much lower costs associated with production and transportation. For example, the freight-adjusted average cost for aggregates by local aggregate producer was reported at $16.40 per ton for 2022 [10]. Even at the high end of aggregate quality, locally quarried aggregates are not likely to approach the high cost of calcined bauxite. However, the texture and friction performance of local aggregates for the South Carolina market (southeastern United States) have not been assessed in comparison to calcined bauxite.

Based on distributor prices available via the internet as of 2024, epoxy resins used for HFST costs ranged from around 400-500 dollars for a 4-gallon application (2 gallons each of the two-part system). At a standard application thickness of 60 mils this equates to about $3.74 to $4.67 per square foot. Ultra-High-Performance Concrete (UHPC) may be a cost-efficient alternative to resins. A 2013 FHWA study showed nonproprietary UHPC material costs without steel fiber at around $500 per cubic yard [11]. Even if adjusted for inflation to 2024 using the Bureau of Labor Statistics Consumer Price Index (CPI) Inflation calculator, it would be about $671.28 [12]. This would give a unit cost of $0.52 per square foot at 0.25 inches thick.

However, the use of UHPC as an alternative binder for HFSTs has not been thoroughly assessed. UHPC has exceptional compressive strength, durability and bond strength, characteristics that are also desirable in epoxies. Because a UHPC-based HFST has the potential to provide adequate friction to improve safety and reduce crashes at a lower material cost while utilizing local materials in South Carolina or the larger southeastern region with lower carbon emissions, it is worthy of further study. Additionally, HFSTs provide durable aggregate surfaces, but the binder can break down after 7-12 years, resulting in lower and differential friction. UHPC may provide a more durable solution with a longer service life [13].

1.2. Project Objectives

The primary objective of this research was to develop and assess the performance of a UHPC-based HFST that utilizes locally sourced materials, including aggregates for use on roads and bridges in South Carolina (and by extension, the larger southeastern region). Apart from the aggregates, the remainder of the materials used in this study are not specific to any region and are therefore applicable to any region, as are the findings related to them in this study. To complete the primary objective, the following sub-objectives were addressed in this research:

1) Conduct a literature review that includes the latest developments in UHPC mix design and applications, the current state of the practice for measurement and evaluation of pavement friction and texture, the state-of-the-practice for HFST applications, a review of friction surface treatments and the current practices for microtexture assessment such that suitable experimental protocols can be developed.
2) Evaluate aggregates available locally to the southeastern United States for their performance in comparison to calcined bauxite. The potential effects of gradation, chemical composition, mineralogy, abrasion resistance, surface texture and the friction should be utilized for evaluation to enable suitable comparison.
3) Develop a suitable non-proprietary UHPC mix design for use as an HFST binder. Assess various silica fume sources for comparison of performance. Evaluate mixtures for particle packing, flow, set time, bond strength, abrasion resistance, compressive strength, and shrinkage behavior to determine the ideal materials and mix designs.
4) Assess application methods for a UHPC-based HFST, including variations of mixing in coarse aggregate with the binder and revealing with surface retarders and washing or broadcasting aggregate onto the UHPC binder. Additionally, evaluate the effects of aggregate moisture and vibration. Compare the performance to traditional HFST materials in terms of friction and various texture parameters.
5) Evaluate the friction, texture, and polishing resistance of UHPC-based HFSTs in comparison to traditional HFST materials and the effect of polishing on friction and texture.

CHAPTER 2: LITERATURE REVIEW

2.1. Ultra-High-Performance Concrete (UHPC)

UHPC is a Portland cement-based concrete mixture that, as its name implies, exhibits high performance across many parameters, including compressive strength, bond strength, durability, permeability, and abrasion resistance. UHPC development began in the 1990s with proprietary and non-proprietary formulations becoming readily available through the 2000s [1]. The advent of UHPC represents the culmination of years of research and development of several concrete materials advances, including the use of SCMs, high-range water reducers (HRWR) or superplasticizers, fiber reinforcement and optimized particle packing, which work together to create concrete with compressive strengths in the range of 17 to 21.7 ksi [1,2].

HRWRs allow flowable fresh concrete with very low water-to-cement ratios, often around 0.20, leading to higher strengths by reducing porosity in the structure [3]. Additionally, silica fume is nearly ubiquitous in UHPC formulations as its pozzolanic reactivity improves strength, and its small particle size enables optimized particle packing, thereby decreasing permeability and further improving the strength [3]. Fibers serve to improve the ductility, allowing much higher total strain before failure [4]. Working together, these elements produce a concrete that can reduce the required cross-sectional area, provide unique architectural applications, and improve the service life of structures [3].

2.2. Tire-Pavement Interactions

The simplest and earliest understanding of friction is built upon the work of Guillaume Amontons, known as the Amontons friction model [17]. Amontons found that a "friction force is directly proportional to the applied load" and that it is "independent of the apparent area of contact" [18]. The Amontons model of friction is not directly applicable when considering the friction between a pneumatic tire and a pavement surface, due to the many factors beyond the contact between surfaces that influence the observed resistance to motion [17]. However, while understanding pavement friction requires a more complex modeling of surface interactions than the models described previously, the basic principles are still at work. The interactions between a pavement surface and a vehicle tire can best be understood by breaking down the texture of the pavement surface into wavelength bands, as shown in **Table 2.1**: Pavement Texture Wavelengths (adapted from [19-21]). The smaller wavelength bands, microtexture and macrotexture, are understood to generate the positive effects of vehicle friction. Larger wavelengths of texture produce negative effects associated with ride comfort, noise and rolling resistance (affecting fuel economy) [17].

Table 2.1: Pavement Texture Wavelengths (adapted from [19-21])

Texture	Horizontal Dimensions	Vertical Dimensions	Source
Microtexture	0 to 0.5 mm	0 to 0.2 mm	Surface of aggregate
Macrotexture	0.5 to 50 mm	0.2 to 10 mm	Aggregate size and gradation, finishing
Megatexture	50 to 500mm	10 to 50 mm	Flaws and distresses
Unevenness/Roughness	>500mm	Exceeding designed tolerance	Flaws and distresses, rutting(transverse)

The World Roads Association (PIARC) defines microtexture as:

> *"Surface irregularities of a road pavement with horizontal dimensions ranging between 0 and 0.5 mm and vertical dimensions between 0 mm and 0.2 mm. Note: microtexture is related to the asperities of the coarse aggregate, the sand particles and the road surface in contact with the rubber of tires. It makes the surface feel more or less harsh but is normally too small to be observed by the eye* [19]*."*

and macrotexture as:

> *"Surface irregularities of a road pavement with horizontal dimensions ranging between 0.5 and 50 mm and vertical dimensions between 0.20mm and 10mm. Note: macrotexture is related to aggregate size, mixture design and laying (compaction), as well as to the surface treatment applied (if any). It has wavelengths in the same order of size as tire tread elements in the tire-road interface* [21]."

2.3. Pavement Friction Components

According to Andresen and Wambold, macrotexture and microtexture contribute to the friction model in three ways: shear, adhesion, and hysteresis, where the total friction is the sum of these three factors [17]. The shear refers to material wear or tearing. If the surface is considered non-rigid, then shearing can occur in the surface material, and if the surface is considered rigid, shear comes from the wearing of the tire, as a small amount of rubber is sheared off and deposited on the surface [9]. The shearing of the surface becomes the critical component of friction when dealing with surface contaminants (winter weather phenomenon of ice and snow) [17]. However, under normal operating conditions, the magnitude of friction generated from adhesion and hysteresis is "80 to 90 percent of the braking slip force [17]," therefore, the effect of shear is often ignored or considered insignificant [9]. Adhesion is generated by the "small-scale bonding and interlocking of the vehicle tire rubber and the pavement surface" and is generally considered to be a factor of the individual aggregate surfaces or microtexture [9]. Hysteresis occurs as the tire elastically deforms and recovers as it rolls over the surface and is a function of the macrotexture.

During this elastic recovery, some of the energy is lost in the form of heat, which contributes to resistance of motion in the form of friction [9].

2.4. Friction Treatment Options

The friction and texture of a pavement surface can degrade over time due to the effects of traffic and weathering. This reduction in friction can lead to safety concerns as adequate friction is necessary for maintaining vehicle traction. Lack of friction is especially concerning in areas where roadway geometry increases risks, such as small radius curves, curves with insufficient superelevation, and areas where driver visibility is limited. When determining a strategy for friction improvement, agencies must consider several variables, including lifecycle cost and benefits, available skilled labor and materials, and the condition of existing pavements. When possible, agencies may wish to address inadequate friction along with pavement distress through maintenance actions that improve both. There are numerous treatments that agencies can consider to address pavement preservation and friction improvement requirements. A summary of possible surface treatments that can address friction, with brief descriptions and observed frictional performance, is presented in **Appendix A**.

2.5. High Friction Surface Treatment (HFST)

HFSTs are a pavement treatment designed to restore or improve the coefficient of friction between the road surface and vehicle tires in order to improve the safety and reduce crashes, with the typical formulation of a "thin layer of high-quality polish-resistant aggregate bonded to the pavement surface with a polymer resin binder [4]." They can be employed in areas with high rates of accidents to compensate for geometric issues such as tight curve radii or insufficient superelevation, enabling better control of vehicles [8]. By increasing friction, HFSTs can also decrease the stopping distance by 25 to 30 percent [2,3,7]. FHWA recently published a study on Crash-Modification Factors (CMF) that estimates that HFSTs "reduce wet crashes by 83 percent and total crashes by 57%" [2,3]. Although the data vary by location and the type of sites that were treated, HFSTs have a proven record of crash reduction wherever they have been installed. The application methods range from manual (bucket mix and squeegee with hand broadcast aggregate) to fully automated spraying of resin and spreading of aggregate using specialized equipment [2,3,7].

The expected service life with high friction is seven to twelve years when properly constructed on pavement in good structural condition, but "varies from 2-10 years depending on various factors, including underlying pavement condition, construction quality, material used, age, environmental conditions, truck volume, and geometric characteristics [13]." The failure at the end of the service life tends to be rapid and not following the trend of aggregate wear, as it is due to the failure of the epoxy binder leading to loss of aggregate [13].

The aggregate used in HFSTs is typically a calcined bauxite of very fine gradation with maximum particle size of three to four millimeters with 95% passing the number 6 sieve and five percent passing the number 16 sieve [4]. While other aggregates can be used, calcined bauxite remains the premier and preferred choice due to its abrasion resistance and the high level of friction it provides

due to the microtexture of the aggregate surfaces. The production and shipping of calcined bauxite make it an expensive construction material and is a large part of the high construction costs for HFSTs. Much of the calcined bauxite comes from China with other sources in India, Guyana, Australia, Brazil, Guinea, and Jamaica [4,8]. Calcined bauxite is produced by heating bauxite (aluminum ore) to high temperatures (from 1,000 to 1,500 degrees Celsius) in a rotary kiln such that calcination occurs, a chemical process that removes moisture and impurities and increases the hardness [4]. What remains after calcination is predominantly aluminum oxide, Al_2O_3, with some aluminum silicate [4]. After calcination, the aggregate is crushed to the desired gradation for the specified application [4]. Major distributors in the US include Great Lakes Minerals and FX Minerals. Because of the energy required for kiln operation and shipping across oceans to the US, in addition to financial burden, calcined bauxite also contributes to excess carbon emissions when compared to local quarry aggregate materials. Costs are around $750 per ton.

The binders used for HFSTs are typically epoxy resin and polymer resin. They are applied in a thin film 50 to 65 mils (0.05 to 0.065 inches) thick in order to provide approximately 50% embedment of the aggregate which provides both adequate aggregate retention and adequate aggregate exposure for high texture and friction [8]. Resins can cost around 400-500 dollars for a 4-gallon set (2 gallons each of the two-part mix), which equates to $3.74 to $4.67 per square foot at 60 mils thick.

Initial friction values for HFSTs that agencies may require include DFT60 which range from 0.75-0.9 [8] and a BPN starting at 65 that can be up to the high 90's, and in some cases exceed 100 [22]. No macrotexture depth is specified by SCDOT, however a typical HFST can expect an initial MPD of around 1.9 mm which wears down to a terminal texture of around 1.1 [23]; other agencies may specify a minimum MPD of 1 mm [8].

2.5.1. South Carolina HFST

FHWA's case study report on South Carolina Department of Transportation's (SCDOT) choice to use HFST as an alternative to a major reconstruction project over a troublesome one-mile section of US-25 in Greenville County is summarized here [24]. The contributing factors to crashes at this location included improper drainage due to the concrete barrier divider, excessive speeds, and inadequate super elevation and sight distance. The proposed reconstruction project would have addressed these issues but at a high cost of five million dollars and would have impacted traffic over a three-year period. The chosen HFST alternative came at a reduced cost of one million dollars and only a 6-month construction time. This treatment reduced wet condition crashes 68 percent and total crashes by 56 percent. Across the state, a study of seven HFST locations showed "81 percent reduction in wet crashes and 71 percent reduction in total crashes" indicating the benefit of HFSTs to travelling public on South Carolinas roadways [24].

An analysis of crash data across 15 HFST application in SC from 2003 to 2016 showed an overall 73.85% reduction in crashes when corrected for traffic. **Figure 2.1** shows the crash rate before and after HFST application at these 15 locations.

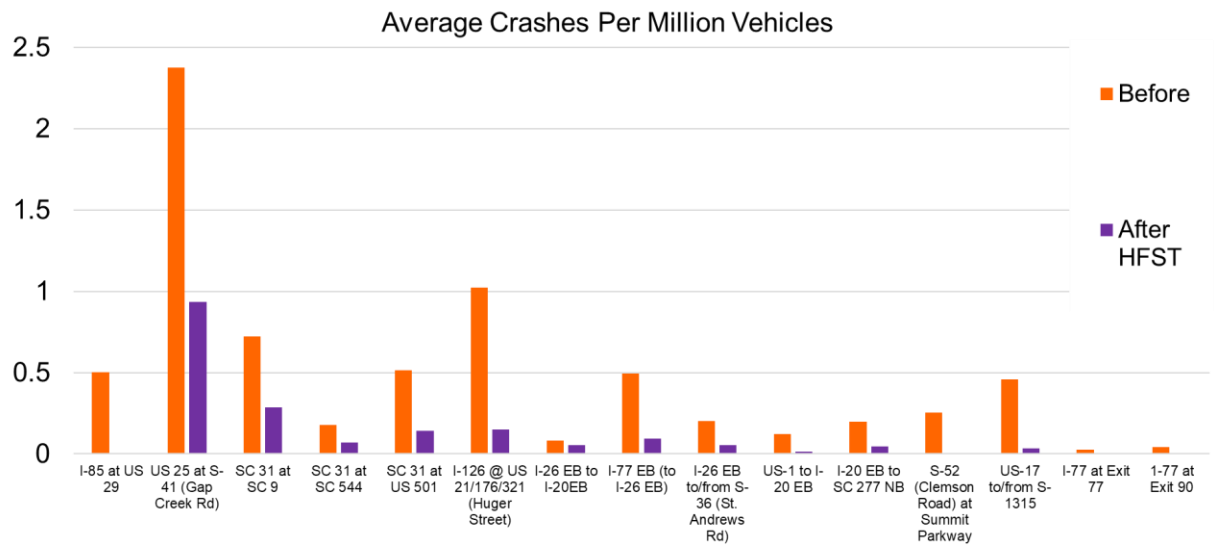


Figure 2.1: SC Crashes Before and After HFST

CHAPTER 3: EXPERIMENTAL PROGRAM

The experimental program for this research was broken into key steps that build on each other. 1) The first step was material selection and procurement. 2) This was followed by aggregate testing and UHPC mix design development which occurred simultaneously and partially independent of each other. 3) The results of the aggregate testing and mix design were then used to develop and evaluate UHPC-based HFST's. 4) Finally, the results of the UHPC-based HFST evaluation were analyzed to inform the development of recommendations for applying these treatments at full scale. The full program is depicted in the flow chart **Figure 3.1**. Additional details for each step are provided in the following section. While generally the flow depicted was followed, much of the work in the subsequent phases was conducted simultaneously with previous phases as sufficient data was gathered to move forward in experimental work and additional tests on mix design continued throughout the project.

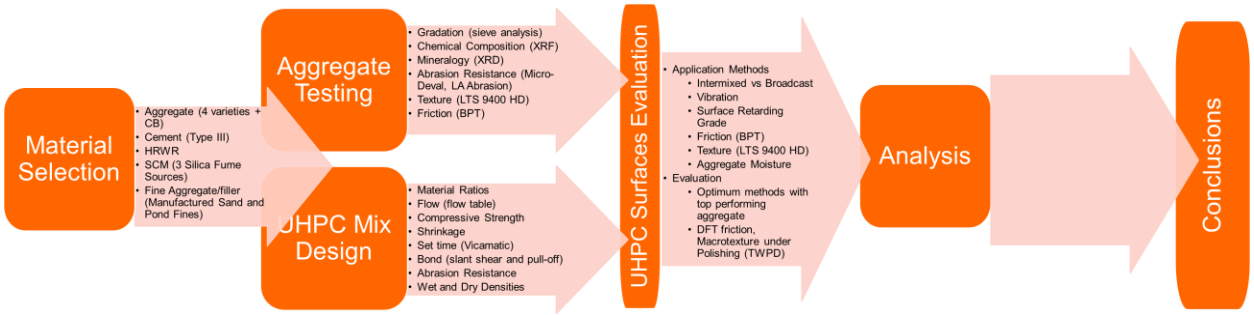


Figure 3.1: Experimental Flow Chart

3.1. Material Selection

The experimental program for this research begins with material selection. To limit the experimental matrix, while still exploring relevant material variables the following materials have been selected for research.

3.1.1. Aggregates

Four varieties of aggregates local to the southeastern United States were selected from the SCDOT coarse aggregate qualified products list. The aggregates were chosen for their reported abrasion resistance (low percent loss according to LA Abrasion). These include two granites from Charlotte, NC and Augusta, GA, a trap rock from Butner, NC, a steel slag from an Electric Arc Furnace (EAF), and finally calcined bauxite was sourced from a distributor in Newell, West Virginia.

3.1.2. Cement

An ASTM C150 Type III portland cement was used for all UHPC samples. Type III portland cement is a finer version of Type I portland cement and results in a faster initial strength gain. Based on a recent mill test report the following properties of the cement used are given, however, there may be slight variation between batches used in the experimental work. The Type III portland

cement had a specific surface area via Blaine's Finess of 485 m^2/kg and a particle size distribution shown in **Figure 3.3**. The chemical composition of this cement is shown in **Table 2.1**.

Table 3.1: The Chemical Composition of the Type III Portland Cement

SiO_2	Al_2O_3	Fe_2O_3	CaO	MgO	SO_3	Na_2O	SO_3	TiO_2
20.0%	4.5%	3.6%	65.4%	0.2%	2.6%	0.4%	2.6%	0.3%

3.1.3. HRWR/Superplasticizer

A single variety of HRWR was selected for this study, Viscocrete 6100 made by Sika. It was selected for its applicability to UHPC. Viscocrete 6100 provided one of the largest water reductions while having the shortest slump life and fastest setting times of the available HRWRs.

3.1.4. Supplementary Cementitious Materials (SCMs)

Three different Silica Fumes (SFs) were used for this study, each coming from a different source. SF 1 is densified whereas SF 2 and 3 are undensified, shown in **Figure 3.3**. The amorphous and crystalline contents are listed in **Table 3.2**, as determined by ratio of integrated intensities from X-Ray Diffraction (XRD) of phases identified. The SF XRD patterns are shown in **Figure 3.2**. Because of the prevalent use of silica fume in UHPC no other SCMs were considered in this research.

Table 3.2: The Crystal Composition of Tested SFs

SF ID	Amorphous Content (%)	Crystalline Content (%)
SF1	92.6	7.4
SF2	93.9	6.1
SF3	98.1	1.9

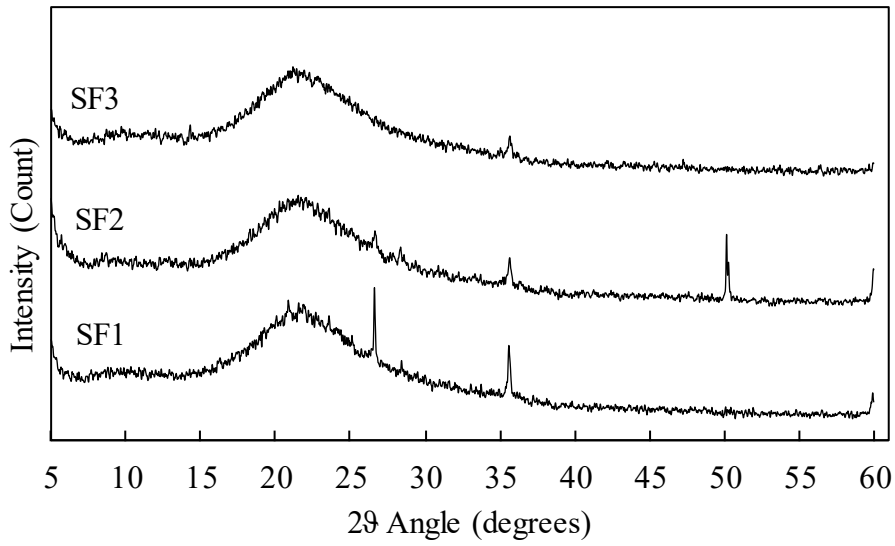


Figure 3.2: XRD Pattern of Tested SFs

3.1.5. Fine Aggregate

A manufactured granite sand aggregate, and pond fines from Liberty, SC were used to provide two gradations of fine aggregate for mix design. The gradations for which are displayed in **Figure 3.3**.

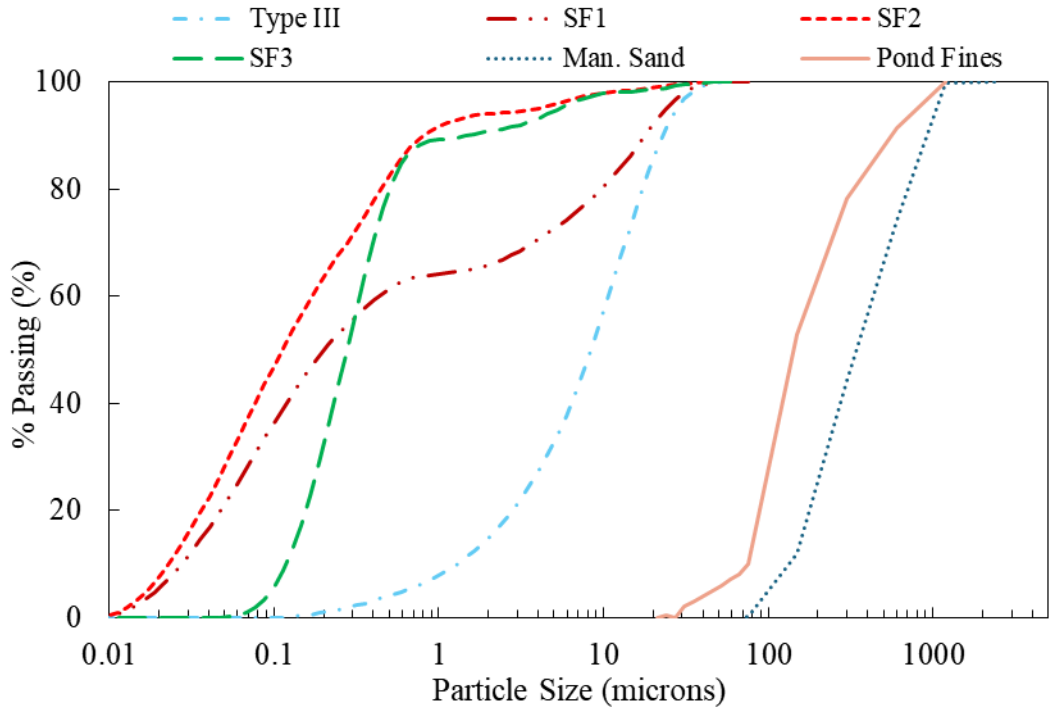


Figure 3.3: The PSD of UHPC Constituent Materials

3.2. Aggregate Testing

Aggregates available locally to South Carolina were evaluated for their performance in comparison to calcined bauxite. The effects of gradation by crushing and sieve analysis, the chemical Composition by X-ray fluorescence (XRF), the mineralogy by XRD, the abrasion resistance by Micro-Deval and Los Angeles Abrasion, the surface texture by laser scanning, and the friction by the British Pendulum Test were all utilized for evaluation. Additionally, the effects of gradation and abrasion on the texture and friction were evaluated.

3.3. UHPC Mixture Design

The UHPC mixture design portion of this study was composed of two primary components: continuous particle packing and discrete particle packing. The continuous particle packing study developed UHPC mixture proportions using the Modified Andreasen and Andersen (MA&A) method for 3 different silica fumes at two separate HRWR dosages. The continuous particle packing performance parameters tested included: flow, setting time, bond strength (pull-off and slant shear), compressive strength, abrasion resistance, coefficient of thermal expansion, autogenous shrinkage, and drying shrinkage.

After completing the continuous particle packing section the worst performing mix was selected for discrete packing to determine if its properties could be improved to exceed the bond and compressive strength thresholds. Discrete packing focused on the influence of intermixing HFST gradation calcined bauxite with the optimized UHPC proportions previously developed. The discrete particle packing parameters included wet density, dry density, compressive strength, bond strength (pull-off and slant shear), abrasion resistance, thin-layer shrinkage, and drying shrinkage.

3.4. UHPC Surface Evaluation

The testing of UHPC-based HFST surfaces was divided into two phases. The first phase focused on developing the materials and methods that could produce adequate HFSTs with comparable properties to that of traditional HFST materials. Because this first phase was focused on binders, only calcined bauxite aggregate was used. The testing evaluated the effects of aggregate moisture, comparing the effects of intermixed coarse aggregate and broadcasted aggregate, the effects of vibration induced aggregate embedment, and the effects of increasing grade of set retarders used for aggregate exposure in intermixed surfaces. The surfaces were evaluated for friction using the British Pendulum Test (BPT) and various macrotexture and microtexture parameters.

The second phase evaluated UHPC-based surfaces employing the top performing aggregates from the aggregate testing, and the top performing application methods for UHPC-based HFSTs. The performances of these surfaces were evaluated by assessing the friction with the Dynamic Friction Tester (DFT) and macrotexture. Polishing using the Three Wheel Polishing Device (TWPD) was conducted on samples to determine the polishing effects on the texture and friction.

3.5. Analysis

Analysis of the data for each phase of experimentation was conducted to draw reasonable conclusions based on the findings. Additional brief analysis of overall impacts of the research includes the costs including materials for construction of UHPC-based HFST's in comparison to traditional HFST construction. Consideration of the performance across friction, texture, abrasion resistance and bond strength were used to distinguish among available materials and methods.

CHAPTER 4: MICROTEXTURE CHARACTERIZATION OF BULK-AGGREGATE SAMPLES FOR APPLICATION IN HIGH-FRICTION SURFACE TREATMENTS

4.1. Objective

This study sought to develop a standard laboratory test to quantify the microtexture of bulk aggregate samples for application in HFSTs in conjunction with standard abrasion tests (MD and LAA). These tests sought to compare various microtexture parameters in spatial, frequency, and statistical domains and assess the effects of gradation and abrasion. Additionally, a comparison was made to discover the best predictors of friction as measured by the British Pendulum Test (BPT), and in comparison, to macrotexture parameters generated from the same profiles. The parameters were also assessed in their ability to distinguish and rank order quality among aggregates. The desired outcome was to present a method and parameters that can be used as an objective measure of aggregate performance in a HFST both in terms of abrasion resistance and friction and that allows a direct comparison between laboratory and field measurements.

4.2. Methods and Materials

4.2.1. Aggregate Selection

Five aggregates were selected for this study based on local availability in the southeastern United States and high abrasion resistance relative to other available aggregates. Among them were two granites identified as Granite-1 and Granite-2, a trap rock, a steel slag, and a calcined bauxite, the standard material for applications in HFSTs. Granite-1 is sourced from northeastern Georgia, Granite-2 from southwestern North Carolina, and the Trap Rock from Central North Carolina quarries. The slag is a byproduct of steel production from EAF and calcined bauxite is a manufactured material made from heating high alumina content rock. The elemental compositions and primary crystal phases of each were determined using fused disc X-ray fluorescence (XRF) and powder X-ray diffraction (XRD), respectively, shown in **Table B.1** of **Appendix B**. Natural materials often consist of multiple minor crystalline phases that increase variability of measured properties. As a manufactured material, calcined bauxite is an exception demonstrated by clean XRD peaks with a high degree of certainty in phase identification. The aggregates were also crushed to other gradations, as described in the following sections. The aggregates are shown in **Figure 4.1**. The 'as received' gradations of each aggregate were determined by sieve analysis as shown in **Figure 4.2**. Calcined bauxite gradation was based on a smaller sample size of 200 grams (less than typical testing quantity).



Figure 4.1: Aggregates as Received (Scale in millimeters)

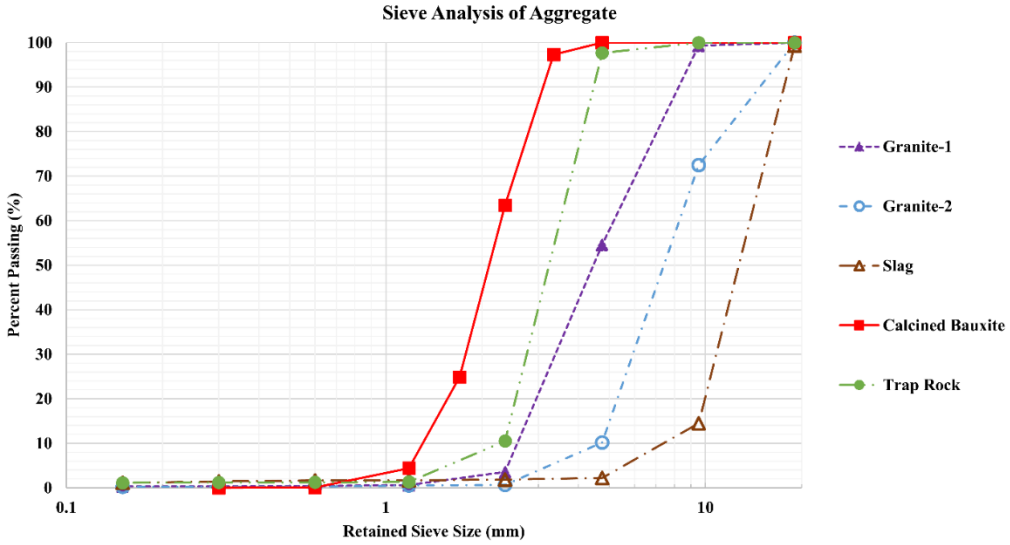


Figure 4.2: Aggregate Gradation as Received

4.2.2. Laser Scanning Process

The microtexture of the aggregate samples were scanned using the AMES Laser Texture Scanner (LTS) 9400HD. This LTS has a maximum profile resolution (sample spacing) of 0.00635 mm. Because the LTS is designed to rest on a pavement surface when in use, a sample holding stage was constructed with adjustable height and a stable surface for mounting the scanner. A removable tray held aggregate samples of approximately 400 grams between two steel plates that made up the sample holder. The aggregates were placed in the holder and leveled then the reference plate for the LTS was placed on top of the stage. As needed, the aggregate samples were lightly agitated and tamped to provide an even surface for scanning that limited dropouts from excessive deep points. The aggregate was then scanned with the LTS.

For each test, five replicate samples were made by removing the aggregate from the sample holder, reordering the particles by pouring from one container to another and then placing them back into the sample holder, leveling, and rescanning. To be efficient while still acquiring adequate sampling, LTS was set to obtain 20 high-resolution scanlines across the surface for each scan operation.

When filtering profiles to isolate the microtexture waveband of texture, steep drops (such as between aggregates) create noise artifacts. The large change in height over the relatively short length results in sharp peaks in the filtered profile. While the LTS accompanying software (Ames Texture Scanner 3.2.0.76) was used for outlier removal and macrotexture parameters, it was found to be inadequate for microtexture filtering. Therefore, MATLAB code was developed to filter to microtexture, filter out the noise artifacts, and produce microtexture parameters. The Virgina Tech method of outlier removal was applied in the AMES software to the microtexture data before exporting to MATLAB. Invalid data was removed in MATLAB.

It is important to select the appropriate baseline for calculation of texture parameters. Li et al. showed that as the baseline length increases so does the parameter value [25]. This study selected a 1-mm baseline from which microtexture parameters were calculated as that was shown to be the ideal by Sergios et al. who found 1-mm baselines provided superior prediction of skid resistance across five parameters (including MPD) compared to 5, 10, and 20 mm baselines [26,27]. After filtering the profiles were divided into 1-mm segments. Parameters were calculated as the mean of all the segment's values. For every scan, a total of seven parameters were determined. Five parameters were calculated from the filtered profile segments, which included three depth parameters—Micro-Mean Profile Depth (Micro-MPD), Micro-Root Mean Square (Micro-RMS), Micro-Arithmetic Roughness (Micro-Ra), and two statistical parameters— Micro-Skewness (Micro-Rsk) and Micro-Kurtosis (Micro-Rku). Additionally, utilizing the AMES software's three-point spike removal and bridging invalid data, macrotexture parameters (for surface samples) and Power Spectral Density (PSD) were determined. The AMES software generated the average elevation PSD from the 20 scanlines using a constant frequency interval of 0.01. The PSD data was exported and the slope and intercept of a linear fit to the logarithm of the average of elevation Power Spectral Density (PSD) to the logarithm of wavelength were calculated as they have been established by other researchers as potential texture parameters [26,27]. While care was taken to verify software input parameters and analysis methods were used consistently as described for data processing, software inputs and outputs are a potential source of minor variability in the data, but any error is believed to negligibly impact the findings of this study. MPD was calculated based on ASTM E1845 methodology but adapted for the 1-mm baseline length instead of the standard 100 mm. The mean value of the1-mm baseline segment of measurement was shifted to zero by subtracting the mean from each data point in the array. The array was then divided in half and the peak value of each half is determined. The mean depth of the segment is the difference between the overall mean (which was set to zero) and the average of these two peak values. The average of all of the mean segment depths is reported as the micro-MPD. The other microtexture parameters were based on their standard mathematical formulations on the same shifted 1-mm baseline. These methods differ from the common imaging techniques such as AIMS in that they are based on a profile that represents the bulk sample as whole instead of samples of individual aggregate particles.

The spatial parameters act as depth measurements with units of millimeters. Skewness refers to tails of the distribution, where negative skewness indicates more troughs than peaks and positive skewness indicates more peaks than troughs in the profile [9,28]. Kurtosis is a measure of outlier content, where a value of 3 is normally distributed, above 3 indicates significant presence of outliers and less than three indicates low outlier content [28]. Some conventions subtract 3 from kurtosis, however it is presented with Rku =3 as normally distributed in this study. To differentiate these parameters from those typically applied to macrotexture or unfiltered profiles the prefix micro is applied to them herein, e.g., micro-MPD.

4.2.3. Aggregate Abrasion Testing

To obtain the desired gradation for all testing, the aggregates were crushed using a Bico Chipmunk jaw crusher, which was repaired and modified during this study to provide the desired small gradations. Additionally, to achieve the small gradations used in HFSTs it was necessary for the aggregates to be subjected to several cycles of crushing. The aggregates were abraded using the LA Abrasion test per ASTM C131-06 procedures. The "D" gradation, defined as passing the #4 sieve and retained on the #8 sieve (P4R8), was selected for testing as it was closest to HFST gradation [8]. Five hundred rotations of the LAA drum with 5000 grams of aggregate and approximately 2500 g of 46.8 mm steel charge were completed and the aggregate retained on the #12 sieve was weighed. Five replicate measurements of texture were scanned on a representative sample of the remaining aggregate.

The aggregates were also abraded using the MD apparatus with procedures adapted from ASTM D7428-15 and in part based on methods used in research conducted at the National Center for Asphalt Technology (NCAT) on alternative aggregates for HFSTs [29,30]. The aggregates were tested at the 'as received' gradation and at a crushed gradation of passing the #4 sieve and retained on the #16 sieve (P4R16). Because the calcined bauxite and trap rock gradations 'as received' were close to P4R16, the 'as received' gradation data was used for both gradations, therefore data was duplicated in comparative and statistical analysis. A sample of aggregate weighing 505 grams was placed in the MD chamber with 0.75 L water and 1250 grams of 9 mm steel charge and rotated at 30-minute intervals. After each interval, the samples were washed and sieved over the #30 sieve, with particles passing the #30 discarded. They were then dried, and five replicate measurements of texture were scanned on a representative sample. The aggregates were then returned to the MD chamber with the same mass of water and steel charge and abraded again for four cycles for a total of 120 minutes of abrasion. A schematic of the abrasion testing plan is shown in **Figure 4.3**.

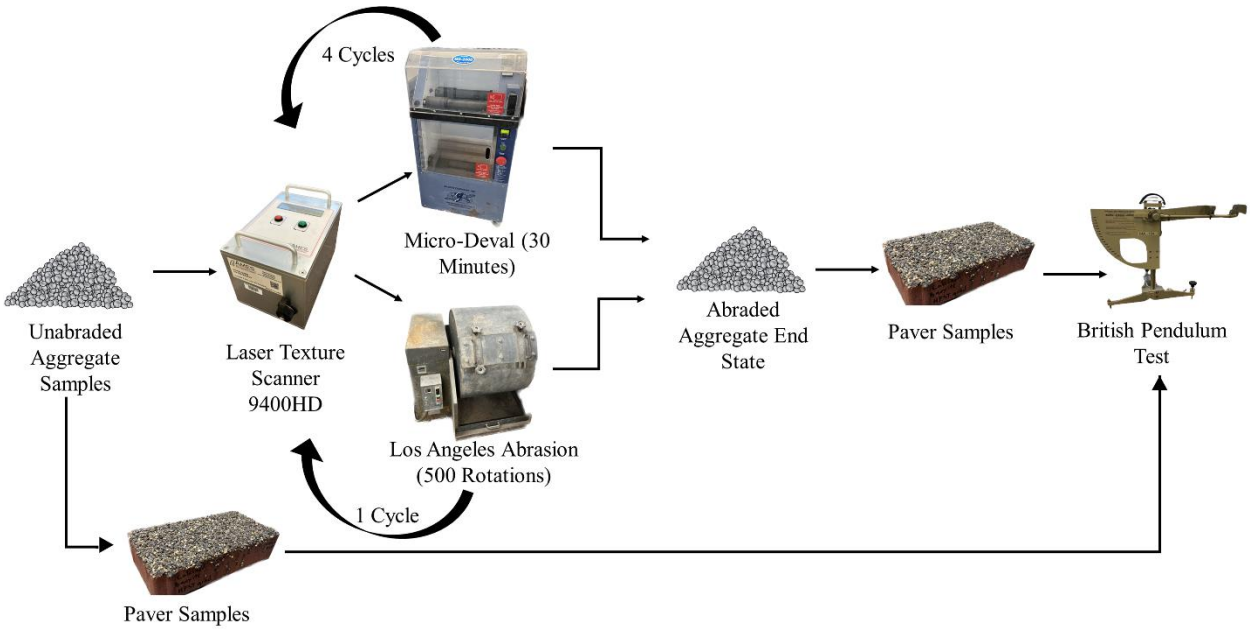


Figure 4.3: Abrasion Testing Schematic

One hundred twenty minutes of MD at P4R16 and 500 rotations of LAA at P4R8 yielded similar average total percent mass loss (20.5% and 19.2%, respectively) across all the aggregates allowing for a valuable comparison of microtexture and friction at the end state of the aggregates between the abrasion tests.

4.2.4. Friction Sample Testing

Sample HFST surfaces were constructed using the aggregates to evaluate the friction and compare texture results from bulk aggregate samples to constructed surfaces. Concrete pavers with dimensions 197 mm x 95 mm were utilized as a base. Thirty ml of HFST resin was applied to each paver (approximately 1.5 mm thick as prescribed for HFSTs) [4]. Aggregate samples were then hand broadcasted to cover the surface in excess of 2 lb/ft^2 per resin manufacturer recommendation. The resin cured for a minimum of 24 hours. The samples were then brushed and subjected to 40 cycles of aggressive rubbing across the surface (20 passes along the width and 20 passes along the length) with a wood board, based on methods used by other researchers [29,30]. This removed weakly bonded aggregate and provided a more uniform surface. Compressed air was used to clean the surface of any wood particles and dust remaining.

Surfaces were constructed at four aggregate gradations: 'as received,' P4R8, P4R16, and HFST. The 'as received' gradation surfaces required additional resin which was adjusted to provide approximately 50% embedment of the aggregate particles. The P4R8 and P4R16 were generated by crushing the slag and granites and sieving the trap rock and calcined bauxite. The samples collected at the end of abrasion testing were sieved to the original P4R8 and P4R16 gradations, removing the finer particles retained previously. The retained abraded aggregates were then

embedded in the same manner as the unabraded aggregate allowing a comparison between before and after abrasion samples with minimal influence of gradation changes from abrasion. The HFST gradation was created to mirror the manufactured gradation of calcined bauxite HFST aggregate as closely as possible, with calcined bauxite's as received gradation used as reference. Sieve analysis was conducted on a 200-gram representative sample over the #4, #6, #8, #12, #16, #30, and #50 sieves. The other aggregates were crushed and sieved to obtain sufficient material to match equivalent masses on each sieve. The desired mass of aggregate from each sieve was then mixed to create equivalent particle size distribution at the HFST gradation for each aggregate. The sample surfaces are shown in **Figure 4.4**.

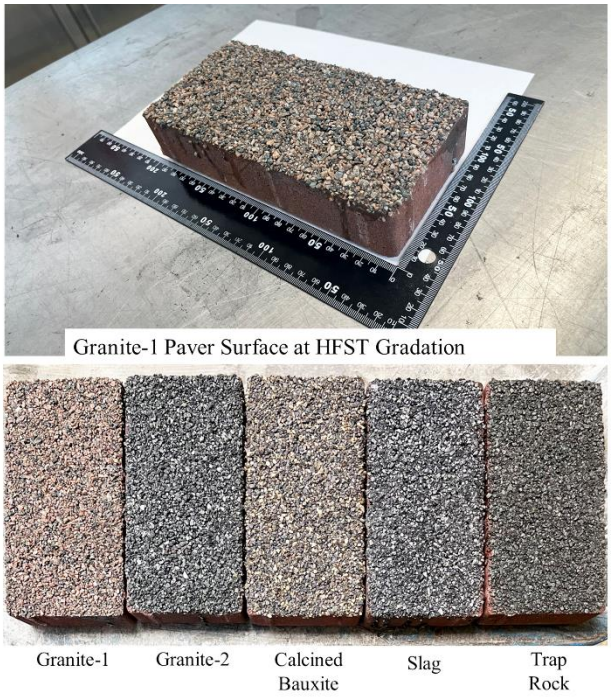


Figure 4.4: Sample HFST Surfaces (Scale in mm)

Two texture scans were completed for each surface at 180 degrees from each other along the length. In addition to the microtexture parameters, the macrotexture parameters of MPD, RMS, Ra, Rsk, and Rku were collected using the LTS software. Minor differences in the samples' overall slope was a potential, but presumably negligible, source of variability.

The friction of the samples was evaluated by the BPT. The test was conducted according to ASTM E303-23 with a TRL-55 rubber slider as recommended by the BPT manufacturer for pavement surfaces. For each surface, the British Pendulum Number (BPN) was recorded as the average of 5 successive swings after two setting swings. The samples were rotated 180 degrees, and the test was conducted again. The average of the two BPNs was taken as the mean BPN, while all 10 data points were used for ANOVA testing among samples. Surfaces prepared with 'as received' resulted in high macrotexture (up to MPD of 4.77 mm) and therefore were not tested to avoid damage to the BPT. Potential sources of additional variability include the possibility of

unrepresentative aggregate samples used in testing (samples were assumed to be representative but sample splitting was not conducted), the possibility of a water leak in the MD apparatus and any other differences due to researcher induced effects, error, oversight, and equipment operation or standard test variations across the testing not described herein.

4.3 Results and Discussion

The outcomes of testing were analyzed through ANOVA and regression modeling, which determined if observed effects were statistically significant and quantified how models accounted for the variability of the data. These were determined by ANOVA P-value (<0.05 significance), model estimates (slope of regression) and coefficients of determination also called the R^2. Across ANOVA tests the assumption of normal distribution of residuals was verified by inspection of normal quantile plots and although not perfect across all tests, they were deemed acceptably normal for the purposes and outcomes of this study. Additionally, limitations on the application of regression results are described. The assumption of equivalent variance was also assessed by visual inspection of box plots of the data. While differences in variance were observed it is not believed to skew the p-values determined because ANOVA can tolerate differences in variance when sample sizes are nearly equal, and the experimental design utilized identical sample sizes. Statistical testing was conducted using JMP Pro 16 software.

4.3.1 Effects of Aggregate Gradation on Microtexture

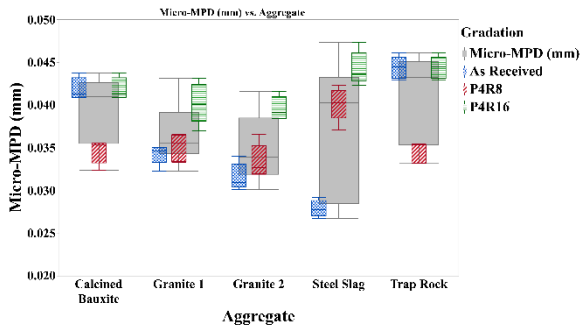
Because testing was conducted at varying gradations, the first test determined if gradation was a significant factor to the measured microtexture. Since microtexture is attributed to the surfaces of exposed aggregate, in theory a unique microtexture could be defined for aggregate sources independent of size and gradation. Factorial ANOVA was conducted on unabraded aggregate samples at P4R8, P4R16, and 'as received' gradations with aggregate type, gradation, and the interaction term of aggregate*gradation used as model effects and each of the microtexture parameters as response variables. One-way ANOVA was also conducted for each aggregate individually with the gradations as model effects and the microtexture parameters as response variables. The results are summarized in

Table B.2**Table B.2** in Appendix B.

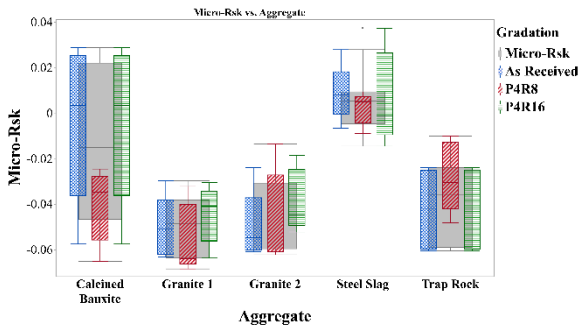
The gradation, aggregate type, and interaction term were statistically significant for all spatial parameters, micro-Rku and PSD intercept, indicating that while these microtexture parameters can distinguish among aggregates, the gradation should be considered, and the significant interaction term indicates that the effect of gradation differs among the aggregates. This effect of gradation seemingly undermines the previously defined divisions of macrotexture and microtexture. However, understanding that texture occurs across the wavelength spectrum, and the wavebands are somewhat arbitrary, the result is not entirely unexpected. For instance, the presence of aggregate particles with dimensions less than 0.5 mm will have an influence on the profile in the microtexture wavebands, but that is attributable to the size and gradation, not just the aggregate surface itself.

In contrast, micro-Rsk and PSD slope were ostensibly robust against the effects of gradation with insignificant p-values for gradation effects in both factorial ANOVA and one-way ANOVA for each aggregate, while the effects of aggregates were statistically significant. This implies that these parameters can distinguish texture among aggregates without accounting for gradation. This is demonstrated in **Figure 4.5**, where box plots of the quartiles of data for Micro-MDP which was influenced by gradation can be compared to that of micro-Rsk and PSD slope. The quartiles of all gradations data for each aggregate are in solid gray set behind the individual gradation box plots. Clear differences among the gradations for each aggregate are seen for micro-MPD, while differences are not significant for micro-Rsk and PSD slope. Micro-Rsk and PSD slope also appear to have more power to distinguish among aggregates, as indicated by the clear differences in the gray box plots of all data. However, they also show a wider variability within the total data range, and the models have poor R^2 relative to the other parameters, with micro-Rsk being superior to PSD slope.

(a)



(b)



(c)

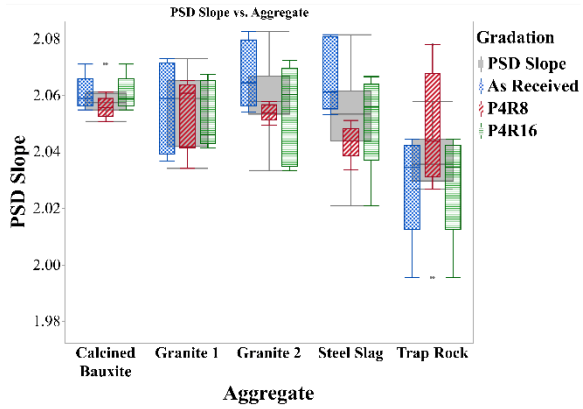


Figure 4.5: Box Plots of Aggregate and Gradation Effect on Microtexture, (a) Micro-MPD, (b) Micro-Rsk, (c) PSD Slope

4.3.2 Repeatability

Because gradation was found to be significant in affecting microtexture, it was considered as a factor in all other analysis to include evaluating the repeatability of the study's laboratory methods themselves. A repeatability coefficient, c_r, can be calculated according to methods described by Bartlett and Frost, where the standard deviation (SD) is estimated from an ANOVA of replicate measurements of the same subject, where the mean square error (MSE) is the variance of the test, and the square root of MSE is the within subject SD in **Equation 4.1** [28,31].

$$c_r = 1.96 \times \sqrt{2} \times * SD_{within\ subject} \quad (4.1)$$

Only data from unabraded aggregates at P4R8 gradation was used for calculation to provide a single c_r for comparative purposes (as a different c_r would result from other gradations). ANOVA was conducted with aggregate type as the model effect and the microtexture parameters as response variables. The repeatability coefficients were calculated as: $c_{r\text{-Micro-MPD}} = 0.0045$ mm; $c_{r\text{-Micro-RMS}} = 0.0021$ mm; $c_{r\text{-Micro-Ra}} = 0.0016$ mm; $c_{r\text{-Micro-Rku}} = 0.1930$; $c_{r\text{-Micro-Rsk}} = 0.0421$; $c_{r\text{-PSD Slope}} = 0.0311$; and $c_{r\text{-PSD Intercept}} = 0.0705$. These coefficients mean that two repeat measurements on the same aggregate will differ by no more than the coefficient 95% of the time, assuming no external sources of variability [31].

The mean microtexture values from unabraded aggregate samples were compared to paver surface samples of the same aggregate and gradation. Although the mean differences between them were low, not all were less than repeatability coefficients. The pavers generally although not universally produced microtexture depth values with a bias of higher microtexture. The differences were likely due to the difference in particle orientation, where leveling of the bulk samples tended to orient particles with flatter sides up while broadcasting of aggregates onto the surface samples allowed for a more random particle orientation and a larger interaggregate spacing. Additionally, the crushing method used and sieving for the gradations likely introduced variability in size and shape

between the chosen sieves, and since gradation was shown to be significant to microtexture, very precise size distribution between the bulk samples and surfaces is necessary for the bulk samples to be used as an accurate predictor. This is demonstrated by comparing the average micro-MPD of bulk to surface samples, where only the 'as received' gradation resulted in the same aggregate rank order and with only one aggregate slightly differing by more than the repeatability coefficient. Micro-Rsk, which factorial ANOVA showed to be robust against gradation effects, was a better (although not perfect) predictor of rank order of aggregate across the other gradations. Micro-Rku also demonstrated superior ability to maintain rank order with differences between the bulk and surface sample within the c_r when compared to other microtexture parameters. A sample of rank comparison is shown in **Table B.3** in **Appendix B**.

The connecting letters reports from Tukey's honest significant difference tests are also included, where for each group, aggregates connected with the same letter did not have statistically significantly different means based on the data variance, which showed even when the Micro-Rsk surface rank order was not predicted precisely by the bulk sample, the ranks only changed within the same connecting letter. Additionally, the micro-Rsk rank orders across the three gradations indicates the ability of micro-Rsk to consistently rank slag at the top. However, the parameter's variability makes consistently distinguishing among the other aggregates across the gradations less reliable, which is reflected in model R^2 of 0.55 which indicates only slightly more than half of the variability is accounted for.

4.3.3 Effects of Abrasion on Microtexture

Texture and friction loss occur over time on pavements due to traffic and environmental effects. LAA and MD test aggregate's resistance to abrasion by subjecting them to tumbling with a steel charge. Percent mass loss is then utilized as the measure of quality, where low loss indicates high quality. However, these tests apply different abrasive energy than that experienced by pavements. Changes in microtexture from abrasion were investigated. Factorial ANOVA was conducted with the level of abrasion, aggregate type, and the interaction of abrasion and aggregate as model effects and the microtexture parameters as response variables, the results of which are shown in **Table B.4** in **Appendix B**. MD abrasion was modeled as a continuous variable with data at 0, 30, 60, 90, and 120 minutes of abrasion. For LAA data were only collected for 0 and 500 rotations, therefore, the results are a binary comparison between non-abraded and abraded samples.

4.3.3.1 Micro-Deval

Apart from micro-Rku, across both gradations, all parameters detected a statistically significant effect of MD abrasion. Aggregate type was statistically significant for all parameters and significance varied for the interaction term of aggregate*abrasion. With increasing abrasion, the regression slopes of depth parameters consistently trended to lower microtexture, more negative micro-Rsk, increasing PSD slope, and decreased PSD intercept, all statistically significant. Interpretation of the negative direction of slopes for depth parameters demonstrated depth decreased with abrasion as expected. Similarly, micro-Rsk becoming more negative is expected, assuming that primarily the higher asperities on the aggregate surfaces are exposed to abrasion and as the higher points polish the profiles will skew more negative. Micro-Rku was significantly

affected by abrasion in the P4R16 model only, but the physical interpretation is like the other parameters, the extreme highs and lows (outliers) become less extreme, decreasing kurtosis. However, the non-statistically significant effect of abrasion on micro-Rku warranted further investigation. The direction of regression slopes of PSD slope and intercept are not easily linked to physical trends.

The 'as received' gradation produced much better models (by R^2) than the P4R16. This was likely because the larger particle sizes in 'as received' had more mass, giving greater ability to absorb the energy of the steel charge, which made them more likely to polish than break, which microtexture measurements were able to measure clearly. Secondly, the opposite was true of the smaller gradation, which were more likely to break (revealing new microtexture) than polish and in breaking cause changes to the particle size distribution introducing gradation variability which is related to previous research that showed smaller aggregate gradations have higher mass loss in MD abrasion [32]. Still, the R^2 for the P4R16 models were in tolerable ranges except for PSD slope.

4.3.3.2 Los Angeles Abrasion

LAA produced a statistically significant effect on Micro-Rsk, micro-Rku and PSD parameters, and although not statistically significant, the spatial parameters showed an increase in texture which defies expectations of polishing. However, as crushing was introducing variability in the MD test, this effect was much more exaggerated by LAA, which used larger steel charges at higher drop distances. If polishing was occurring in the LAA rotations, its effect was masked by simultaneous crushing. Kuzmanić et al. similarly described the higher energy of LAA resulting in breakage and creation of new particles (although no steel charge was used) and a greater observable changes in texture resulting from MD compared to LAA at equivalent mass loss levels [33]. Kamani and Ajalloeian also observed a great decrease in texture from MD compared to very little change from LAA [34]. Furthermore, as suggested by Deiros Quintanilla, the presence of water in MD testing likely allows more fine particles to be removed from the surface of aggregates, while the dry LAA may allow larger aggregate particles to be coated in a thin layer of fine dust which provides some protection from further polishing [35]. Another possible source of difference and variability between LAA and MD is that the aggregates' differing minerology and specific gravity behavior could result in different performance in dry versus wet conditions as observed by Nålsund [36]. This difference between MD and LAA effect is illustrated by the trends of Micro-MPD plotted for each aggregate of the MD of 'as received' as compared to LAA of P4R8 shown in **Figure 4.6** also demonstrates the variability for measurements for individual aggregates due to the aforementioned factors and inherent variability in samples of natural materials. Among the models with significant effects from abrasion only micro-Rku and PSD intercept modeled with adequate R^2. Again, the results of micro-Rku warranted further investigation.

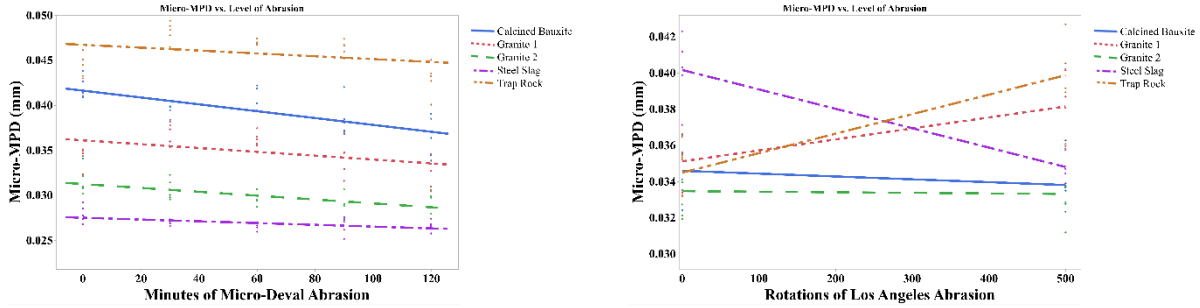


Figure 4.6: Abrasion Effect on Micro-MPD for (a) Micro-Deval (b) Los Angeles Abrasion

4.3.3.3 Other Abrasion Observation

In assessing micro-Rku, it is noteworthy that across all the factorial models in this study micro-Rku consistently had the highest R^2 (0.95, 0.97, 0.93, and 0.90), and this is despite containing a model for which abrasion was not a statistically significant model effect. However, a higher R^2 does not necessarily mean better model. It implied that micro-Rku was perhaps the most effective model for distinguishing among aggregates, but observing the entire data set of micro-Rku for the bulk aggregates yielded an interesting finding. The distribution of data shows that micro-Rku was not normally distributed across the aggregates. The histogram and normal quantile plot show a bimodal distribution with the higher distribution due to calcined bauxite, which is made clear by comparison of micro-Rku data sorted by aggregate **Figure 4.7**.

(a) (b)

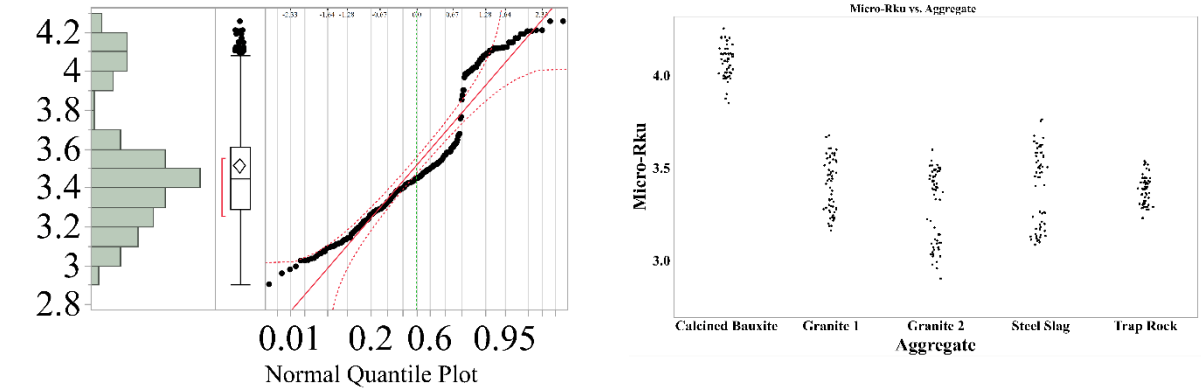


Figure 4.7: Distribution of micro-Rku data by (a) Histogram and Normal Quantiles (b) Data sorted by Aggregate

Normal quantile plots of residuals from abrasion ANOVA showed acceptable distribution, so ANOVA assumptions were not violated. However, the test is reflecting the distinct differences in means. Therefore, because calcined bauxite had such a distinct micro-Rku and all the factorial ANOVA models included aggregate type as a model effect, the high R^2 is reflects the model's power to observe this difference. The results are more indicative of the unique properties of calcined bauxite than the utility of micro-Rsk as a parameter. Calcined bauxite's high kurtosis was from the complex pore structure of the aggregate providing excessive high peaks and low troughs.

4.3.4 Friction Testing

Friction testing of the sample surfaces enabled a comparison among the microtexture parameters as predictors of tire friction on HFSTs and a comparison of microtexture to macrotexture parameters. Additionally, the effects of abrasion on friction were assessed.

Microtexture was poorly correlated with friction using only the data collected on the HFST sample surfaces. However, this was due to the range of data given the variability inherent to the BPT, i.e., all of the samples were in the same range of high friction. Several reference surfaces including asphalt, painted asphalt, concrete, and manufactured ceramics of various lower textures were scanned and measured with the BPT to calibrate the regression model to a wider range of data which improved the models with an outlier removed. Comparison of Micro-MPD effect on BPN showed the calibration surfaces improved the R^2 from 0.064 to 0.706. Additionally, it was discovered that with the wider range of data, the regression was better fit to a log scale than linear with an R^2 of 0.815. Given the variability of the models within the range of data that is desired for HFSTs and the limited additional data, the calibrated regression models are representative of the general physical phenomena relating microtexture to BPT friction but should not be considered highly precise predictive models, especially since the samples included surfaces not representative of real pavement textures and a larger quantity of data is centered around the higher values. The models do however suggest what could be considered high friction occurs at micro-MPD exceeding approximately 0.035 mm based on the methods used determining the parameter in this study. Zuniga-Garcia and Prozzi showed there is not one universal relationship between texture and friction, and the relationship is also related to the type of pavement surface [37]. However, Zuniga-Garcia and Prozzi still highlighted the utility of using both macrotexture and microtexture in friction prediction models. The results of regression testing are summarized in

Table B.6 in **Appendix B** with PSD slope multiplied by -1 to enable logarithmic regression. Data used were the average values for each surface sample.

Among all the models, ln(micro-MPD) was the best as measured by R^2. Microtexture parameters were consistently superior to macrotexture. The relationship between PSD intercept and BPN showed increasing friction with higher intercept, thus validating the negative slope direction of the regression on the abrasion samples.

Comparison of unabraded to abraded aggregates mirrored the results seen with microtexture. MD led to decrease in friction for all aggregates, while the effect of LAA decreased some but increased others indicating that crushing was occurring along with polishing. The results are shown in **Table B.5** in **Appendix B**.

Comparing the friction across P4R8, P4R16, and HFST gradations, the performance varied across the aggregates, but HFST had the highest average BPN across the unabraded aggregates with calcined bauxite at HFST gradation having highest friction observed.

In evaluating the utility of mass loss as a quality indicator, slag aggregate presents an interesting case. Slag had the greatest loss in friction (-28.8 BPN after MD) and texture relative to mass loss, indicated by steeper slopes in **Figure 4.8**. However, it was on the lower end of total mass loss, with only calcined bauxite having less. This is in stark contrast to the findings of El-Ashwa et al. who found that under MD abrasion slag increased in texture index as measured by the AIMS and had very little loss in angularity relative to other aggregates tested [38]. One possible explanation is that harder aggregates will preferentially polish over breaking which is supported by some data presented. However, calcined bauxite which lost less mass did not have as much texture and friction loss. This is a possible indicator that mass loss alone does not capture the way aggregates abrade, and in this case abrasive energy appears to affect the slag in a way that may makes it less suitable for an HFST, as it went from the highest friction sample at P4R16 to the lowest friction after MD. These findings cannot be broadly applied to all slag aggregates but are sufficient to draw conclusions for the specific slag source used in this study.

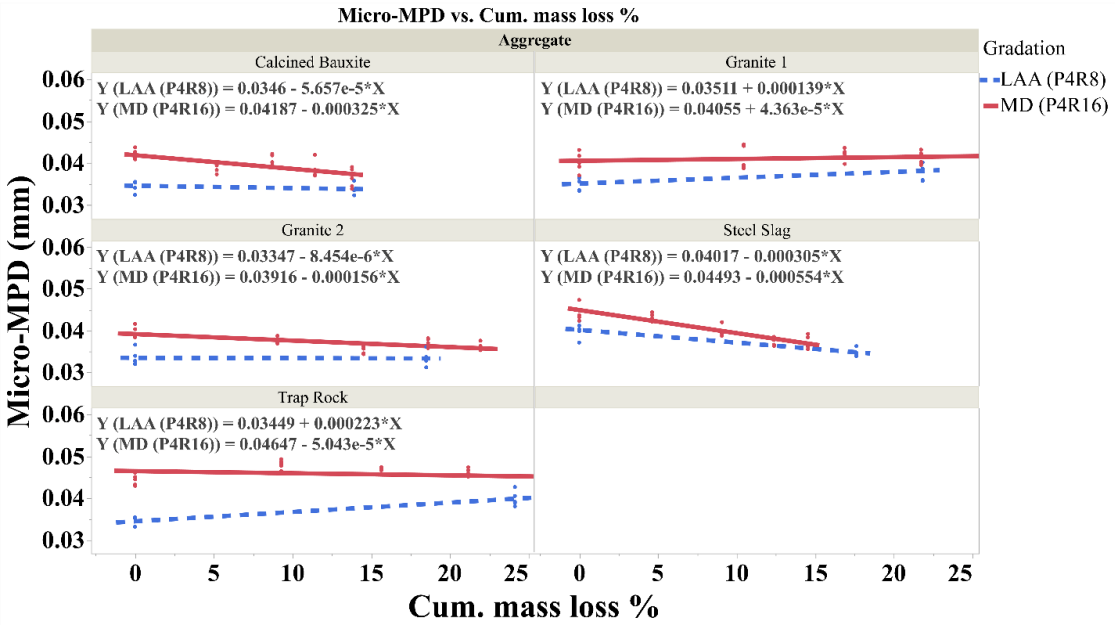


Figure 4.8: Micro-MPD vs Cumulative Mass Loss

4.4 Conclusions

This study developed a novel technique for measuring the microtexture of aggregate samples for use in HFST applications. This method could in some cases adequately predict the microtexture offered by the same aggregate in an HFST application, given the gradation was very consistent between them. This technique was also able to detect the changes in microtexture that occur due to abrasion in the MD and LAA tests. Coupled with BPN friction, the microtexture measurements showed that LAA testing is prone to crushing more than polishing and is therefore a poor representation of abrasion experienced by aggregates on pavement surfaces, and while MD is better, it likely still has some crushing effects present. Abrasion mass loss was also shown to be a poor representation of loss of texture as the methods utilized in this study (microtexture in conjunction with BPT friction after abrasion) were able to reject an aggregate as suitable for HFSTs that mass loss alone would have deemed high quality.

Among the depth micro-texture parameters (MPD, RMS, Ra), the significance was not distinguishable, but ln(Micro-MPD) had the highest R^2 with friction of all models. PSD intercept was the second-best parameter to depth measurements to correlate with friction while providing consistent reliable results. Micro-Rku alone was able to identify the unique texture features of calcined bauxite, which was the best performing of all the aggregates. Micro-Rsk showed some utility in being less sensitive to the effects of gradation, albeit with higher variance. Both statistical parameters give a unique insight even though they are not strongly correlated with friction. The PSD intercept model performed nearly as well as depth parameters, while PSD slope performed poorly. There is possibility of improving the microtexture and PSD parameters by adjusting the filtering and analysis processes, but further study is required to determine the effects of any adjustments. Additionally, generating PSD parameters adjusting the constant frequency interval of

0.01 used in the AMES software could potentially improve the results but further study is needed to determine what the effects would be and if there is an ideal range.

Microtexture parameters were superior to macrotexture in modeling the BPT friction. Additionally, microtexture was found to correlate much better with BPT friction on a logarithmic scale than on a linear scale.

Based on the aggregates selected in this study, calcined bauxite was found to be a superior aggregate among the testing conducted. In contrast, while the crushed slag aggregate provided high initial friction and texture it had the highest loss of friction and texture under abrasion. Granite 2 was the worst performing aggregate overall with low initial texture and friction and high loss under abrasion. Granite 1 and the trap rock showed potential as suitable HFST aggregates with adequate friction before and after abrasion maintaining BPN above a threshold of 65, which is the lower end of observed friction for HFSTs according to a report by the Western Transportation Institute [39].

The laser scanning method utilized to capture microtexture of bulk aggregate samples has a distinct advantage over the commonly utilized imaging methods in that the same methods and data analysis methods can be applied directly to pavement surfaces as well, allowing a direct comparison of laboratory and field values. Additionally, the use of parameters describing bulk samples in lieu of individual aggregate samples more closely approximates the state of the aggregates when measured in pavement surfaces. There is a possibility of improving the microtexture and PSD parameters by adjusting the filtering and analysis processes (e.g., adjusting the frequency interval used in Ames software), but further study is required to determine the effects of any adjustments.

CHAPTER 5: UHPC-BASED HFST MIXTURE PROPORTIONS OPTIMIZATION

5.1. Problem Statement

A reduction in materials costs for HFSTs is necessary to increase the breadth of their application therefore, numerous projects have investigated alternative HFST aggregate sources [5,30,56-58]. While cursory investigations have studied cementitious based friction treatments the efficacy of UHPC-based HFSTs has yet to be explored [59,60]. There currently exists no comprehensive study that outlines how UHPC compares to epoxy-resin for the criteria necessary for an effective HFST.

5.2. Objective

This chapter investigated the use of UHPC as a potential binder alternative for HFSTs and an assessment of the suitability of the prevalent particle packing methods to develop UHPC to act as an HFST binder. Testing focused on the fresh properties, bond strength, compressive strength, and shrinkage of UHPCs designed using the MA&A methodology and Wet Packing Density method. Comparisons were made between the UHPC samples and epoxy-resin binder to assess mechanical properties and performance relative to existing standards for HFSTs and roadway remediations.

5.3. Methods

5.3.1. Mixing Procedure

Most UHPC mixtures were mixed using a 20-quart Hobart Mixer with a 0.5 HP motor at three speeds of: low (planetary motion 60 rpm and paddle 107 rpm), medium (planetary motion 113 rpm and paddle 198 rpm), and high (planetary motion 207 rpm and paddle 365 rpm). Mixing and batching occurred in laboratory conditions (23±1℃ and 50±5% relative humidity), and batching was completed directly before mixing. The mixing procedure used for this study is based on recommendations from literature and previous experimental work [61,62].

An important first step when mixing UHPC is the dispersion of the Silica Fume and the blending of the solid particles through a two-minute dry mix at low speed with the cement, silica fume, sand, and pond fines. After blending, the water is added in two steps. First, 70% of the batch water is added at low speed over 30 seconds and then the remaining 30% of the batch water is added with the HRWR over a subsequent 30 seconds at the low speed. The speed is then set to medium and mixed until the UHPC becomes cohesive and then given another 30 seconds of mixing time to develop fluidity. This step typically takes between four and eight minutes. After cohesion, mixing is stopped for 30 seconds during which the paddle and bowl are scraped to ensure all material is properly mixed. Once the 30 second wait has elapsed, the mixer is set to high speed and mixed for one minute. After this high speed mix the UHPC is ready unless steel fibers or calcined bauxite is intermixed. If steel fibers are included, the steel fibers are added over another subsequent minute long period on low speed, where the fibers are hand dispersed to ensure no fiber balls disrupt the cementitious matrix. If calcined bauxite is intermixed the speed is decreased to

low, and the calcined bauxite is intermixed over a minute long mixing time. **Figure 5.1** summarizes this procedure.

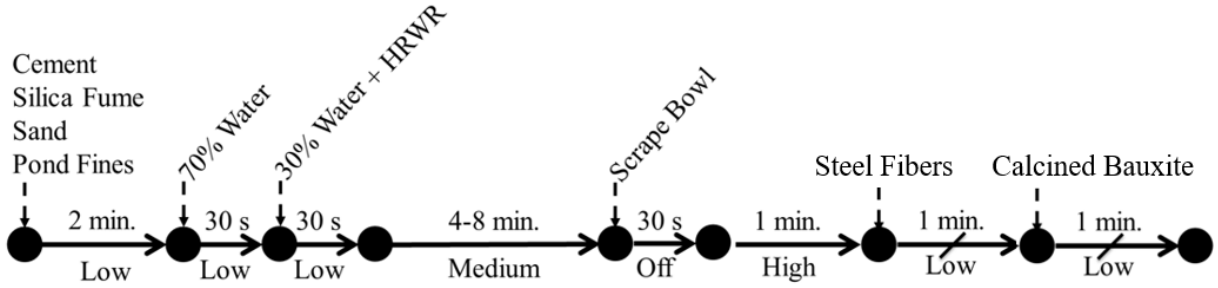


Figure 5.1: Mix Procedure for UHPC Samples

An alternative mixing procedure and mixer was used for the thin-layer shrinkage mixtures due to their small volumes. Mixing was completed in a vacuum mixer at a shear rate of 350 RPMs and 12.9 psi of vacuum with all powder materials, water, and HRWR included until the mix became cohesive (two to three minutes), at which point the bowl was scraped for 30 seconds, then finished with another 350 RPM and 1.8 psi vacuum for one minute. The mixing ended if calcined bauxite was not included. However, if calcined bauxite was included, it was mixed by hand for one minute due to the larger particle size. **Figure 5.2** summarizes this procedure.

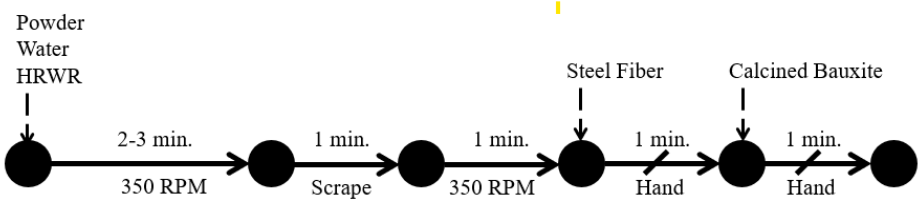


Figure 5.2: Mix Procedure for UHPC and Intermixed Vacuum Mixing

5.3.2. Flowability

The flowability was measured directly after mixing the UHPC samples and the intermixed calcined bauxite samples with oven-dry calcined bauxite in a room at laboratory conditions. The test procedure followed a modified version of ASTM C1437-20 as recommended by ASTM C1856-17 for the UHPC samples. The intermixed calcined bauxite samples followed the method outlined by ASTM C1437-20 directly. The mold for both tests is a truncated cone with 70 mm upper diameter, 100 mm lower diameter, and a height of 50 mm. Each flowability reading was completed in triplicate, and the average and standard deviation are included in the results section. A threshold of 100-150% flow was selected for comparison based upon the definition of UHPC outlined in ASTM C1856-27.

5.3.3. Setting Time

The setting time of the UHPC mixes was measured using an automatic Vicat apparatus following ASTM C807-21. The automatic setup utilizes a water bath maintained at 23±0.5℃ by a recirculating chiller, a circular brass ring mold with a 76 mm inner diameter and 40 mm tall, and a 2±0.05mm diameter stainless steel needle (total mass=300±0.5 g). To calculate the initial setting time, the last penetration exceeding 25 mm and the first penetrating less than 25 mm are inserted into **Equation 5.1**. Secondarily, the final set for this testing is set at 0.5 mm, as opposed to 0 mm for conventional testing, due to the ability of a surface defect to obscure the accurate final set by outputting a slight penetration when none is truly present. To calculate the depth at which a penetration of 0.5 mm occurs, **Equation 5.1 is** modified to instead solve for the interpolation of a 0.5 mm penetration. There is an existing criterion for setting time (cure rate) in the SCDOT HFST Supplemental Specification but it is not used as a criterion for this project due to the necessity of accelerators to achieve a three-hour setting time.

$$Initial\ Set = \left(\left(\frac{H-E}{C-D}\right) * (C - X)\right) + E \tag{5.1}$$

where:

X = Penetration Depth of Desired Reading

E = Time to penetration greater than X

H = Time to penetration less than X

C = Penetration reading at time E

D = Penetration reading at time H

5.3.4. Pull-Off Bond Strength (Pull-off Method)

Tests to determine the tensile strength of the UHPC mixes, intermixed calcined bauxite mixes, and an epoxy-resin surface were carried out at seven and 28-days. The test procedure followed the methodology recommended by ASTM C1583-20. Overlays were cast on both full-age (>28 days old) concrete and asphalt substrates. The concrete substrates were cut from a larger slab, and the surface was prepared to an ICRI surface preparation of six by a pneumatic scabbing hammer. All substrate surfaces were cleaned of loose debris after the surface preparation. The pull-off bond strength of the substrates is listed in **Table 5.1**. The failure modes are shown in **Figure 5.3** and are designated in the results section if not along the overlay-substrate interface. The average and standard deviation of the test results are shown in the results section. The SCDOT HFST Supplemental Specification outlines a minimum pull-off bond strength of 250 psi or 100% failure in the substrate and is used as the evaluation criteria for this project.

Table 5.1: Pull-Off Bond Strength of Substrates

Substrate	Pull-Off Bond Strength (psi)	Std. Dev. (psi)
Concrete	489	32
Asphalt	46	13

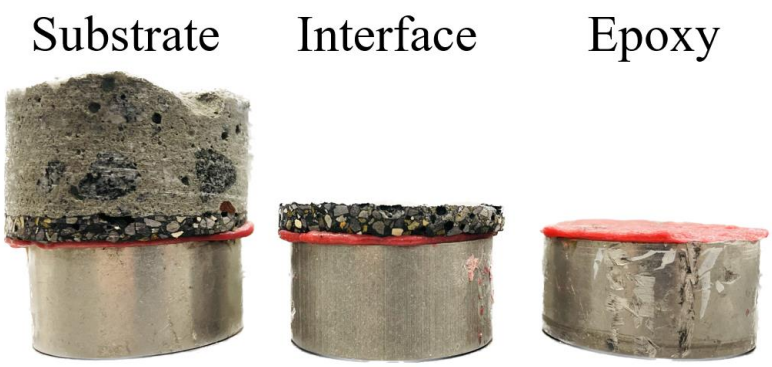


Figure 5.3: Failure Modes of the Pull-Off Bond Strength Test

5.3.5. Slant-Shear Bond Strength

The shear bond strength was measured per ASTM 882-23 at 1, 7, and 28-days for the UHPC, the intermixed calcined bauxite UHPC, and an epoxy-resin. The test substrate was a full-age concrete 3" x 6" cylinder with a compressive strength of approximately 10,000 psi, which was tested in accordance with ASTM C39-23. The concrete substrate was cut at a 60° angle to provide an equivalent surface area for each half of the cut cylinder. The surface was not prepared before testing/casting. The bond strength was calculated using **Equation 5.2**, where the surface area was 14.13 in^2 for all samples tested, and the ultimate load capacity was based on the test results. To convert to the shear bond strength, **Equation 5.3** is applied, where the total bond strength is converted to the shear component along the sample interface. Lastly, this test has different failure modes based on where the sample failed, as shown in **Figure 5.4**.

To determine if a cementitious systems break was sufficient for exposure conditions the general guidelines provided in ASTM C928-20 were utilized. ASTM C928-20 is the standard specification for rapid-hardening cementitious materials for concrete repairs and determines if a roadway patching material is viable for exposure conditions. Since these patches are placed in locations already prone to failure, a more conservative recommendation is expected. This standard sets out a bond strength requirement of at least 1000 psi at one-day and 1500 psi at seven days. Converting these values to the shear component of that bond strength using **Equation 5.3** sets the minimum ultimate slant shear bond strength at one-day to 450 psi and at seven days to 650 psi [63]. The ultimate slant shear bond strength is used rather than the bond strength, as it is dependent on the

angle of the cut relative to loading, whereas the ultimate slant shear bond strength already accounts for the angle.

$$S = \frac{L_u}{A_I} \qquad (5.2)$$

Where:

S = Bond Strength

L_u = Ultimate Load

A_I = Interface Area

$$S_S = 0.5 * S * \sin(60°) \qquad (5.3)$$

Where:

S = Bond Strength

S_S = Slant Shear Bond Strength

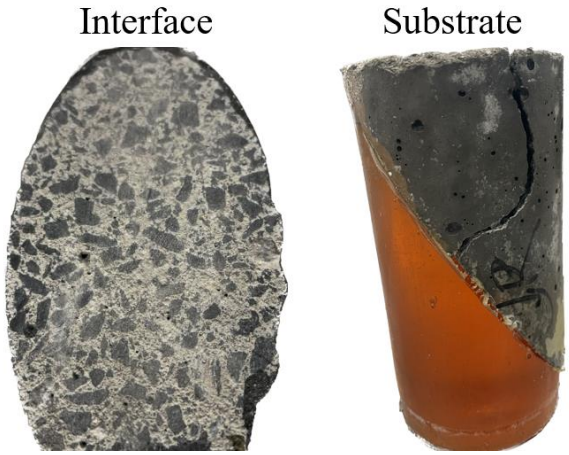


Figure 5.4: Failure Modes of the Slant-Shear Test

5.3.6. Abrasion Resistance

The abrasion resistance was measured on two full age UHPC samples, intermixed samples, concrete, asphalt, and epoxy-resin cylinders using a modified version of ASTM C944-19 (**Figure 5.5**) under laboratory conditions based on the methodology outlined by Lyons [64]. The test samples were 6" diameter cylinder cut to 2.5±0.5" tall sections (this process led to some surface defects, increasing the test's variability). This allowed for flat initial surfaces and exposed the test

surface during the initial testing stage. The test was completed at 250 rotations per minute under a load of 40±1 N applied to the spindle. The weight of the samples was taken at 0, 5, 10, 15, and 20 minutes of abrasion time. Before measurement, the surfaces were sprayed with compressed air to remove any loosely adhered particles or dust. The volume loss, calculated by dividing mass loss by sample density at each age, is listed in the results section and includes the average volume loss at the varying abrasion times of the two samples. Due to the abrasion resistance testing following a modified version of ASTM C944-19 no existing criteria were utilized for analysis and instead is used only as a relative measure of quality.



Figure 5.5: Abrasion Resistance Setup

5.3.7. Compressive Strength

The compressive strength was measured at one, seven, and 28-days on 2-inch cubes per ASTM C109-23 for the UHPC samples and the intermixed calcined bauxite samples with oven-dry calcined bauxite. Additional SF3-3.5 and SF3-4.5 were tested at 1, 7, and 28-days with intermixed calcined bauxite at saturated surface dry to determine its impact on the performance of UHPC. Three cubes were tested for each sample, and each sample's average and standard deviations were provided in the results section. If one test sample deviated from the average by 8.7% or more, the average of the two cubes closest to the average value was taken. However, if those two values deviated by more than 7.6%, the test results were thrown out, and the test was repeated. The existing criteria outlined by the SCDOT HFST Supplemental Specification requires a three-hour 1000 psi compressive strength and seven-day 5000 psi compressive strength. Due to the setting time exceeding three-hour requirement that data point was removed as a criteria point. Additionally, a comparison was made to the existing UHPC threshold set out by ASTM C1856-17 of 17 ksi for classification as UHPC.

5.3.8. Drying Shrinkage

The drying shrinkage of UHPC samples with and without intermixed calcined bauxite was completed in accordance with ASTM C596-23 with measurements at 3, 7, 14, 21, and 28-days after casting. The readings conducted at three days were the initial readings, and all subsequent readings' ages were the time from casting minus three days. Drying shrinkage values were calculated to the nearest 0.001% but were reported to the nearest 0.01%. The results and standard deviation for this section are included in the results section. The criterion for this test was set based upon the ultimate tensile strain capacity of unreinforced ordinary portland cement systems of 0.02%, due to the thin nature and high degree of restraint prevalent in pavement overlays.

5.3.9. Autogenous Shrinkage

The assessment of autogenous shrinkage to supplement drying shrinkage results was completed on only the UHPC samples and conducted per ASTM C1698-19. The autogenous strain for a given age is equal to the length reading at that time minus the reading at the final set divided by the initial length of the sample. Length changes were recorded to the nearest 0.001 inches criterion for this test, that match those of the drying shrinkage test.

5.3.10. Coefficient of Thermal Expansion

The coefficient of thermal expansion was tested on triplicate samples 28-days or older for UHPC, concrete substrate, asphalt substrate (only one sample), and epoxy-resin systems tested per AASHTO T336. Samples were 4" x 8" cylinders cut to a height of 7±0.2" to ensure the test surfaces were flat and parallel. This test was primarily used as a comparison between different surfaces but also highlights the degree of differential shrinkage between different surfaces. It is important to note that the effects of thermal expansion will compound with drying/autogenous shrinkage leading to strain/stress buildup.

5.3.11. Wet Density

The wet density was measured directly after mixing for all discretely packed samples and an additional sample at a calcined bauxite to cementitious materials ratio of 4.0 under standard laboratory conditions. The test procedure followed a modified version of ASTM C138-23, where 3x6 cylinder molds were used as the reference measure. The measured density of the UHPC is calculated using **Equation 5.4** from ASTM C138-23 and the theoretical density of the UHPC is calculated using **Equation 5.5** from ASTM C138-23. These values allowed for the determination of the solids concentration, voids ratio, and air content, which are found using **Equations 5.6-5.10**, respectively. The resultant densities and void/solids concentrations are included in the results and discussion section. The objective of this test for particle packing is to maximize the wet density.

$$D = \frac{M_C - M_m}{V_m} \tag{5.4}$$

Where:

D = Measured Density

MC = Mass of Concrete

Mm = Mass of Measure

Vm = Volume of Measure

$$T = \frac{M}{V} \tag{5.5}$$

Where:

T = Theoretical Density

M = Mass of all components

V = Absolute volume of every component

$$V_s = \frac{\sum M}{\sum V} \tag{5.6}$$

Where:

Vs = Volume of the solids

∑M = Summation of component masses for a batch

∑M = Summation of component volumes for a batch

$$Solids\ Concentration = \frac{V_s}{V_m} \tag{5.7}$$

Where:

Vs = Volume of the solids

Vm = Volume of the measure

$$Voids\ Ratio = \frac{V_m - V_s}{V_m} \tag{5.8}$$

Where:

Vs = Volume of the solids

Vm = Volume of the measure

$$Air\ Content = \frac{D}{T} \quad (5.10)$$

5.3.12. Dry Density

The dry density was taken on the triplicate concrete cylinders previously cast for wet density measurements after seven days of curing for all discretely packed samples and an additional sample at a calcined bauxite to cementitious materials ratio of 4.0 under standard laboratory conditions. The test procedure follows ASTM C39-23s hardened density procedure. After recording the masses, the density of the samples was calculated using **Equation 5.11**. Furthermore, additional properties were recorded using **Equations 5.6-5.10**, which were previously outlined in the wet density section. The results and pertinent analysis are included in the results and discussion section. The objective of this test is to maximize the dry density.

$$\text{Dry Density} = \frac{W_{SSD}}{W_{SSD} - W_{SUB}} * \gamma_w \quad (5.11)$$

Where:

W_{SSD} = SSD Weight of Sample

W_{SUB} = Submerged Weight of Sample

γ_w = Density of Water

5.3.13. Thin Layer Shrinkage

The early age shrinkage of thin UHPC sections was measured using the thin-layer measurement system by Schleibinger Testing Systems. This system utilizes two lasers, reflectors, and sensors to determine the lateral deformation of thin sections with measurements recorded every 150s (**Figure 5.6**). This study tested all the discretely packed samples on two different substrate surfaces, an unrestrained and restrained surface.

The unrestrained surface was created by adhering a plastic laminate sheet onto an underlying flat tile of dimensions 5" x 10". Once the plastic laminate sheet is applied, a 3D printed form was placed onto the surface, with the two end plates caulked to the surface to ensure a well bonded mold. Allowing for the proper compaction of the samples and the avoidance of sample leaks.

The restrained surface was created on 197 mm x 95 mm concrete brick pavers. The top surface was prepped using pneumatic scabbing hammer to an ICRI surface prep level of approximately six. After prepping the surface, a tape barrier was placed around the surface of the sample to create an 8 mm layer of UHPC without flowing off the sides. Concrete substrates were saturated before testing for at least one hour. Once the substrate surface was prepared, samples were batched and mixed in standard laboratory conditions by the mix procedure outlined for vacuum mixing. This procedure was chosen to ensure consistency between small volume samples. Once mixed, the UHPC sample was added to the substrate surface, spread by a trowel, and then consolidated using

a vibrating table for 15±5 seconds. The sample was then placed on the thin-layer measurement system, the reflectors placed onto the sample, the lasers adjusted, and the sampling process started.

After 13 hours, the data was exported and the first hour is removed from the data. This was due to the first hour being a random period where the reflectors either display expansion or contraction based upon the initial settling of the samples. This data is not considered in analysis. The decision to limit the testing to the subsequent twelve hours is due to the minimal change experienced between 8 and 24 hours. The results from this testing are included in the results and discussion section. The criterion for this test was set based upon the ultimate tensile strain capacity of unreinforced ordinary portland cement systems of 0.02%, based upon the thin nature and high degree of restraint prevalent to pavement overlays.



Figure 5.6: Thin-Layer Measurement System

5.4 Phase 1: Continuous Packing of UHPC (MA&A Method)

5.4.1. Background and Mixture Proportions

As a baseline an initial comparison was made between non-proprietary UHPC, intermixed calcined bauxite UHPC, traditional UHPC, and an epoxy-resin binder (some testing also included a comparison to conventional concrete and asphalt) for a variety of common HFST evaluation criteria. These mixture proportions were developed based upon existing common UHPC design procedures, pavement concrete/asphalt surfaces, and epoxy-resins. To create a wide range of non-proprietary UHPCs three different silica fumes were used with differing particle sizes and amorphous contents. This allowed for more variety when optimizing the particle packing of UHPC.

To maximize the particle packing of the UHPC mixtures their constituent material proportions were optimized by the MA&A Method (**Eqn. 5.12**) to minimize the deviation from the theoretical packing curve. All mixes were optimized around a q-value of 0.19 based on the recommendation

of Liu et al. [51]. The upper bound for the MA&A was based upon the maximum sand particle size (1.18mm), and the minimum was dependent on the smallest SF particle size (0.01 microns for SF1 and SF2 and 0.1 microns for SF3 and Traditional UHPC. The mixture proportions generated via optimization through the MA&A method are shown in **Table 5.2,** and the packing curves are shown in **Figure 5.7**. Generating the mixture proportions required an iterative process, where the relative proportions were modified to decrease the difference between the real and theoretical curves. Iterations of varying component ratios were completed until the R^2 no longer increased. To mitigate the influence of nonlinear change in cumulative percent finer on the R^2 the sampling rate was also nonlinear (more frequent sampling at smaller sizes).

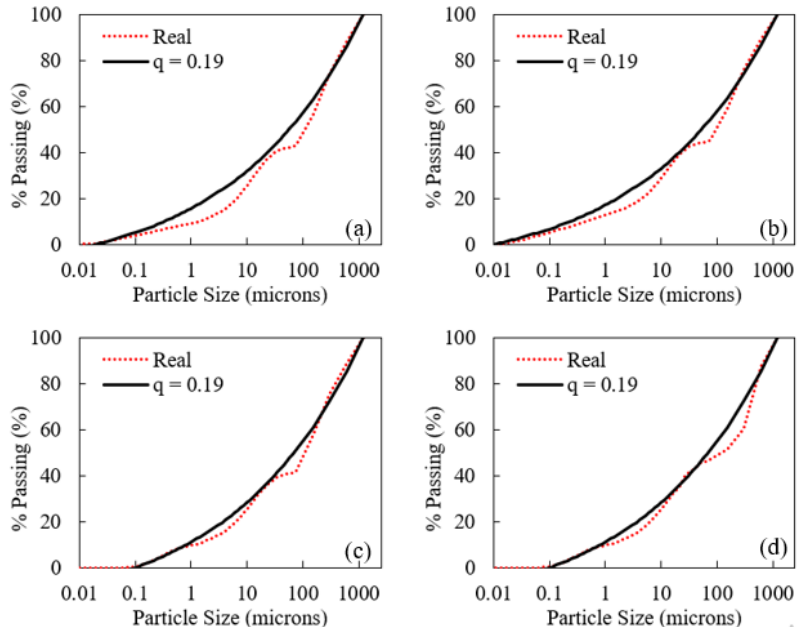


Figure 5.7: MA&A Curves of (a) SF1 Mixes (b) SF2 Mixes (c) SF3 Mixes (d) Trad. UHPC

$$CPFT = \left[\frac{d-d_{min}}{d_{max}-d_{min}}\right]^{q} * 100 \qquad (5.12)$$

Where:

CPFT = Cumulative Percent Finer Than

d = Particle Fraction Testing

d_{min} = Minimum Particle Size

d_{max} = Maximum Particle Size

q = Distribution Exponent

Table 5.2: Mixture Proportions for UHPC Mixes

Sample ID	C/CM (-)	SF/CM (-)	S/CM (-)	PF/CM (-)	W/CM (-)	HRWR/CM (-)	Steel Fiber (% Vol)
SF1-3.5	0.80	0.20	0.7	0.4	0.2	0.035	0.0
SF1-4.5	0.80	0.20	0.7	0.4	0.2	0.045	0.0
SF2-3.5	0.80	0.20	0.6	0.4	0.2	0.035	0.0
SF2-4.5	0.80	0.20	0.6	0.4	0.2	0.045	0.0
SF3-3.5	0.85	0.15	0.6	0.5	0.2	0.035	0.0
SF3-4.5	0.85	0.15	0.6	0.5	0.2	0.045	0.0
Trad. UHPC	0.85	0.15	0.6*	0.5*	0.2	0.045	2.0

*Siliceous Sand

Additional testing was completed using intermixed calcined bauxite, the mixture proportions for those mixes are shown in **Table 5.3**. The mixture proportions were kept the same as the original UHPC mixes but contained calcined bauxite at a calcined bauxite to cementitious material (CB/CM) ratio of 3.0. The CB/CM ratio is based upon experimental testing, where 3.0 was the most calcined bauxite possible while still being cohesive to provide ample HFST aggregate for friction generation.

Table 5.3: Mixture Proportions for Intermixed Calcined Bauxite Mixes

Sample ID	C/CM (-)	SF/CM (-)	S/CM (-)	PF/CM (-)	W/CM (-)	HRWR/CM (-)	CB/CM (-)
SF1-3.5-CB	0.80	0.20	0.7	0.4	0.2	0.035	3.0
SF1-4.5-CB	0.80	0.20	0.7	0.4	0.2	0.045	3.0
SF2-3.5-CB	0.80	0.20	0.6	0.4	0.2	0.035	3.0
SF2-4.5-CB	0.80	0.20	0.6	0.4	0.2	0.045	3.0
SF3-3.5-CB	0.85	0.15	0.6	0.5	0.2	0.035	3.0
SF3-4.5-CB	0.85	0.15	0.6	0.5	0.2	0.045	3.0

A traditional UHPC was created by utilizing steel fibers and siliceous sand. Steel fibers with an average diameter of 0.2 mm and a length of 13 mm (aspect ratio of 65) were used for the traditional

UHPC. The specific gravity of the fibers was 7.8 and had an ultimate tensile strength of 2000 MPa. A two percent total mixture volume dosage was added to improve compressive strength and durability. The siliceous sand was predominately quartz and was sieved/ground using a disc mill to two separate gradations. The SCM used for the traditional UHPC mixture is SF3 and the HRWR dosage is 4.5%.

A low viscosity epoxy-resin was utilized for the epoxy-resin samples as a representative traditional HFST binder. The epoxy-resin met the specification requirements set out by the SCDOTs HFST supplemental specification for all mentioned properties [65]. Epoxy-resin samples were mixed using the manufacturer recommendations and allowed to cure until the specified test age or at least 28 days. Similarly, an asphalt reference surface was cast by gyratory compactor. The asphalt followed the aggregate and binder contents for a Surface B mixture and was heated to 85±5°C in an oven before being compacted in a gyratory compactor for 100 gyrations under a 600 kPa load at rate of 30 gyrations per minute. Asphalt samples were allowed to oxidize for 28 days to reach a full age state before testing.

5.4.2. Results and Discussion

5.4.2.1. Flowability

The flowability of the six selected UHPC mixes by the modified flow table test is shown in **Figure 5.8**. The designed mixes extend across the recommended workability identified previously from 100-150% flow, which provides a workable UHPC mixture that was easily consolidated without segregating. Segregation is a key concern for UHPC as an HFST, as proper aggregate embedment, fiber dispersion, and the strength would become less reliable [66]. The mixes containing a higher dosage of HRWR on average flowed 17% greater than the lower dosage mix, as HRWR sterically repulses the cement particles resulting in less trapped water. SF1 mixes had the lowest flowability in part due to their higher impurities content, but also due to the aggregate content necessary to match the MA&A curve being greater. The SF2 mixes had intermediate flowability in part due to their slightly lower sand content and 20% silica fume replacement. The most workable of the mixes was SF3, which extended slightly past the recommended range of 150% at 4.5% HRWR dosage. This is in part due to the lower SF content and lower sand content. Overall, this indicates that the UHPC mixes have sufficient flowability for construction. Lastly, while not included in the figure the traditional UHPC mixture had a flowability of 150% hitting the maximum recommended all while having two percent steel fiber addition reducing flowability. The increase in workability associated with switching aggregate sources is a function of aggregate angularity and HRWR attraction.

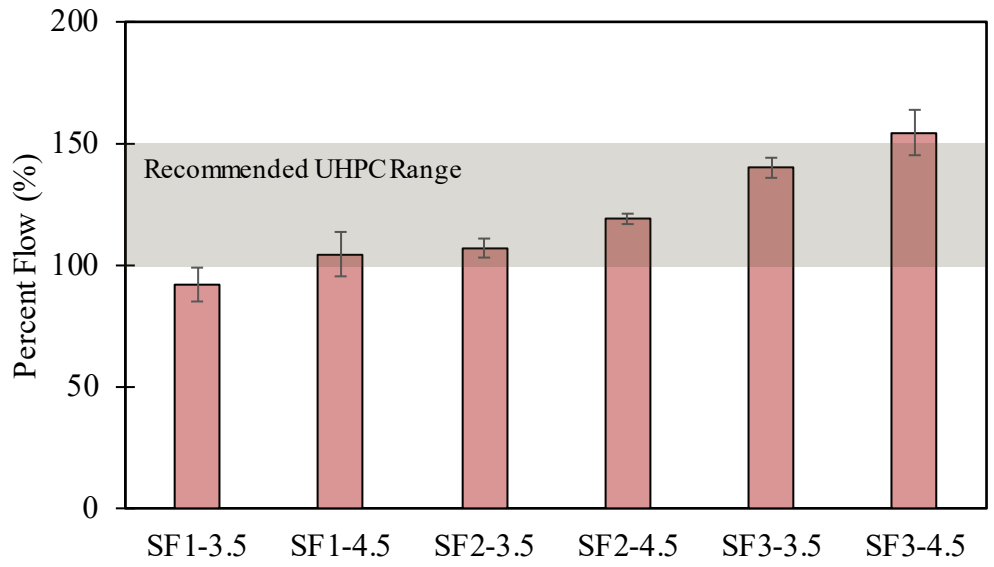


Figure 5.8: Flowability of Selected Mixes using the Modified Flow Table Test

The mixes containing intermixed calcined bauxite had significantly reduced workability and forced testing to switch from the modified flow table test to the regular flow table test (**Figure 5.9**). If the modified flow table test results were displayed each would have received a flow value of 0%. However, the regular flow table test shows these mixes still performed inadequately, not being significantly impacted by the drops of the flow table. The order of sample flows still followed the results of the UHPC samples for the same reasons but were in the order of magnitude of 5-20% flow. This is inadequate for proper consolidation using vibration and indicates that mixes containing high dosages of calcined bauxite would require external compaction to achieve sufficient consolidation.

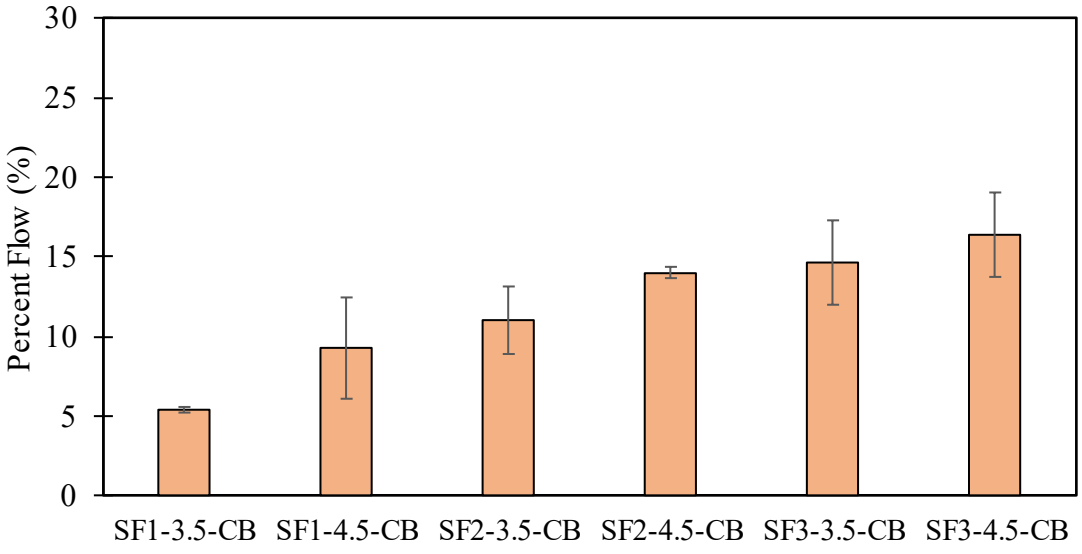


Figure 5.9: Flowability of Intermixed Calcined Bauxite by the Flow Table Test

From these test results the UHPC mixes without calcined bauxite created using the MA&A methodology should have adequate flowabilities for construction. However, the usage of intermixed calcined bauxite results in a significant reduction in the workability of the mixture and could significantly hamper the ability for those samples to be consolidated.

5.4.2.2. Setting Time

The setting time of the UHPC mixes was completed to determine the time required to open to traffic. Samples did not include HFST aggregate as it is anticipated that the inclusion of calcined bauxite would only obfuscate the test results by penetrations encountering solid HFST aggregate particles. The results of the setting time testing are shown in **Figure 5.10**.

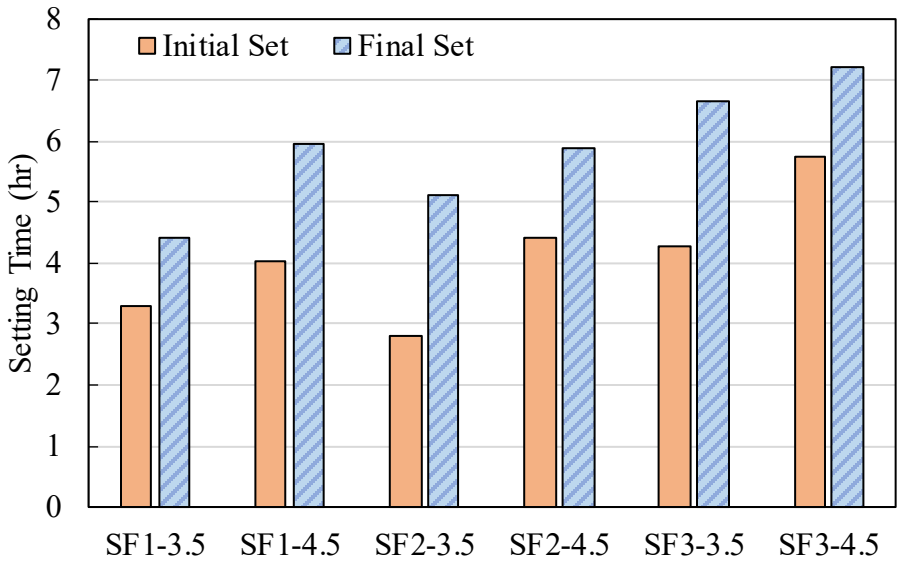


Figure 5.10: Setting Time of Continuously Packed UHPC Mixes

The extended setting time of these samples relative to conventional concrete is due to the high dosage of HRWR. The range of initial setting times was between 2.75 and 5.75 hours, with SF 1 and SF 2 having comparable initial and final setting times, but SF 3 having an extended initial setting time. The final setting times varied from 4.25 to 7.25 hours, in the same order as initial setting time. The time difference between the initial and final set varied between 70 and 140 minutes and was independent of HRWR dosage, with some 3.5% dosages being greater and some 4.5% dosages being greater. The setting time values from this testing is less than typically found for UHPC mixes (but also greater than conventional concrete) without any set accelerating agent and are probably in part due to the usage of a higher specific surface area cement (Type III), allowing for a faster rate of reaction. This accelerated setting time is beneficial for the application of these UHPC mixes for HFST applications, as a faster setting time is preferred, as it allows earlier opening to traffic.

Importantly, these set time values are greater than the setting time of resin-based binders, which are required to have a maximum gel time (equivalent to setting time) of three hours. To match this three-hour threshold, ordinary portland cement systems require either a set accelerator or nanomaterials, which accelerate setting time either physically or chemically depending on type [67,68]. However, using these materials generally increases the difficulty of placing and increases cost.

5.4.2.3. Pull-Off Bond Strength

The pull-off bond strength of the UHPC overlays was completed on concrete substrates at seven and 28-days and on asphalt surfaces at only 28-days. Based upon the FHWA recommendation for HFST binders, a passing test result is one that either exceeds 250 psi or fails in the substrate [8]. Initial testing on asphalt surfaces at seven days indicated low strengths and failures in the substrates, which passed the test but did not provide any useful supporting information to categorize effectiveness.

The pull-off bond strength test results of continuously packed samples are included in **Table 5.4**. This testing indicates that all samples on concrete substrates exceeded the required 250 psi and either exceeded or matched the performance of the epoxy-resin. At seven-days the UHPC samples varied between 96-134% of the epoxy-resin strength (300-425 psi). Whereas at 28-days the samples varied between 74-114% of the epoxy-resin samples strength (275-475 psi). This decrease in the proportion of the UHPC strength to the epoxy-resin's is due to the epoxy-resin refinement of its chain structure, whereas for ordinary portland cement systems the rate of hydration decreased rapidly due to the low water-to-cementitious material ratio.

Testing on the asphalt surfaces for all UHPC overlays experienced failure in the substrate. Asphalt not being chemically adhered provides a weaker bond and fails at significantly lower tensile strengths. However, this failure in the substrate while passing the test procedure does not adequately provide context for compatibility. A key parameter of tensile strength for asphalt overlayed samples is how the overlay fortifies the substrate. For resin-based systems, which often have much lower viscosities, there is a drawdown into the asphalt substrate's void structure, which enhances bond strengths. Other researchers have indicated this is due to the formation of a continuous network structure in the epoxy-resin asphalt region [69]. This is why the 28-day epoxy-resin overlay on an asphalt experienced 197 psi of bond strength. This differs from the cementitious binders, which have higher viscosity and do not penetrate the pore structure as effectively. Instead, UHPC systems form a thicker layer on the surface. As such, while the samples passed the strengths were 30-50% of the epoxy-resin overlay, which is between 64-87 psi.

In turn, these results provide the preliminary observation that epoxy-resin binders are preferrable for asphalt substrates, as they can fortify the overall tensile strength. However, testing on how the epoxy-resin drawdown impacts the long-term roadway coefficient of friction and permeability is needed to confirm that the epoxy-resin does not strongly impact long term safety. For concrete substrates, the results are similar, indicating either epoxy-resin or cementitious binders are acceptable. Epoxy-resin systems have previously been confirmed as acceptable, but cementitious

materials require confirmation that the shrinkage and coefficient of thermal expansions are acceptable.

Table 5.4: Pull-Off Bond Strength Results of UHPC Samples

Sample ID	Concrete (psi)				Asphalt (psi)	
	7-Day	% of Epoxy	28-Day	% of Epoxy	28-Day	% of Epoxy
Epoxy	315	100%	380	100%	197†	100%
Trad. UHPC	432	137%	436	114%	92†	46.7%
SF1-3.5	424	134%	377	99.2%	76†	38.6%
SF1-4.5	415	132%	478	126%	87†	44.1%
SF2-3.5	329	104%	278	73.1%	85†	43.1%
SF2-4.5	303	96.1%	430	113%	75†	38.1%
SF3-3.5	308	97.8%	280	73.7%	64†	32.5%
SF3-4.5	323	103%	342	90.0%	68†	34.5%

†: Failure in the Substrate

After making these initial judgements an assessment was made of how intermixed calcined bauxite influences the pull-off bond strength (**Table 5.5**). The initial assumption being that the calcined bauxite replacing a proportion of the UHPC would decrease the tensile strength. Testing was again completed at seven and 28-days after initial casting on concrete substrates and at 28-days on asphalt substrates.

Testing on the asphalt surfaces with the intermixed samples failed in the substrate but did not provide additional strength as seen by the epoxy-resin. However, testing on the concrete substrates provided mixed results. At seven days all mixes performed worse than the epoxy-resin systems but most still passed the FHWA recommendation, falling between 60-90% of the epoxy-resin tensile strength. The most concerning component being that both SF3 mixes fell below the FHWA recommendation at 231 and 191 psi, respectively. The intermixed calcined bauxite mixes varied between 190-280 psi at seven-days. Where these mixes proved advantageous was when tested at 28 days, where all mixes provided strengths greater than 250 psi. Strengths at 28-days on concrete substrates varied between 350-440 psi. Furthermore, strengths typically exceed that of the epoxy-resin being between 94-133% the strength of the epoxy-resin samples at 28-days. This increase in strength is probably due to the further hydration of the cementitious system due to water absorbed by the calcined bauxite being released. Based upon these results a key area of interest is determining if a different proportion of calcined bauxite could balance the early age tensile strength

achieved by the UHPC systems without calcined bauxite and the later age strength achievable with intermixed calcined bauxite.

Table 5.5: Pull-Off Bond Strength Results of Intermixed Samples

Sample ID	Concrete (psi)				Asphalt (psi)	
	7-Day	% of Epoxy	28-Day	% of Epoxy	28-Day	% of Epoxy
Epoxy*	315	100%	380	100%	197†	100%
Trad. UHPC*	432	137%	436	114%	92†	46.7%
SF1-3.5-CB	252	80.0%	410	108%	73†	37.1%
SF1-4.5-CB	284	90.1%	367	96.6%	77†	39.1%
SF2-3.5-CB	277	87.9%	358	94.2%	87†	44.1%
SF2-4.5-CB	253	90.3%	372	97.9%	73†	37.1%
SF3-3.5-CB	**231**	73.3%	420	133%	99†	50.2%
SF3-4.5-CB	**193**	61.2%	405	107%	65†	33.0%

* Not Intermixed, just included for ease of comparison.

† Failure in the Substrate

5.4.2.4. Slant Shear Bond Strength

The shear bond strength of HFSTs is critical, as hard braking or sliding generates large shear stress, which attempts to separate the overlay from the substrate [5]. Ensuring delamination does not occur is critical as it destroys the overlay. This testing was completed at one, seven, and 28-days after initial casting. Initially, epoxy, UHPC, traditional UHPC, and intermixed calcined bauxite mixes were tested. However, the one-day testing on epoxy-resin systems failed in the substrate at a relatively low strength of 0.32 ksi. In comparison the cementitious samples were failing along the interface at approximately 1.0 ksi at one day. As such, further testing was not conducted on the epoxy-resin and the results were not included in the tables to avoid the false assumption that a higher strength means a better result. The epoxy-resin provided a better shear bond strength than any of the cementitious samples and managed to efficiently distribute those forces to the substrate, causing failure in the substrate (**Figure 5.4**).

Table 5.6 provides the test results for the UHPC samples. This table highlights the one, seven, and 28-day maximum shear stresses before failure. Designations were not made between failure modes, as all samples failed along the interface. For one day testing ultimate slant shear bond strengths varied between 0.7-1.2 ksi, with all samples greatly exceeding the required shear bond strength. At seven days the ultimate slant shear bond strength varied between 1.4-2.2 ksi, again

exceeding the required shear bond strength. Lastly, as a check to see the continued development of ultimate slant shear bond strength testing was completed at 28-days and the strengths varied for the UHPC mixtures from 2-2.7 ksi. These results indicate that UHPC, while not as successful at handling shear loads as the epoxy-resin still provides adequate bond strength, which minimizes the risk of failure on concrete substrates. Importantly, testing on the traditional UHPC samples identified a further increase in bond strength from the inclusion of steel fibers. While one day strengths were not collected to avoid insufficient curing the seven and 28-day results highlight a 52% and 44% increase in bond strength in comparison to the UHPC samples. Steel fibers help to better distribute the loads placed upon the system and further increase the area able to handle the stress concentration along the interface before failure. Previous researchers have already highlighted their effectiveness at increasing ultimate slant shear bond strengths [71].

Table 5.6: Slant Shear Bond Strength Results for UHPC Samples

Sample ID	Concrete (ksi)					
	1-Day	Std. Dev.	7-Day	Std. Dev.	28-Day	Std. Dev.
Trad. UHPC	---	---	2.7	0.2	3.2	0.03
SF1-3.5	0.7	0.12	1.5	0.2	2.0	0.25
SF1-4.5	1.0	0.09	1.5	0.1	2.7	0.19
SF2-3.5	1.2	0.17	2.0	0.1	2.0	0.29
SF2-4.5	1.1	0.10	2.2	0.2	2.3	0.17
SF3-3.5	0.9	0.16	1.4	0.1	2.2	0.27
SF3-4.5	1.0	0.12	1.8	0.2	2.2	0.30

In addition to the testing completed on UHPC samples intermixed calcined bauxite samples were also tested at one, seven, and 28-days. The results of which are included in **Table 5.7**. One-day testing on the intermixed samples varied between 0.39-0.61 ksi, with two sets of samples falling below the threshold imposed for passing. The seven-day testing on intermixed samples varied between 0.90-1.38 ksi, with all samples exceeding the specified minimum. Lastly, the 28-day test results varied between 1.83-2.00 ksi of bond strength. These results highlight that the bond strength of intermixed calcined bauxite samples is only insufficient at early ages and quickly develops. Based upon this failure it is anticipated that intermixing calcined bauxite at a different replacement level could result in sufficient performance.

Table 5.7: Slant Shear Bond Strength Results for Intermixed Samples

Sample ID	Concrete (ksi)					
	1-Day	Std. Dev.	7-Day	Std. Dev.	28-Day	Std. Dev.
Trad. UHPC*	---	---	2.66	0.24	3.24	0.03
SF1-3.5-CB	0.55	0.04	1.02	0.17	1.93	0.20
SF1-4.5-CB	**0.42**	0.05	0.94	0.15	1.83	0.04
SF2-3.5-CB	0.57	0.04	0.90	0.13	1.84	0.25
SF2-4.5-CB	0.53	0.07	1.22	0.19	2.00	0.06
SF3-3.5-CB	0.61	0.05	1.38	0.18	1.93	0.09
SF3-4.5-CB	**0.39**	0.08	1.36	0.14	2.00	0.06

*Not Intermixed, included for ease of comparison.

When comparing the UHPC and intermixed calcined bauxite samples, a significant reduction in performance is noted at earlier ages. The intermixed calcined bauxite samples were only 40-70% that of the UHPC samples at one day. This improves at seven days when the range converts to 45-96% and becomes even more similar at 28-days with samples varying from 69-97% of their UHPC counterparts. Further testing on intermixed calcined bauxite samples at different replacement rates may highlight the ability to achieve more comparable results, as the inherent voids in the system are replaced with epoxy-resin, which boost bond strength.

5.4.2.5. Abrasion Resistance

Abrasion resistance results were taken for the UHPC mixes, the traditional UHPC, intermixed UHPC, and substrates. Unfortunately, the epoxy-resin was not included as a tested surface due to an incompatibility with the testing equipment. However, based upon the general knowledge base of epoxy-resin binders it is anticipated that they would have performed better than the UHPC and concrete substrates with minimal volume loss [72]. Previous research has highlighted that one of the main concerns for HFSTs is the HFST aggregate wearing away while the epoxy-resin binder stays in place resulting in lower coefficient of frictions when compared to initial conditions [73].

Abrasion resistance highlights the ability to handle repeated loading without seeing significant surface loss. For HFSTs this is a critical parameter, as low abrasion resistance would necessitate high layer thicknesses to account for the loss of surface material. Since this test was modified to operate with equipment limitations, current standard specifications for abrasion resistance are not applicable. Instead, the test results operate as a relative comparison tool.

The abrasion resistance test results for the UHPC samples are included in **Table 5.8**. All samples demonstrated linear abrasion loss, so only the 20-minute results are discussed to accentuate the differences. Testing at the lower force rate resulted in volume losses at 20 minutes of 6.6 cm^3 for the asphalt substrate surface, 3.0 cm^3 for the concrete substrate surface, and 2.8 cm^3 for the traditional UHPC surface. Whereas the UHPC samples' volume loss varied between 3.6-5.9 cm^3 at 20 minutes. This places them firmly between the concrete and asphalt substrates. It is anticipated that the lesser abrasion resistance in comparison to the concrete substrate is in large part due to the usage of manufactured granite fine aggregate, which has a significantly reduced strength when compared to siliceous sand fine aggregate used for the concrete substrate. This finding is reinforced by the traditional UHPC experiencing a lower volume loss than the concrete substrate, even though the cementitious matrix matches that of the UHPC samples. In essence, this may highlight that more traffic is able to pass over UHPC with high quality fine aggregate, which abrades from the surface at a slower rate. However, the short lifetime (7-10 years) of HFSTs may make this benefit a moot point. Further testing on simulated traffic is needed to better understand this performance.

Table 5.8: Abrasion Resistance of UHPC Samples

Volume Loss (cm^3)					
	Time (min)				
Sample ID	0	5	10	15	20
SF1-3.5	0.0	0.7	1.7	2.6	3.6
SF1-4.5	0.0	1.2	2.2	3.5	4.5
SF2-3.5	0.0	1.4	2.8	4.1	5.6
SF2-4.5	0.0	1.1	2.5	3.9	5.0
SF3-3.5	0.0	1.5	2.9	4.9	5.9
SF3-4.5	0.0	0.7	1.5	2.4	3.6
Trad. UHPC	0.0	0.4	1.3	2.0	2.8
Concrete	0.0	0.9	1.8	2.5	3.0
Asphalt	0.0	1.4	3.5	5.0	6.6

Testing was also completed on intermixed calcined bauxite samples to identify how their inclusion influenced the abrasion resistance of the UHPC (**Table 5.9**). Ultimately, the test results supported this hypothesis with the intermixed samples varying from 1.4-2.6 cm^3 of volume loss. In comparison to the other surfaces this is less than half of the asphalt abrasion loss and is less than the traditional UHPC and concrete substrates, which were previously more than the UHPC samples. This may thereby indicate that abrasion resistance of the underlying cementitious material

is of minor consequence, as the calcined bauxite can elevate its performance. Especially considering that the calcined bauxite HFST aggregate extends from the surface of the UHPC and protects the UHPC from some abrading action.

Table 5.9: Abrasion Resistance of Intermixed Calcined Bauxite Samples

Volume Loss (cm^3)					
	Time (min)				
Sample ID	0	5	10	15	20
SF1-3.5-CB	0.0	0.4	0.7	1.2	1.5
SF1-4.5-CB	0.0	0.4	1.0	1.4	2.0
SF2-3.5-CB	0.0	0.4	0.6	1.1	1.4
SF2-4.5-CB	0.0	0.8	1.3	1.6	1.9
SF3-3.5-CB	0.0	0.8	1.6	2.2	2.8
SF3-4.5-CB	0.0	0.6	1.4	2.1	2.6
Trad. UHPC	0.0	0.4	1.3	2.0	2.8
Concrete	0.0	0.9	1.8	2.5	3.0
Asphalt	0.0	1.4	3.5	5.0	6.6

5.4.2.6. Compressive Strength

The compressive strength of the UHPC, traditional UHPC, and intermixed calcined bauxite samples were taken on 2" cubes to determine if sufficient strength gain was achieved at early ages and to determine if the later age strengths justified the designation of UHPC. The early age performance follows part of the compressive strength requirements set out in the AASHTO MP 41 specification, expecting to achieve the 5000 psi at seven days as required for resin systems [74]. The AASHTO MP 41 specification also requires 1000 psi of compressive strength at 3 hours, but this is inside of the set time for cementitious systems and falls out of the range of traffic opening and is not monitored. The last requirement is set out by ASTM C1856-17, the ASTM standard practice for testing UHPC, which requires a compressive strength of at least 17 ksi for classification as UHPC. This designation is not a performance requirement, but a classification requirement.

Testing on the UHPC samples focused on one, seven, and 28-day strengths (**Figure 5.11**). At one day all samples gained sufficient strength to pass the seven-day requirement of 5000 psi, with a range of 6.9-9.5 ksi at one day. The seven-day strengths further increased, ranging from 11.0-11.9 ksi, which doubled the requirements in place for HFST resin systems. From this information and

as expected these UHPCs should handle any traffic load placed upon it with minimal risk of failure. Lastly, the compressive strengths at 28-days ranged from 12.3-15.2 ksi, which fell below the specification for UHPCs. In the authors' opinion, designation as UHPC is still appropriate due to the utilization of a UHPC design methodology, compressive strengths are of secondary importance for this use case, and the critical parameter bond strength is superior to traditional concretes.

Furthermore, testing on the traditional UHPC samples identified compressive strengths at one day of 6.9 ksi, seven days of 14.8 ksi, and 28-day of 17.5 ksi which strengthens the claim that the UHPC design process was principally impacted not by the quality of the cementitious binder, but by the fine aggregate and fiber inclusion. As such, calling the other samples UHPC still appears appropriate.

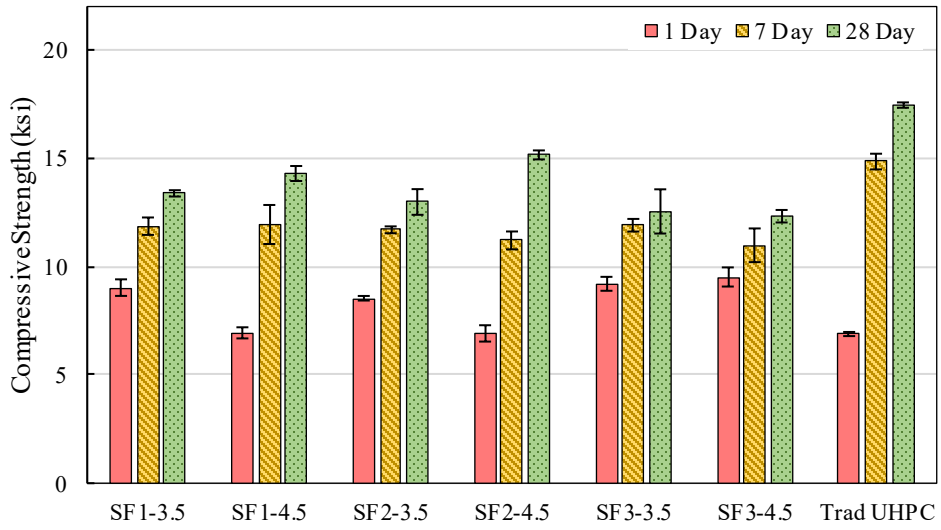


Figure 5.11: Compressive Strength of UHPC Samples

Figure 5.12 displays the results for compressive strength testing completed on intermixed calcined bauxite samples. As demonstrated by previous testing on slant-shear and pull-off bond strength testing, the early age strength of samples containing calcined bauxite was less than their UHPC counterparts. However, when tested in compression one day strengths for intermixed calcined bauxite samples varied from 7.2-8.4 ksi or alternatively were 76-110% the strength of their UHPC counterpart. This similarity in compressive strength between intermixed and UHPC samples is due to compressive loadings allowing the calcined bauxite to benefit the matrix due to its strong inherent compressive strength. Calcined bauxite's inherent strength further bolstered the mixes at seven days and at 28-days. Seven-day compressive strengths for intermixed calcined bauxite samples varied from 11.3-13.0 ksi and were 94-111% the strength of their UHPC counterparts. The 28-day compressive strength results varied from 16.1-18.6 ksi, with three of the six tested samples exceeding the 17 ksi threshold for classification as UHPC. Furthermore, these samples were 120-140% greater than their UHPC counterparts, which is interesting considering the porosity left due to the inter particle spaces due to the high calcined bauxite content. Based on this

strength increase it is possible that decreasing the calcined bauxite content to a proportion that does not exhibit additional porosity could lead to further increases in compressive strength, but further testing is needed to confirm this hypothesis.

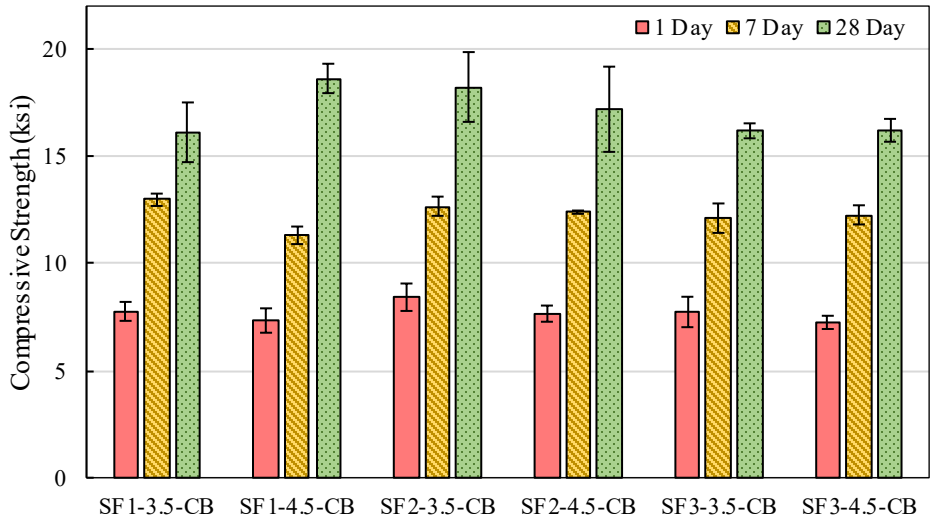


Figure 5.12: Compressive Strength of Intermixed Calcined Bauxite Samples

5.4.2.7. Drying Shrinkage

Drying shrinkage is designated as the reduction in volume that occurs due to negative capillary pore pressure, caused by the evaporation of capillary water [75,76]. Drying shrinkage is the principal form of shrinkage on mature concrete samples and is unavoidable. Shrinkage by itself is not a significant factor for UHPC and concrete in general. Concrete typically shrinks approximately 0.06% of their total length due to the evaporation of pore water [76]. Over a hundred-foot span this would equate to an approximately 0.75-inch reduction in the total length. The concern for cementitious systems is the lack of tensile strain capacity, as restrained shrinkage induces tensile stresses that result in cracking and subsequent deterioration of the surface and ride quality [77]. Typically, the tensile strain capacity for non-fiber reinforced concrete is approximately 0.02% (200 microstrain) [76,78]. However, for traditional UHPCs this value is greater often greater than 1% but relies upon the ductility granted by fibers for the increase and is largely post peak behavior [79]. This section identifies the drying shrinkage of UHPC-based HFSTs and determines if further mitigation techniques or fibers are needed.

Figure 5.13 displays the results of the six tested UHPC samples to determine the magnitude of their drying shrinkage. Testing found that samples had little variation in drying shrinkage, which is expected as all were optimized using particle packing methodologies, which mitigate the total void content. 25-day drying shrinkage theoretical strains varied from 600-800 µstrain. This range places the shrinkage caused by the usage of UHPC firmly above the threshold of tensile strain

capacity for ordinary portland cement systems. To mitigate this risk further testing is needed to mitigate the total shrinkage of these concretes.

Several strategies are employable to solve this problem. The simplest strategy is that the inclusion of the intermixed calcined bauxite will reduce shrinkage via the filler effect, for CB=3.0 mixtures a 50% reduction in shrinkage is expected as calcined bauxite occupies 50% of the total mixture volume. Additionally, mitigation techniques such as the inclusion of shrinkage reducing admixtures could decrease the shrinkage by decreasing the capillary pore pressure by changing the surface tension at the interfacial areas. Lastly, the inclusion of fibers could increase the tensile strain capacity of the UHPC samples and eliminate the concern of large cracks forming.

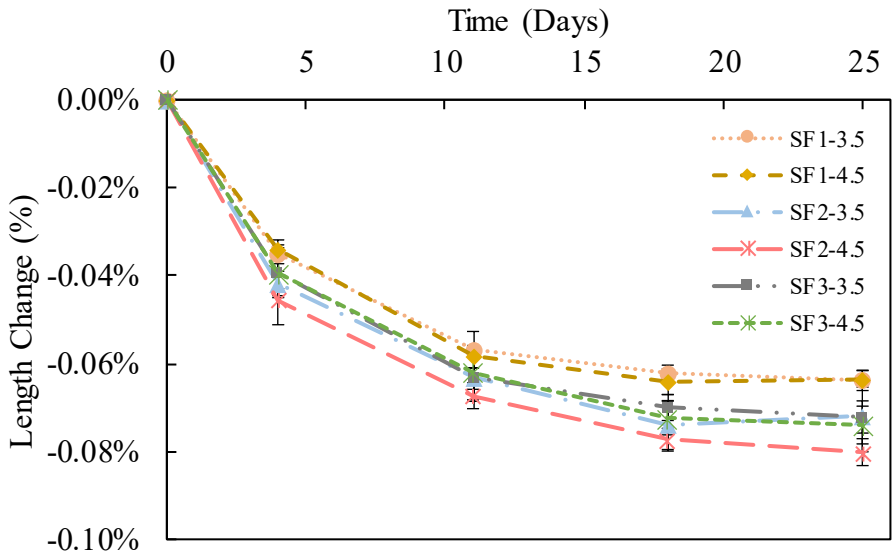


Figure 5.13: Drying Shrinkage of UHPC Samples

5.4.2.8. Autogenous Shrinkage

Autogenous shrinkage is an early age shrinkage caused by the consumption of water during the hydration of cement. Autogenous shrinkage is an important effect to monitor in UHPC because of the low water-to-cementitious material ratio and the high cementitious material volume. Measurements of autogenous shrinkage are undertaken after the final set has occurred, as shrinkage occurring before set does not result in stress buildup as it is allowed to freely deform. As demonstrated in **Figure 5.14** the onset of measurements occurring after the final set resulted in an ordering where the samples with earlier final sets had greater shrinkage and later sets had lesser shrinkage. Theoretical shrinkage strains varied from 400-800 microstrain, which again exceeded the thresholds outlined for tensile strain capacity in the drying shrinkage section. To mitigate the autogenous shrinkage of these UHPCs may require the inclusion of a greater proportion of fillers or a shrinkage reducing admixture.

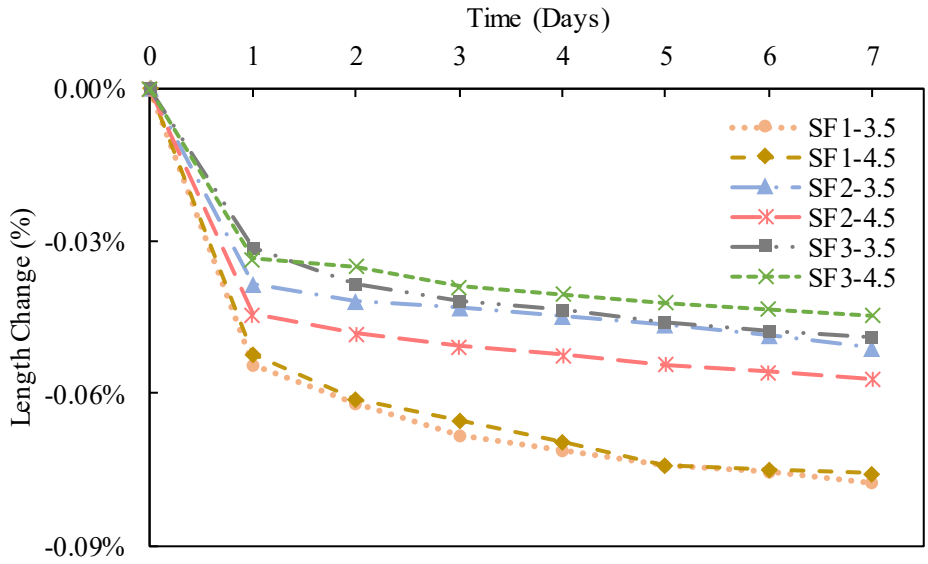


Figure 5.14: Autogenous Shrinkage of UHPC Samples

5.4.2.9. Coefficient of Thermal Expansion

The coefficient of thermal expansion (COTE) quantifies the degree of length change caused by an increase or decrease in temperature. When materials have equivalent COTE, the materials shrink/expand together, and no differential stresses are generated. However, when the materials have differing COTEs, a differential stress is generated, and curling may occur on the pavement surface [80]. Therefore, it is critical to ensure that materials with low tensile strain capacity have similar COTEs to the underlying substrate.

Figure 5.15 and **Figure 5.16** highlight the results of the COTE testing. Minimal variability was observed between the six UHPC samples, which had COTE between 6.5 - 7.2*10^{-6} in/in/°F. These values are 34% of the asphalt substrate and 122% of the concrete substrate. In effect this means that during a ±50°F shift in temperature a differential shrinkage of -0.06% in the asphalt substrates develops compared to -0.006% for concrete substrates. Highlighting the suitability of UHPC-based HFSTs to concrete substrates but drawing additional questions for UHPC-based HFSTs over asphalt substrates as the strain exceeds the expected tensile capacity of the UHPC. To correct for thermal incompatibility would require the inclusion of fibers, as it would increase the tensile strain capacity. However, future field trials/experimental investigations may deem this as a secondary issue as ultra-thin white toppings and bonded concrete overlays have proven sufficiently durable under similar conditions.

In comparison, the epoxy-resin currently used to create HFST surfaces had a COTE of 1.1*10^{-4} in/in/°F, which is 536% greater than the asphalt substrates and 1918% greater than the concrete substrates COTE. This in turn results in a significantly larger differential shrinkage/expansion. During a ±50°F shift in temperature an asphalt substrate would result in a differential shrinkage of -0.440% and the concrete substrate would experience a differential shrinkage of -0.513%.

However, this is not to say that epoxy-resin systems are likely to crack due to differential expansion, as the tensile stress capacity of epoxy-resin (10%) is significantly greater than cementitious systems.

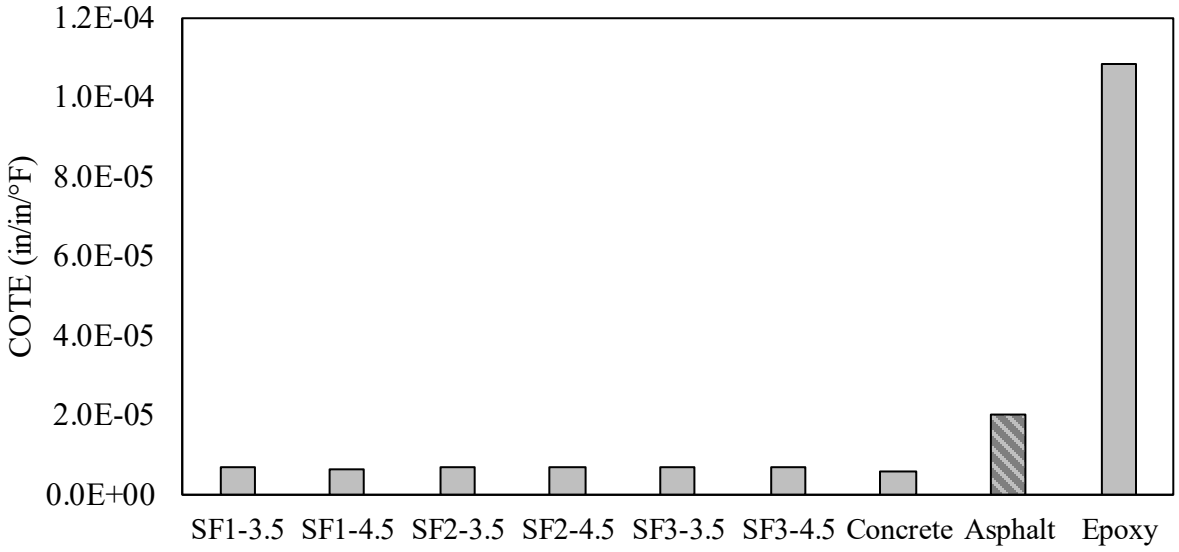


Figure 5.15: COTE Results of UHPC Samples Full Scale

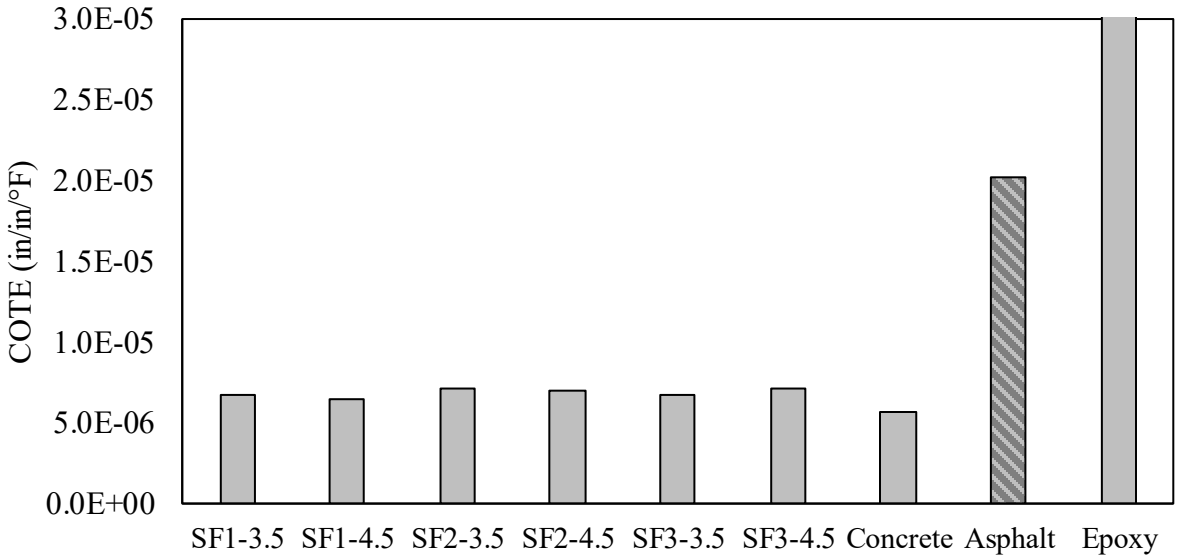


Figure 5.16: COTE Results of UHPC Samples Reduced Scale

5.4.3. Conclusions

Based upon the experimental results of this phase several conclusions are drawn:

1. The preliminary performance of UHPC-based HFST provides adequate mechanical performance on both asphalt and concrete substrates. The bond strength and compressive strength all match or exceed guidelines set in place for equivalent systems.
2. The performance of epoxy-resin HFSTs on asphalt overlays exceeds that of cementitious systems, even though the UHPC was still adequate. Key concerns for UHPC on asphalt surfaces include lesser pull-off bond strength and low compatibility of coefficient of thermal expansion.
3. The performance of UHPC with intermixed calcined bauxite varied with increased compressive strength and lower variability later age bond strength as positives and reduced workability and lower initial bond strength as negatives.
4. The shrinkage of UHPC is the current limiting factor for the introduction of UHPC-based HFSTs and must be reduced to a value less than -0.02% to ensure that cracking does not occur and accelerate deterioration.

5.5. Phase 2: Discrete Particle Packing of Intermixed Calcined Bauxite UHPC

5.5.1. Background and Mixture Proportions

After determining that intermixing calcined bauxite could improve the performance of the UHPC both in terms of compressive strength, abrasion resistance, and pull-off bond strength of UHPC-based HFSTs. It then became necessary to investigate how variable calcined bauxite contents would influence the performance of UHPC-based HFSTs. However, these UHPC mixtures could not be designed using the existing continuous particle packing method, due to the high concentration of particles between 2.36 and 1.18mm making continuous methodologies ineffective (**Figure 5.17**). As shown, to match the initial increased slope caused by the inclusion of calcined bauxite a distribution exponent of 0.9 is required. To match this necessary slope with the other materials would require decreasing their material to cementitious material ratio to 0.01 or less. Secondarily, if the distribution factor remains at 0.25 an offset is formed between the real and ideal curves, which would only be corrected by including less fine material necessary to fill the voids between particles and react through pozzolanic reaction.

Based upon the failure of continuous methodologies at optimizing the HFST aggregate fraction, it is thereby necessary to implement a discrete packing methodology to determine the appropriate dosage of calcined bauxite. Discrete packing methodologies create well packed concretes by experimentally modifying each variable and measuring its density, solids concentration, and void concentration. However, the solids and void concentrations are the more important factors as they neglect the impact of component density. The specifics of how these techniques are completed and analyzed are included in the methods and results sections, respectively.

Since the powder fraction has previously been optimized using a continuous packing methodology the cement, silica fume, sand, pond fines, water, and HRWR to CM ratios are held constant for this study. These ratios were chosen based upon the worst performing mixture (SF3-4.5) from that previous study to determine if HFST aggregate optimization would increase the likelihood of a

continuously packed mixture to move from insufficient strength to sufficient strength. Furthermore, the calcined bauxite to cementitious materials ratio varied between 0.0 and 3.0 for most of the testing completed, however for density testing an additional sample at a CB/CM of 4.0 was tested to better characterize the change after the optimal dosage of calcined bauxite. The mixture proportions tested are shown in **Table 5.10**. Lastly, comparisons were made to the epoxy-resin, concrete, and asphalt as previously discussed in phase one.

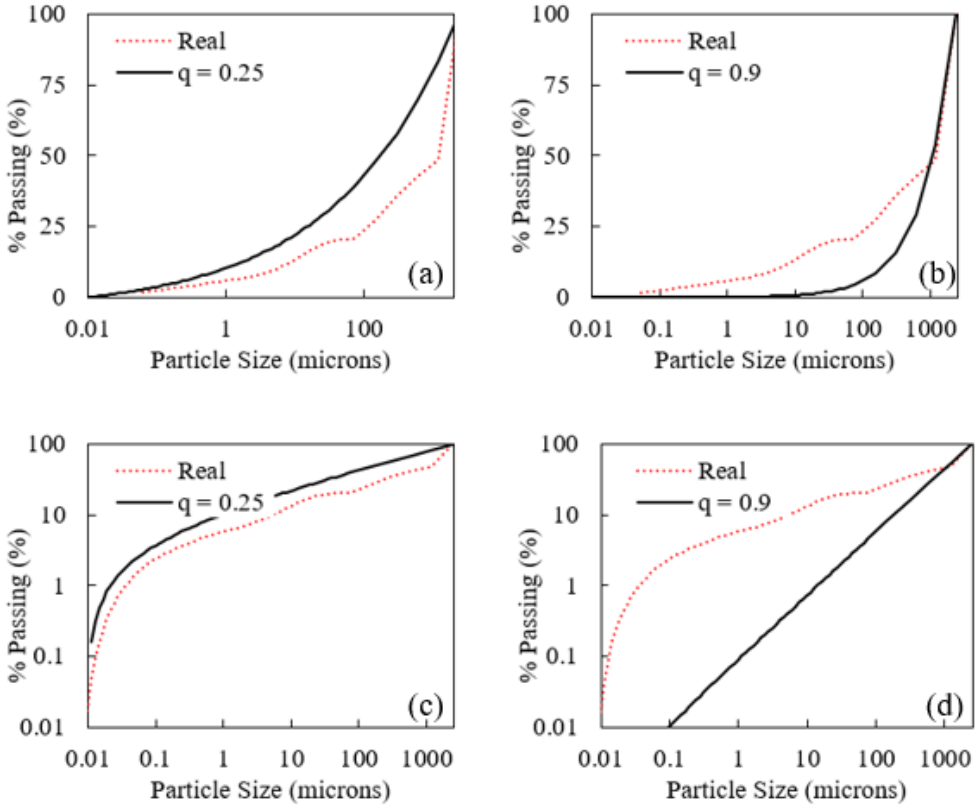


Figure 5.17: The MA&A Packing with Calcined Bauxite for (a, c) q = 0.25 and (b, d) q = 0.9

Table 5.10: Mixture Proportions for Discrete Packing Testing

Sample ID	C/CM (-)	SF/CM (-)	S/CM (-)	PF/CM (-)	W/CM (-)	HRWR/CM (-)	CB/CM (-)
CB-0.0	0.80	0.20	0.7	0.4	0.2	0.045	0.0
CB-1.0	0.80	0.20	0.7	0.4	0.2	0.045	1.0
CB-1.5	0.80	0.20	0.7	0.4	0.2	0.045	1.5

CB-2.0	0.80	0.20	0.7	0.4	0.2	0.045	2.0
CB-2.5	0.80	0.20	0.7	0.4	0.2	0.045	2.5
CB-3.0	0.80	0.20	0.7	0.4	0.2	0.045	3.0
CB-4.0*	0.80	0.20	0.7	0.4	0.2	0.045	4.0

* Only included in density testing

5.5.2. Results and Discussion

5.5.2.1. Flowability

The flowability of UHPCs containing variable CB contents varied considerably, as expected for materials with exceptionally different aggregate contents (**Figure 5.18**). The lower dosages of CB demonstrate exceptional fluidity with 157%, 124%, and 94% flows for CB/CM ratios of 0.0, 1.0, and 1.5, respectively. These intermixed calcined bauxite UHPCs are effectively conventional UHPCs with a low amount of coarse aggregate that has excess paste to separate particles. However, above CB/CM 1.5 a significant decrease in the flowability is observed with CB/CM ratio of 2.0 having a flow of 47% and CB/CM ratio of 2.5 and 3.0 having a flow of approximately 0%. This rapid decrease in fluidity is a function of the increased aggregate content and a decrease in the interaggregate paste thickness [81]. While previously at lower contents the calcined bauxite particles had a large paste layer to interact with, the higher contents have less excess paste and begin to interlock with each other [82]. This is most exemplified by the CB/CM ratio of 3.0 mix, which has sufficient paste to coat the particle surfaces, but does not have the excess paste necessary to fill all the voids left in the matrix. As such, the UHPC exhibits zero flow under the modified flow table test, demonstrating the minimally acceptable cementitious material content.

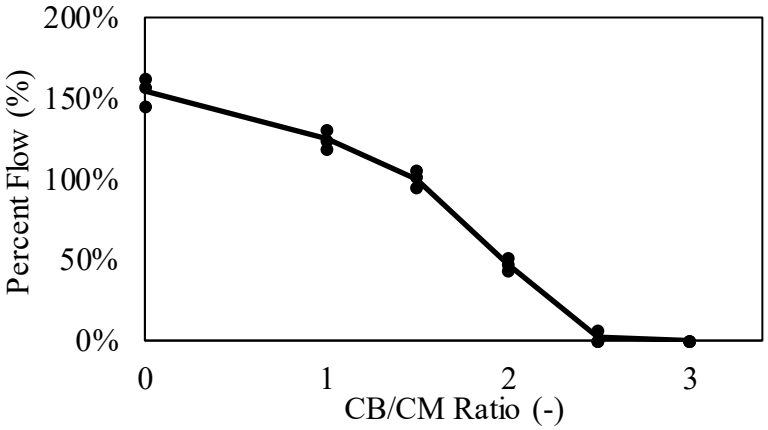


Figure 5.18: Influence of CB/CM Ratio on Flowability

5.5.2.2. Wet Density

The packing density of the UHPC with varying CB/CM ratios was tested in both the fresh and solids states to determine the optimal dosage for maximizing the packing density. This consisted of determining the solids concentration, void concentration, density, and air content. As the CB/CM ratio of 3.0 was the beginning of the transition from a higher packing density to lower an additional sample with a CB/CM was tested at 4.0 for this subsection.

The fresh packing density is shown in **Figure 5.19**. **Figure 5.19a** displays the solids concentrations of these mixes. Samples with CB/CM ratios between 0-3 all exhibited solids concentrations greater than 0.90, which is expected as they were already optimized using a continuous packing methodology. However, when calcined bauxite was intermixed the solids at ratios between 1.0-3.0, the solids concentration was closer to 0.95 indicating a better packed matrix. The packing density increased up to a CB/CM ratio of 2.5, after which it began to decrease at a CB/CM ratio of 3.0 and even more rapidly decreased at a CB/CM ratio of 4.0 where the UHPC content was only able to coat the surface of the aggregate with minimal excess paste to fill interparticle void spaces. As such, it is ultimately evident that optimizing the dosage of CB is primarily determined based upon finding sufficient paste remains to fill the interparticle void spaces. The exact opposite trend was observed for the void ratio content, which is directly tied to solids concentration. With increasing CB content, the void content decreased, as the voids caused by the paste were minimized up to a ratio of 3.0.

Importantly, the density of these mixes continued to increase past the point of decreasing solids concentration. This is predominately due to the density of calcined bauxite being greater than the other components, which thereby meant that any increase in calcined bauxite content would increase the density. This makes utilization of density as a proxy for quality of varying the calcined bauxite content ineffective and justifies the usage of the void and solids concentration. If maximizing density was utilized as the criteria for determining the optimum calcined bauxite content, then excess voids would be included in the system.

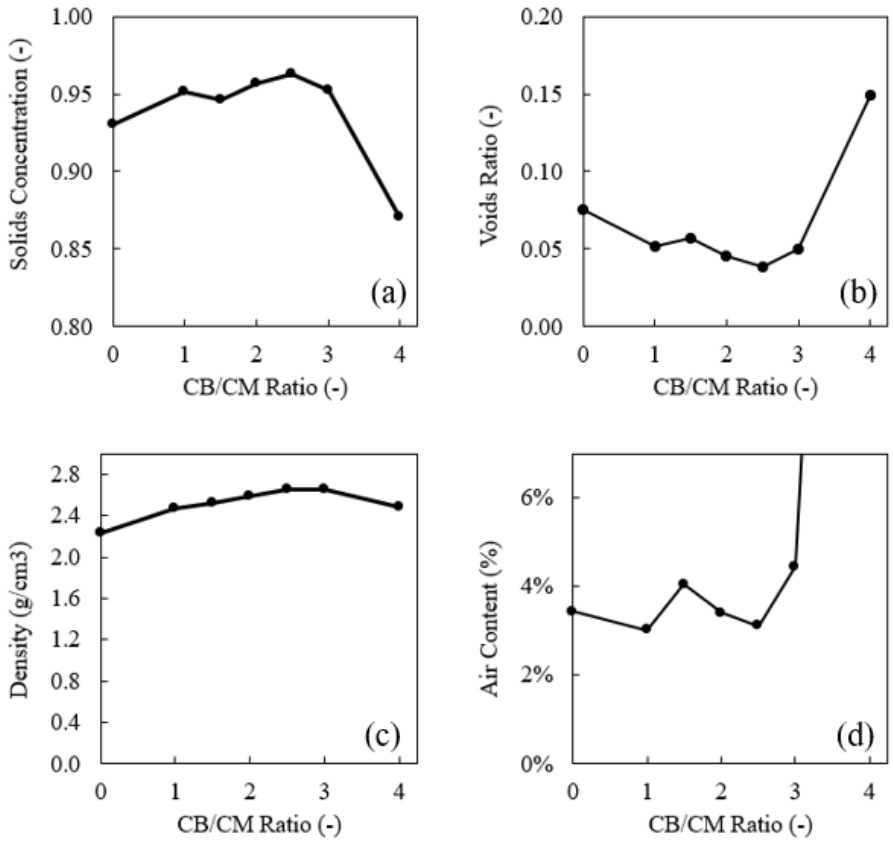


Figure 5.19: Influence of CB Content on Wet (a) Solids Concentration, (b) Voids Ratio, (c) Wet Density, and (d) Air Content

5.5.2.3. Dry Density

In conjunction with testing the wet density the dry density was also tested after seven days of curing. This was primarily conducted to determine if curing and setting would influence the void structure of these samples. Hydration products occupy a smaller volume than the initial unhydrated phases, which brought the possibility of increasing the void content at lower CB content levels and making the higher dosages more appealing.

The results of the dry density testing are displayed in **Figure 5.20**. Based upon the test results for solids concentration appears that the difference between the dry and wet packing densities is minimal. The solids concentration is still maximized at a CB content of 2.5. Furthermore, the solids concentration for the dry densities maximized at 0.956 as opposed to 0.963. The primary observations from this test are the same as those of the previous section. The inclusion of intermixed calcined bauxite had the least concentration of voids and highest solids concentration at a CB content of 2.5. This testing again highlights the importance of not using density as the measure of quality, as density continues to increase after the optimal dosage.

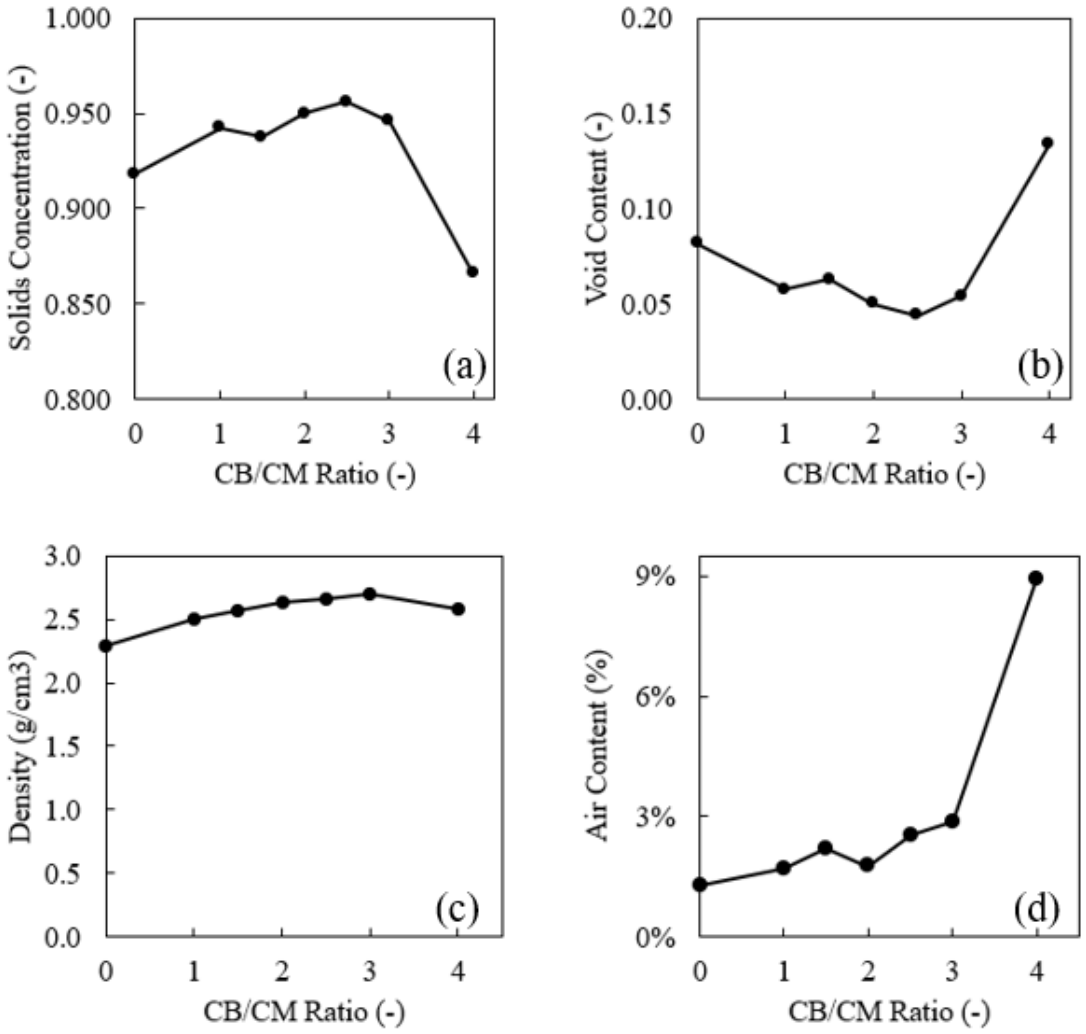


Figure 5.20: Influence of CB Content on Dry (a) Solids Concentration (b) Voids Content (c) Density (d) Air Content

5.5.2.4. Pull-Off Bond Strength

The pull-off bond strength of the varying calcined bauxite content from 0.0 to 3.0 were tested as overlays on concrete substrates at seven and 28-days (**Figure 5.21**). Based upon the FHWA specification for HFST binders a passing test result is one that either exceeds 250 psi or fails in the substrate [8]. Testing indicated at seven days found that samples with CB/CM ratios of 0.0,1.0,1.5,2.0, and 2.5 (borderline at 252 psi) all exceeded that value and would have passed certification. A calcined bauxite ratio of 3.0 on the other hand only achieved pull-off bond strength at seven days of 193 psi, which is below the required bond strength and would not have passed certification. The general trend for tensile bond strength is a slight increase when increased from 0.0 to 1.0, likely in response to additional hydration due to the inclusion of water to account for calcined bauxite absorption and then a gradual decrease in pull-off bond strength from 1.0 to 3.0.

The response at 28-days is similar but has some key differences. For starters, all samples exceeded the required 250 psi of pull-off bond strength at 28-days with strengths varying from 300-400 psi. The same general trends are also first observed with only minor increases in pull-off bond strength for CB/CM ratios of 0.0, 1.0, 1.5, and 2.0. However, after that point a noticeable increase in bond strength from 7 to 28-days is observed. This increase in part may be due to the porosity of these systems, which allows water to permeate into the pore structure and promote further hydration.

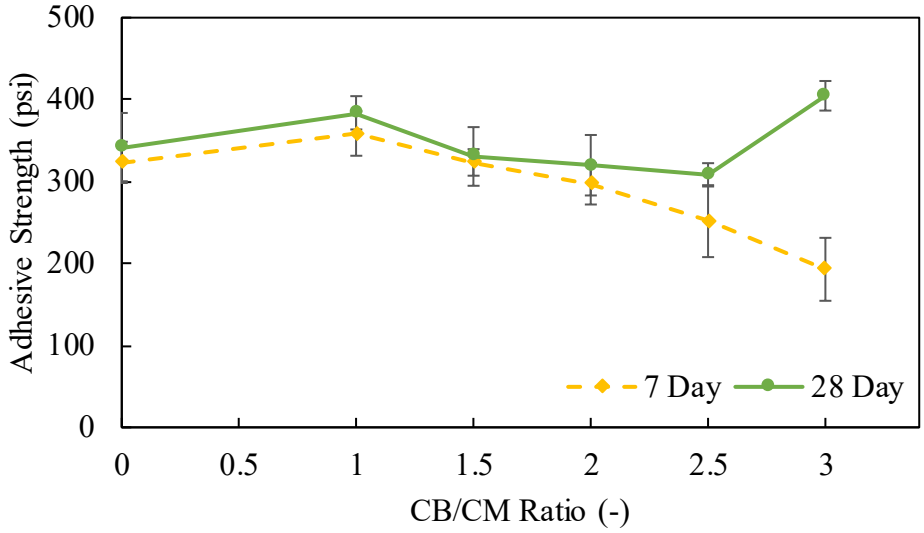


Figure 5.21: Influence of CB Content on Pull-Off Bond Strength

Based upon these results a clear decrease in performance is observed from the inclusion of higher dosages of calcined bauxite. An initial increase in performance is observed at lower CB contents, either as a function of additional mix water from the absorption correction or variability of the test. This decrease is because aggregate particles do not adhere to the surface and as such do not provide additional bond strength. By including more HFST aggregate, the total surface that is being strongly bonded decreases and as a result the ultimate bond strength decrease.

5.5.2.5. Slant Shear Bond Strength

Slant shear testing was completed on concrete substrates at one, seven, and 28-days of curing (**Figure 5.22**). The slant shear bond strength of HFSTs is critical, as hard braking or sliding generates large shear stress, which attempts to separate the overlay from the substrate [5]. Ensuring delamination does not occur is critical as it destroys the overlay. Testing on slant shear varied from CB contents of 0.0 to 3.0.

To determine if a cementitious systems break was sufficient for exposure conditions the general guidelines provided in ASTM C928-20 were utilized. ASTM C928-20 is the standard specification for rapid-hardening cementitious materials for concrete repairs and determines if a roadway patching material is viable for exposure conditions. Since these patches are placed in locations already prone to failure, a more conservative recommendation is expected. This standard sets out

a bond strength requirement of at least 1000 psi at one day and 1500 psi at seven days. Converting these values to the shear component of that bond strength using **Equation 5.3** sets the minimum ultimate slant shear bond strength at one day to 450 psi and at seven days to 650 psi [63]. The ultimate slant shear bond strength is used rather than the bond strength, as it is dependent on the angle of the cut relative to loading, whereas the ultimate slant shear bond strength already accounts for the angle.

The one-day testing on slant shear bond strength generally exceeded the minimum one-day threshold of 450 psi and the seven-day threshold of 650 psi, except for the 3.0 dosage which had an average slant shear bond strength of 390 psi. In contrast the highest bond strength was exhibited by CB/CM content of 2.0, which exhibited a slant shear bond strength of 1471 psi at one day. Importantly, after that dosage the slant shear bond strength rapidly decreased in part due to the reduction in excess paste resulting in a larger relative volume of ITZ. In comparison the one-day value of no calcined bauxite was 956 psi, which while exceptional is far less than the 2.0 slant shear bond strength. This increase is more than likely due to mechanical interlock and load transfer caused by including the calcined bauxite, which are extremely hard and durable. As generally expected, all one-day samples broke along with the overlay interface.

Furthermore, testing at seven-days exhibited a similar trend of calcined bauxite increasing the slant shear bond strength, but the maximum value occurred at a dosage of 1.0, which 2180 psi of slant shear bond strength. At seven-days a plateau existed where CB 1.0-2.0 were of similar strength and after which a significant decrease exists. This is believed to occur as mentioned previously due to the inclusion of voids. As expected, all seven-day samples broke along the overlay interface.

Finally, the 28-day tests importantly exhibited failures in the substrate rather than only along the interface. The samples for CB/CM of 1.0 and 1.5 failed in the substrate at a strength not much greater than the seven-day values. This makes observing how much the bond increased between that period difficult, but when failure occurs in the substrate the concern for the overlay switches from the bond interface to the substrate, an unlikely and therefore preferred outcome. As such, this demonstrates an important finding, as these bonds at later ages can handle substantial shear loads.

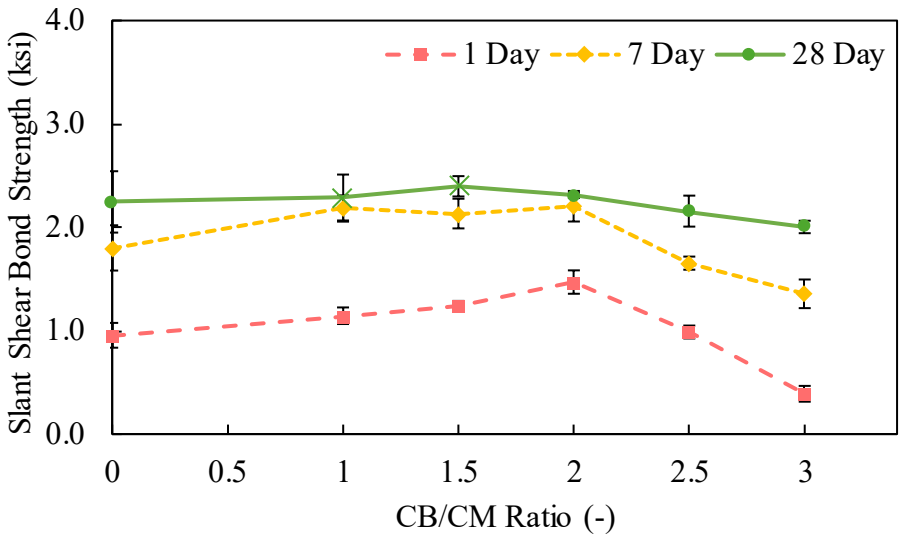


Figure 5.22: Influence of CB Content on Slant shear bond strength

5.5.2.6. Compressive Strength

The compressive strength of intermixed calcined bauxite samples was observed to determine if these samples could classify under existing UHPC thresholds as well as to observe how higher calcined bauxite contents influence the compressive strength of the samples. Compressive strength is the primary mechanical property positively influenced by the inclusion of calcined bauxite, as the aggregates inherent strength and takes the brunt of the load. ASTM C1856-17, the ASTM standard practice for testing UHPC, requires a compressive strength of at least 17 ksi for classification as UHPC and is the goal for 28-day strengths. As a relative measure of quality, the early age performance follows part of the compressive strength requirements set out in the AASHTO MP 41 specification, expecting to achieve the 5000 psi at seven days as required for resin systems [74]. The AASHTO MP 41 specification also requires 1000 psi of compressive strength at 3 hours, but this is inside of the set time for cementitious systems and falls out of the range of traffic opening and is not monitored.

The results of compressive testing are included in **Figure 5.23**. The one-day compressive strengths for the intermixed calcined bauxite samples easily exceeded the 5000-psi requirement with CB/CM 0.0-2.0 samples average compressive strength varying from 9.5-9.7 ksi. The strength of CB-2.5 dipped to 8.6 ksi and the CB/CM of 3.0 dipped further to 7.2 ksi. At seven days a similar trend was observed, but the decrease after CB-2.0 was significantly reduced. The compressive strength increased from 11.0 ksi for CB-0 to 13.5 ksi for CB-1.5. Importantly, this mixture saw a reduction in compressive strength for CB-2.0 relative to the other mixes but may be a function of the brittle nature of UHPC. Lastly, the 28-day compressive strength again saw an increase in compressive strength, but the intermixed calcined bauxite samples began to greatly exceed the CB-0 mix. CB-0 had compressive strength at 28-days of 12.7 ksi, whereas CB-3.0, the lowest performer at one-day, had a compressive strength of 16.2 ksi. Lastly, the compressive strength of

CB-2.0 was again the highest with a strength value of 16.7 ksi unfortunately falling below the threshold for classification as UHPC in accordance with ASTM C1856-17.

From these results several conclusions about compressive strength can be drawn. First, the early age strength is most dependent on ensuring excess paste coats the CB and provides some thickness for dense paste. Having the most densely packed sample provides little excess paste and as such a greater proportion of the total paste is in ITZ, which is weaker than the densely packed outer paste. Conversely, at later ages compressive strength is more dependent on the total calcined bauxite content, as its high inherent strength can transfer load more effectively. This change from high calcined bauxite contents being a negative to a positive is dependent on the improved ITZ density of UHPC. UHPC improves ITZ density due to the high SCM content converting calcium hydroxide into CSH gel [83].

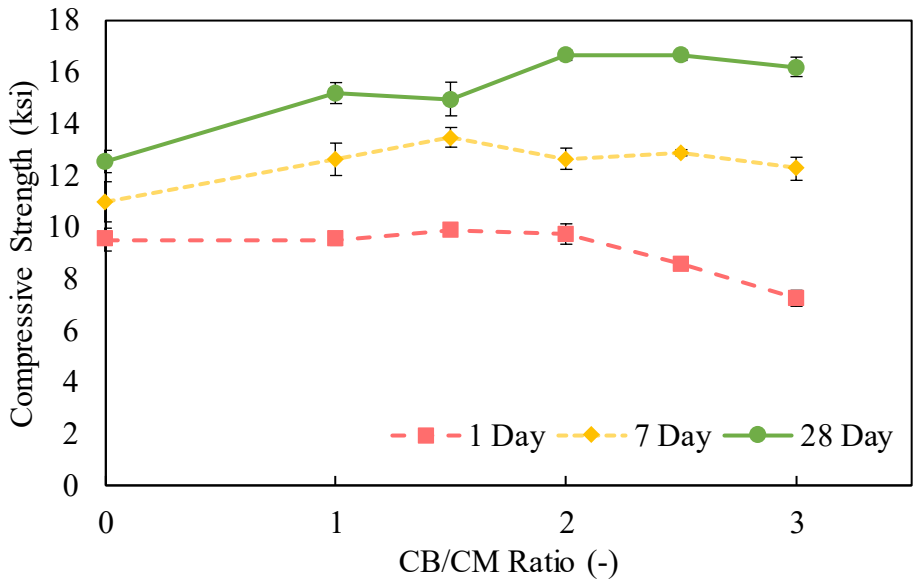


Figure 5.23: Compressive Strength as a Function of Calcined Bauxite Content

5.5.2.7. Abrasion Resistance

The abrasion resistance was monitored at full age for all mixes CB-0.0 to CB-3.0 (**Figure 5.24**). The abrasion resistance was completed on full age samples (>28 days). Since the testing procedure was a modification of the ASTM procedure the test results are only used as a relative comparison tool. Testing indicated that the inclusion of calcined bauxite greatly reduced the abrasion loss going from 3.5 cm^3 to between 2-2.5 cm^3 for the other calcined bauxite replacement rates. This indicates that the hardness and toughness of the calcined bauxite is providing a significant improvement in the abrasion resistance. Further classification of performance is difficult based upon the variability of the test results.

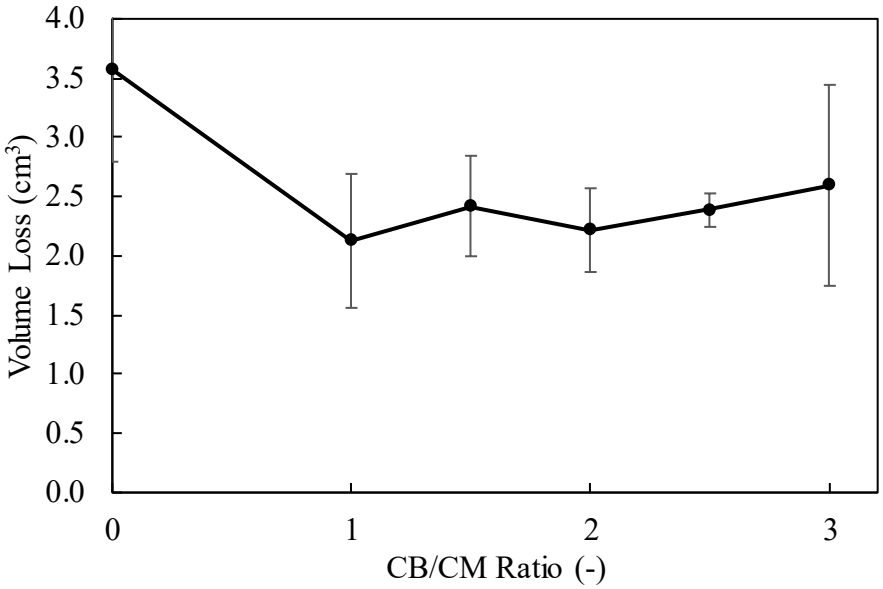


Figure 5.24: Abrasion Resistance as a Function of CB Content

5.5.2.8. Drying Shrinkage

The drying shrinkage of UHPC-based HFSTs was determined to quantify if the reduction in paste volume by including calcined bauxite would sufficiently reduce the shrinkage to below failure levels. **Figure 5.25** displays the results of the samples tested of varying CB content. The CB-0 sample had the highest shrinkage at all ages, culminating in a 25-day drying shrinkage length decrease of 0.07%. This fees well over the strain capacity of most ordinary portland cement systems (0.02%). Experimental observation found a reduction of 21%, 34%, 43%, 52%, and 49% for CB-1.0 to CB-3.0, respectively. Based upon the filler effect from including CB a 25% reduction in shrinkage is anticipated for CB-1.0, 33% for CB-1.5, 40% for CB-2.0. 45% for CB-2.5, and 50% for CB-3.0 due to the relative proportion of CB to the total mixture volume. This performance indicates that the replacement of paste with CB only acts as a filler and in this case does not also act as an internal curing agent, as the aggregate is not prewetted and there is not enough free water to absorb aggregate in the fresh state. Based upon this trend the replacement of paste with calcined bauxite is not a sufficient shrinkage mitigation tool to decrease shrinkage below the 0.02% criterion.

Several strategies are employable to solve this problem. Mitigation techniques such as the inclusion of shrinkage reducing admixtures would decrease the shrinkage by decreasing the capillary pore pressure by changing the surface tension at the interfacial areas. Lastly, the inclusion of fibers could increase the tensile strain capacity of the UHPC samples and eliminate the concern of large cracks forming.

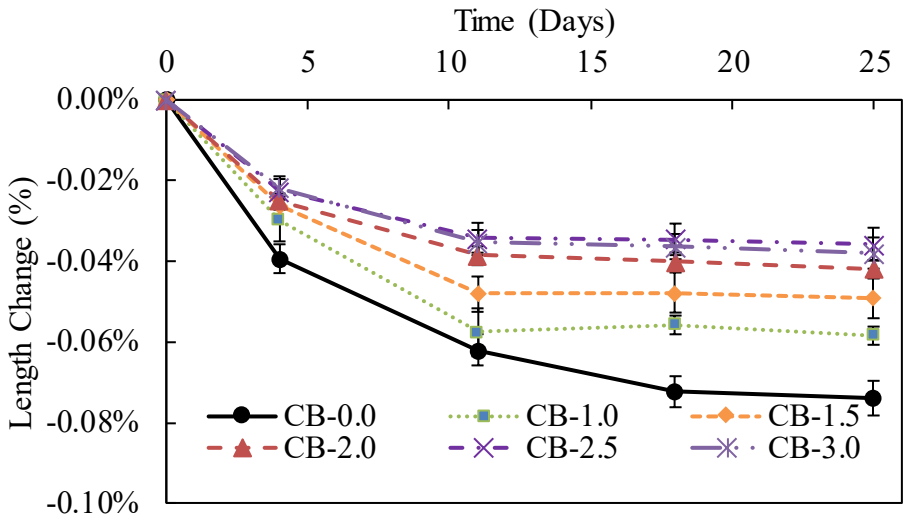


Figure 5.25: Drying Shrinkage as a Function of CB Content

5.5.2.9. Thin-Layer Shrinkage

Thin-layer shrinkage was utilized to monitor the cumulative effect of drying shrinkage and autogenous shrinkage simultaneously over the first 13 hours after initial hydration. However, the first hour is removed due to sample settling disrupting the utility of the data and resulting in large positive or negative shifts depending on sample leveling. This is of minimal consequence, as the tensile strain capacity during this period is often more than 1% [84].

Additionally, this testing provided information on how restraint by the substrate influences the conversion of shrinkage into stress. Samples were tested on both an unrestrained smooth surface and a restrained roughened concrete surface. Based upon the difference in shrinkage between the restrained and unrestrained surface an estimation of the proportion of shrinkage converted into stress on the surface is possible. Doing so would allow for a better estimation of the conversion of shrinkage into tensile strain, which dictates when the sample will fail. It is anticipated that each sample will restrain to a similar degree due to the substrate and that the degree of shrinkage is a function of the CB content.

Figure 5.26 displays the results of the unrestrained surfaces samples. Testing displayed a similar rank order as previously tested, but the relative change in comparison to CB-0.0 is significantly different. The order of shrinkage from greatest to smallest is CB-0.0, CB-1.0, CB-2.0, CB-1.5, CB-2.5, CB-3.0. The difference is that the relative change in comparison to CB-0.0 at 12 hours is 17% for CB-1.0, 50% for CB-1.5, 48% for CB-2.0, and 73% for CB-2.5 and CB-3.0. This reduction is generally greater than that experienced by the drying shrinkage samples, which more closely aligned with the reduction in cementitious material content. This in part could be due to the early age shrinkage being predominately a factor of evaporation rate and w/c ratio [85]. As the batch water corrected for the CB absorption additional bleed water was present delay self-desiccation and further shrinkage.

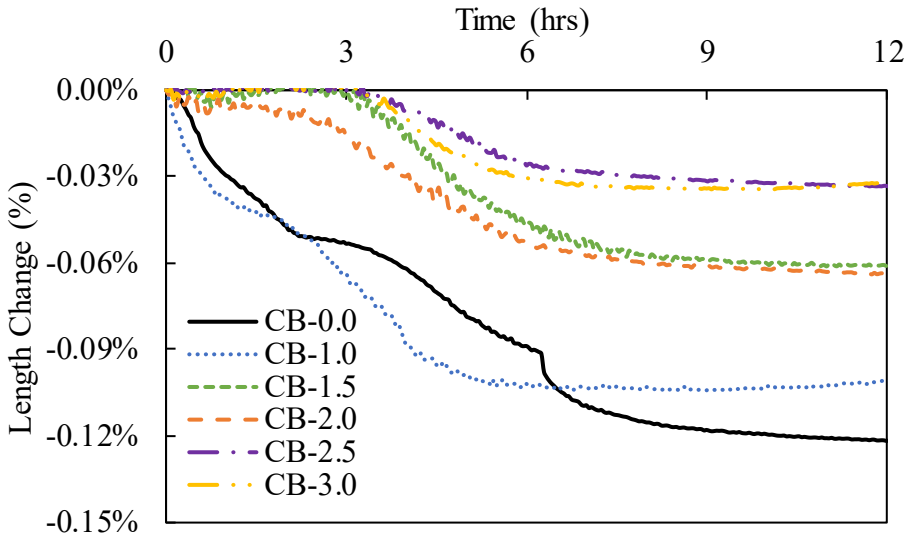


Figure 5.26: Unrestrained Thin-Layer Shrinkage at Varying CB Contents

Figure 5.27 displays the results of the restrained surface samples. A similar behavior was observed for the restrained surface samples to the unrestrained surface samples, where the shrinkage reduction exceeded the filler effect. The difference in the relative change in comparison to CB-0.0 at 12 hours is 34% for CB-1.0, 23% for CB-1.5, 58% for CB-2.0, 71% for CB-2.5, and 84% for CB-3.0. This would appear to mirror the previously mentioned improvement due to the inclusion of water correction for CB's absorption. Additionally, a substantial reduction in comparison was observed, with the maximum shrinkage being 0.075% as opposed to 0.122% for CB-0.0.

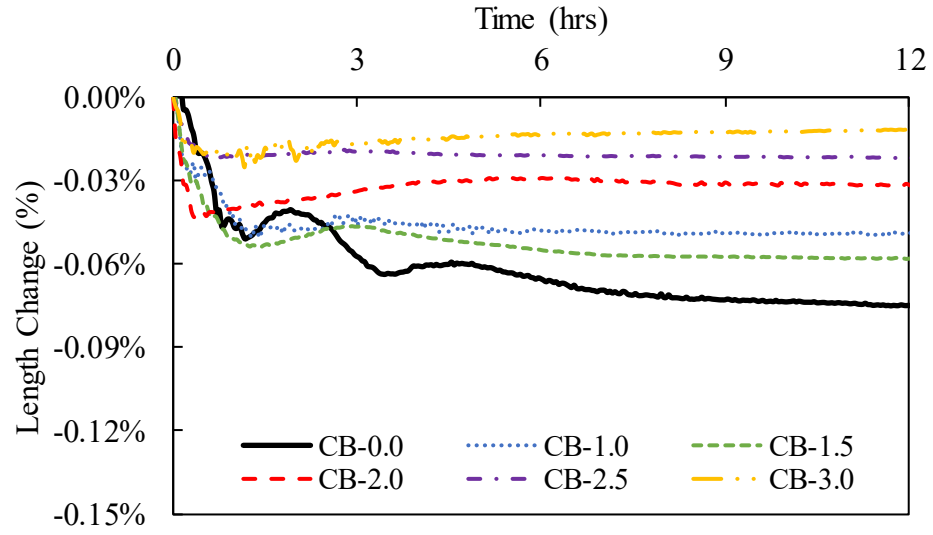


Figure 5.27: Restrained Thin-Layer Shrinkage as a Function of CB Content

By observing the difference between the unrestrained and restrained samples a general reduction in lateral shrinkage of 35-60% is observed, with one sample only having a 4% reduction, which would appear to indicate insufficient adhesion for that sample. Assuming that this reduction is due to the restraint provided by the substrate it is thereby estimated that the conversion of shrinkage to stress by an ICRI surface prep of six is approximately 35-60% for these UHPCs. This is promising, as it shifts the allowable shrinkage of these systems by 40% due to the tensile strain capacity. However, further testing is needed on differing levels of surface to determine if this is a function of surface preparation and material type.

5.5.3. Conclusions

Based on the experimental results of this study, several conclusions have been drawn:

- Optimizing packing density is not the best methodology for creating a superior UHPC-based HFST. While CB-2.5 provides the highest density, it does not offer the highest compressive strength, bond strength, or abrasion resistance. Instead, CB-2.0, which provides an elevated packing density compared to CB-0.0 and CB-0.0, had the highest compressive strength at 16.7 ksi at 28-days.
- Bond strength testing highlighted the importance of cementitious material content, as lower CB mixes provided better bonds at earlier ages, which will decrease the risk of delamination.
- The shrinkage and bond strength of UHPC-based HFSTs increase with increasing cementitious material content. Balancing the cementitious material content to provide adequate bond strength and low enough shrinkage is key for UHPC-based HFSTs.
- Based upon the evaluation criteria the preferred intermixed calcined bauxite UHPC-based HFST mixture is between a calcined bauxite content of 1.5-2.0. These mixes have a reduced shrinkage compared to the CB-0.0 mix and adequate bond/compressive strength. Secondary shrinkage mitigation measures are needed but significantly reduced.

5.6. Phase 3: Influence of Steel and Glass Fibers

5.6.1. Background and Mixture Proportions

This phase of the study assessed the impact of fiber content on the strength and shrinkage of UHPC-based HFST systems with intermixed calcined bauxite. This work sought to determine if fiber content plays a role in mitigating early age shrinkage. The mixture proportions for thin-layer testing varied based upon their calcined bauxite and fiber content. The cementitious binder was designed based upon the weakest but most workable of the designed UHPC formulations (SF3-4.5). The intermixed calcined bauxite contents for this study varied being either 0.0, 2.0, or 3.0 to allow for a variety of shrinkage, workability, and strength conditions. Lastly, two different fibers were chosen for testing, both based upon their ability to resist shrinkage and provide strength to the UHPC. Fiber dosage rates were maintained at 2.0% by volume primarily to achieve greater strength and durability performance. The samples tested and their IDs are listed in **Table 5.11**.

Table 5.11: Mixture Proportions of UHPC Samples Including Fibers

Sample ID	C/CM (-)	SF/CM (-)	S/CM (-)	PF/CM (-)	W/CM (-)	HRWR/CM (-)	CB/CM (-)	Stl.Fbr. (% Vol)	Glass Fbr. (% Vol)
CB0	0.85	0.15	0.6	0.5	0.2	0.045	0.0	0.0	0.0
CB0-S2	0.85	0.15	0.6	0.5	0.2	0.045	0.0	2.0	0.0
CB0-G2	0.85	0.15	0.6	0.5	0.2	0.045	0.0	0.0	2.0
CB2-0	0.85	0.15	0.6	0.5	0.2	0.045	2.0	0.0	0.0
CB2-S2	0.85	0.15	0.6	0.5	0.2	0.045	2.0	2.0	0.0
CB2-G2	0.85	0.15	0.6	0.5	0.2	0.045	2.0	0.0	2.0
CB3-0	0.85	0.15	0.6	0.5	0.2	0.045	0.0	0.0	0.0

5.6.2 Results and Discussion

5.6.2.1. Flowability

The flowability of the tested mixes is shown in **Figure 5.28**. Based upon initial testing by the modified flow table test supplemental testing by the standard flow table test was conducted if no flow was observed. For all mixes tested a decrease in flow is observed with the inclusion of fibers or calcined bauxite. For fibers this is due to fibers large aspect ratio, which increases the cohesive force of the mix. The flow of steel fiber reinforced samples was greater than glass fibers for the same reason, as the glass fibers had a larger aspect ratio than the steel fibers. For calcined bauxite, the reduction in flow is due to reduction in the interparticle paste volume, which increases the interlock between particles and reduces the workability. Importantly, initial testing intended to also include CB3 mixes with fibers, but those mixes were not cohesive due to the further increase of surface area that decreased the interparticle paste volume even greater. This test highlights that the inclusion of fiber makes consolidation more difficult.

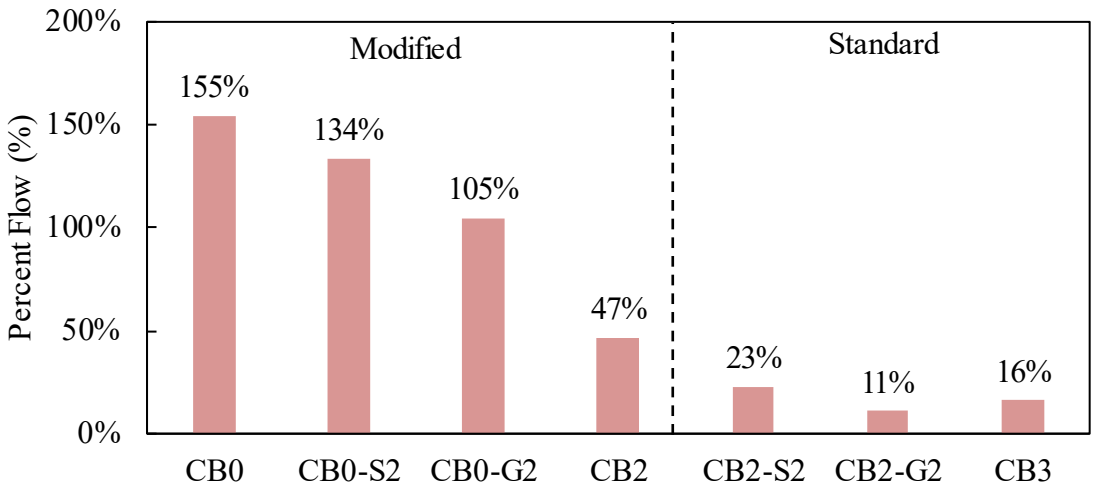


Figure 5.28: Workability of Fiber Reinforced Samples

5.6.2.2. Compressive Strength

The compressive strength of the samples was observed to determine if these samples could meet existing UHPC thresholds as well as to observe the effect of different fibers on the compressive strength. ASTM C1856-17, the ASTM standard practice for testing UHPC, requires a compressive strength of at least 17 ksi for classification as UHPC and was the target for 28-day strengths. Compressive strength test results are included in **Figure 5.29**.

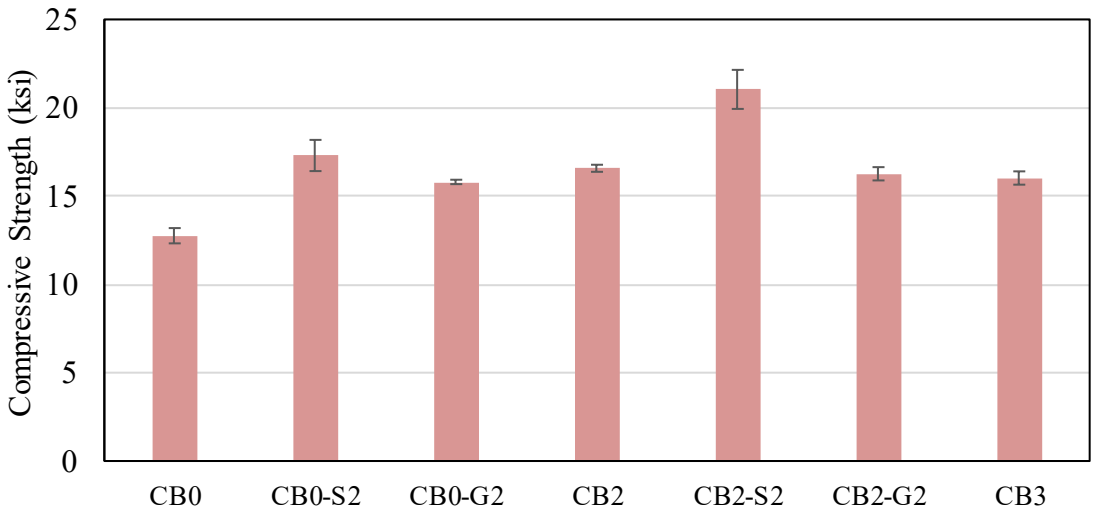


Figure 5.29: Compressive Strength of Fiber Reinforced Samples

The testing indicated that mixes without fibers had reduced compressive strengths in comparison to their fiber reinforced counterparts. CB0 had a compressive strength of 12.8 ksi, CB2 of 16.6 ksi,

and CB3 of 16.0 ksi. In comparison the steel fiber reinforced samples increased the compressive strength by 35% (17.3 ksi) and 26% (21.0 ksi) in comparison to their unreinforced counterparts for CB0-S2 and CB2-S2, respectively. For glass fibers the improvement was less with an increase of 24% for CB0-G2 and a reduction of 2% for CB2-G2 in comparison to their unreinforced counterparts. The reduction in compressive strength is believed to be caused by the reduction in paste volume caused by the need to coat the fibers. The inclusion of steel fibers allowed for the compressive strength to exceed the ASTM requirement for both mixes tested and the CB2-S2 mixture matched the required strength for ACI of 21 ksi the higher requirement [86]. The inclusion of steel fibers also benefits durability, which is still greatly needed to ensure a long service life.

5.6.2.3. Drying Shrinkage

This section identifies the drying shrinkage of UHPC systems made for HFST binders and determines if the reduction in paste volume by including fibers will sufficiently reduce the shrinkage to below tensile failure levels under restrained conditions. Concrete typically shrinks approximately 0.06% of their total length due to the evaporation of pore water [76]. Over a hundred-foot span this would equate to an approximately 0.75-inch reduction in the total length. The concern for cementitious systems is the lack of tensile strain capacity, as restrained shrinkage induces tensile stresses that result in cracking and subsequent deterioration of the surface and ride quality [77]. Typically, the tensile strain capacity for non-fiber reinforced concrete is approximately 0.02% (200 microstrain) [76,78]. However, for traditional UHPCs this value is greater often exceeding 1% but relies upon the ductility granted by fibers for the increase and is largely post peak behavior [79].

The results of this test are included in **Figure 5.30**. Testing as previously noted indicated a reduction in shrinkage proportional to the volume of calcined bauxite included (filler effect). However, the inclusion of fibers appears to have a negligible effect, with CB2-S2, CB2-G2, and CB0-G2 having no impact on shrinkage. CB0-S2 had an 18% reduction in comparison to CB0 and is more than likely a function of the steel fibers restraint against the shrinkage of the samples. Steel fibers can have a chemical and frictional bond to cementitious systems, whereas glass fibers are predominantly frictional [87,88]. The CB2-S2 mixture may not have displayed this change due to the lessened interparticle paste thickness. However, the more important behavior caused by the inclusion of fibers is the increase in tensile stress capacity, as fiber reinforced concrete has additional strain capacity due to secondary cracking.

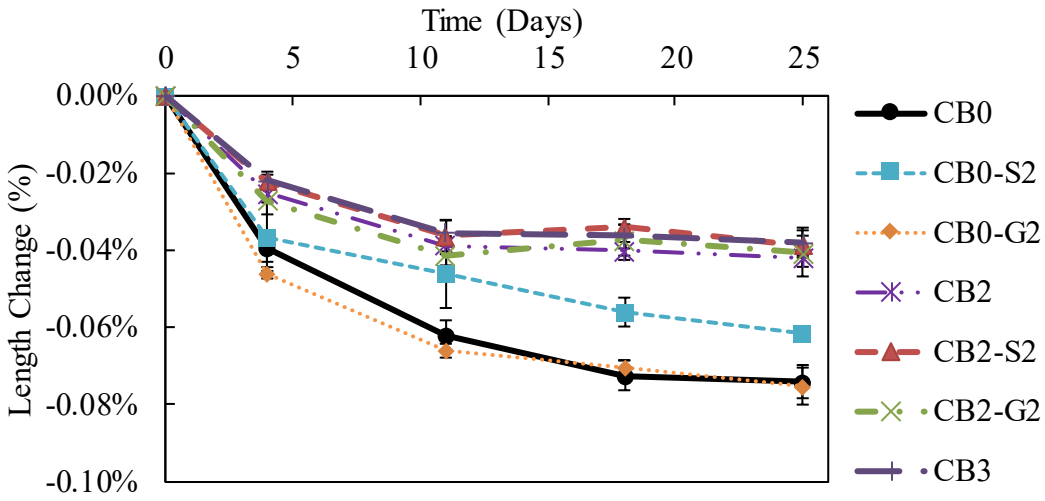


Figure 5.30: Drying Shrinkage of Fiber Reinforced Samples

5.6.2.4. Thin-Layer Shrinkage

Thin-layer shrinkage testing provided information on how restraint from the substrate influences the conversion of shrinkage into stress. Samples were tested on both an unrestrained smooth surface and a restrained roughened concrete surface. Based upon the difference in shrinkage between the restrained and unrestrained surface an estimation of the proportion of shrinkage converted into stress on the surface is possible. Doing so would allow for a better estimation of the conversion of shrinkage into tensile strain, which dictates when the sample will fail. It is anticipated that each sample will restrain to a similar degree due to the substrate and that the degree of shrinkage is a function of the CB content.

Figure 5.31 displays the results of the unrestrained surface samples. The testing indicated that the samples without fibers displayed higher shrinkage than those with fibers. This is in part due to the restraining effect that fibers have on the cementitious material adhering to the paste and resisting the tensile stresses imposed upon them [89]. This results in the generation of stress and strain but is generally offset by the increase in strain capacity by the inclusion of fibers. Testing on CB0 samples demonstrated a 44% reduction for steel fiber inclusions and a 50% decrease for glass fibers. Testing on CB2 mixes demonstrated a 46% reduction with steel fibers and 50% reduction with glass fibers. Ultimately, this resulted in the shrinkage of CB0 mixes with fibers being comparable to CB2 without fibers and CB2 mixes with fibers being comparable to CB3 in terms of 12-hour shrinkage. Further testing is needed to determine if this decrease in visible shrinkage results in sufficient restrained strain to not induce cracking. However, all samples currently tested did not demonstrate visible surface cracking.

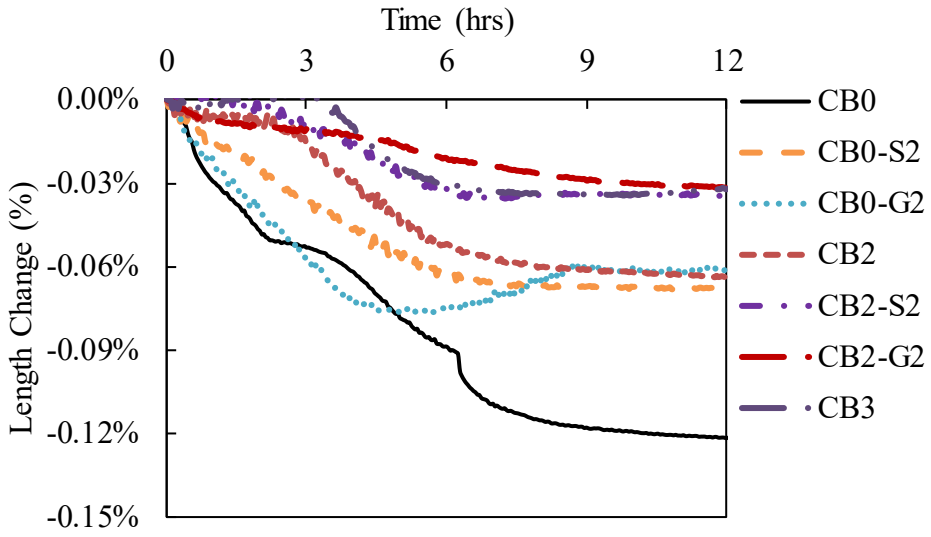


Figure 5.31: Thin-Layer Shrinkage of Unrestrained Fiber Reinforced Samples

Figure 5.32 displays the results of the restrained surfaces samples. The trends generally followed the results of the unrestrained surfaces, but at a lesser shrinkage level indicating restraint from the substrate. The reduction in shrinkage for CB0 with steel fibers was 66% and for glass fibers was 39% when compared to the CB0 mixture without fibers. For CB2 with steel fibers a 51% reduction was observed and for glass fibers a 57% reduction was observed in comparison to the CB2 mixture without fibers. The decrease for samples between restrained and unrestrained surface varied from 26-63% of the total magnitude of shrinkage. Based upon these results this would indicate that on similarly prepped real world samples the shrinkage could be 150% greater than the strain capacity and be unlikely to crack, as the shrinkage is not fully converted in stress. Unfortunately, most unreinforced mixes currently have shrinkage values that exceed that 150% threshold. Further testing is needed to determine if this methodology is an effective tool to determine the restraint provided by a substrate for thin sections, but the results look promising.

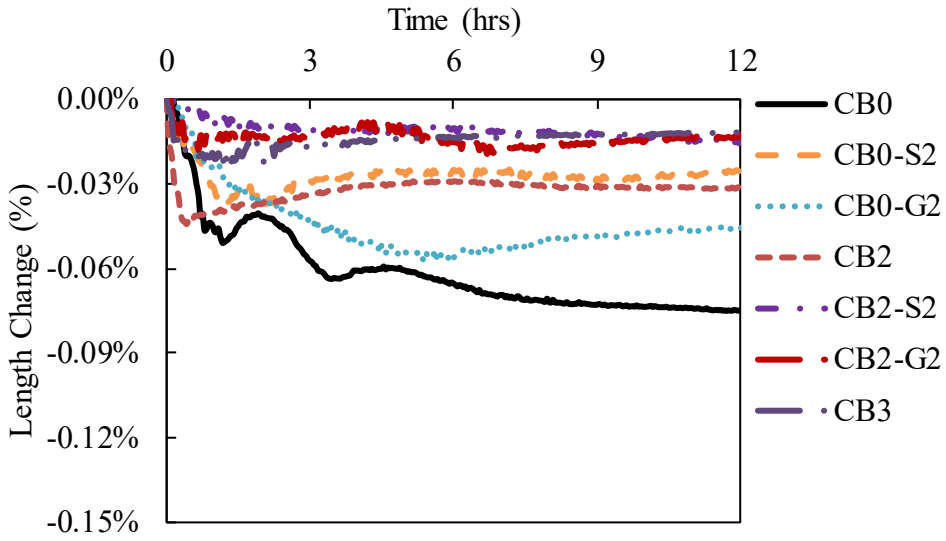


Figure 5.32: Thin-Layer Shrinkage of Restrained Fiber Reinforced Samples

5.6.3. Conclusions

Based upon the experimental results of this study several conclusions are drawn:

- The inclusion of fibers (especially steel) greatly increases (20-30%) the compressive strength of UHPC for both normal and intermixed calcined bauxite samples if sufficient paste is available.
- The drying shrinkage of hardened UHPC samples indicated that the fiber content had a minimal impact, with only the CB0-S2 mixture providing a substantial change. This is probably in part a function of a decrease in the available paste content and the reduced bond of the glass fibers.
- The thin-layer shrinkage demonstrated a clear decrease in shrinkage from the inclusion of fibers. Samples decreased between 40-50% in the unrestrained state and 30-60% in the restrained state. This indicates that the fibers are helping to resist the inward force. However, these samples still exceeded the expected tensile strain capacity and as such could crack.

5.7. Overarching Conclusions

Overall, as a summary of the three phases of UHPC mixture designing and testing the following conclusions can be drawn:

- The preliminary performance of UHPC-based HFST provides adequate mechanical performance on both asphalt and concrete substrates. The bond strength and compressive

strength all match or exceed guidelines set in place for equivalent systems.

- The performance of epoxy-resin HFST on asphalt overlays greatly exceeds that of cementitious-based HFST, even though the UHPC was still adequate. Key concerns for UHPC on asphalt surfaces include lower pull-off bond strength and low compatibility of coefficient of thermal expansion.
- The performance of UHPC with intermixed calcined bauxite varied with increased compressive strength and lower variability later age bond strength as positives and reduced workability and lower initial bond strength as negatives.
- Optimizing packing density is not the best methodology for creating a superior UHPC-based HFST. While CB-2.5 provides the highest density, it does not offer the highest compressive strength, bond strength, or abrasion resistance.
- Bond strength testing highlighted the importance of cementitious material content, as lower CB mixes provided better bonds at earlier ages, which will decrease the risk of delamination.
- The shrinkage of these UHPCs, the central area of concern, was also dependent on cementitious material content. Since most of the preferred mechanical properties and shrinkage performance depend on conflicting relationships, it is necessary to balance these design parameters.
- The inclusion of fibers (especially steel) greatly increases (20-30%) the compressive strength of UHPC for both normal and intermixed calcined bauxite samples if sufficient paste is available. The fibers allow the reinforced mixes to fall under UHPC designation. However, if insufficient paste is available to fully coat the fibers minimal impact is demonstrated.
- The drying shrinkage of hardened UHPC samples indicated that the fiber content had a minimal impact on drying shrinkage, with only the CB0-S2 mixture providing a substantial change. This is potentially due to a decrease in the available paste content that reduces the bond to the fibers.
- The thin-layer shrinkage demonstrated a clear decrease in shrinkage from the inclusion of fibers. Samples decreased between 40-50% in the unrestrained state and 30-60% in the restrained state. This indicates that the fibers are helping to resist the inward force. However, these samples still fall above the expected tensile strain capacity and as such could crack. Testing is needed to determine the true tensile strain capacity of these samples for better characterization.

CHAPTER 6: UHPC-BASED HFST SURFACE APPLICATION METHODS AND EVALUATION

6.1. Problem Statement

The high material cost of HFSTs has limited the breadth of their application across pavement networks where they would otherwise be effective in crash reduction. The efficacy of cementitious binders and the use of surface retarders for the application of HFSTs has not been thoroughly assessed, particularly in the US. Previous efforts for high friction coarse aggregate embedment have not adequately scaled up to full size pavement samples [59,60]. Although the use of retarders for exposed aggregate concrete has been proven in Europe, it has seen only limited use in the United States. There is a lack of standard guidance for use of surface retarders particularly for UHPC pavement applications.

6.2. Objective

This study sought to develop and evaluate application methodologies for a non-proprietary UHPC-based HFST binder to generate adequate friction and texture and durability in comparison to traditional epoxy-based systems. The effects of various grades of surface retarders, aggregate moisture, aggregate broadcasting methods, and external vibration were also assessed. Mean profile depth (MPD) macrotexture, and friction by the British Pendulum Test (BPT), and Dynamic Friction Tester (DFT) where used as primary performance parameters along with polishing utilizing the Three Wheel Polishing Device (TWPD).

6.3. Methods and Materials

At the outset of the experimental work some initial trial batches of UHPC HFST surfaces were cast to identify experimental parameters of interest and further develop the experimental design. Based on this initial testing a HFST aggregate content of 3.0 as a ratio to cementitious materials was selected. Furthermore, a 12-hr cure time was selected for surface retarded samples. Finally, the samples with broadcasted aggregate (which was initially in saturated surface dry condition (SSD)) exhibited white deposits on the surfaces of and in between aggregates which were evaluated using a scanning electron microscope with energy dispersive X-ray Spectroscopy (EDS). The remainder of the experimental work was divided into two phases with the first focused on assessing the suitability of various application methods and the second on evaluating the performance of UHPC-based HFST variations. Only oven dried (OD) condition HFST aggregate was used in phase two based on the findings using SSD aggregate.

6.3.1. Phase 1: Evaluation of Application Methods

6.3.1.1. UHPC Mix Design Materials

A non-proprietary UHPC mix design was developed. The primary criteria in selection of the mix design included adequate flow to enable aggregate embedment and placement and adequate strength such that durability would be comparable to that of epoxies. Notably the desirable UHPC

properties for this application include bond strength and abrasion resistance. The constituent materials of the binder were limited to silica fume (SF) as the singular supplementary cementitious material, a liquid form polycarboxylate high range water reducer suited for use in UHPC, a manufactured sand fine aggregate (at two gradations for better particle packing) and Type III cement (to enable the earliest possible opening to traffic). No fibers were included in the UHPC surface mix.

The final mix design materials were batched as a ratio of mass to the total mass of cementitious materials (Cm = cement and silica fume combined). The ratios were: water = 0.2, sand = 0.6, fine sand = 0.5, silica fume = 0.15 and a HRWR dose 0.035. For the samples made from intermixing the HFST aggregate, a ratio to Cm of 3.0 was used and it was assumed for the mix design of broadcasted aggregate samples. Calcined bauxite was the only HFST aggregate used.

6.3.1.2. Surface Retarders

Surface retarders are a type of cement set retarders that are formulated to be applied to a finished concrete surface such that after the bulk of concrete has set, the very top layer of the concrete that has not set is removable through washing with water, scrubbing or pressure washing. The intent of these products is to enable consistent aggregate exposure. A total of 6 surface retarders were selected for this study, two from a particular manufacturer (identified herein by prefix VE) and four from another (identified by prefix SE) at varying grades where the higher number following the prefix denotes a deeper etch.

6.3.1.3. Sample Construction

Generally, two types of surfaces were created for this study, intermixed, and broadcasted. Intermixed refers to samples where the coarse aggregate was added into the UHPC and mixed prior to placing the surface. The aggregate was then revealed through surface retarders and washing. Broadcast refers to samples where the UHPC was placed on the surface and then the aggregate was added onto the surface. Broadcast samples included aggregates in SSD and oven dry (OD) condition, each further divided into gravity embedment of aggregates and the use of vibration for embedment samples. Reference surface samples were also constructed utilizing epoxy resin binder. Pre-manufactured paver bricks of dimensions 197 mm x 95 mm were used as the substrate base for the surfaces.

The volume of UHPC applied to the surface was proportioned to produce a layer ideally between 5 and 8 mm when finished. As needed, the samples were vibrated to get an even and consolidated surface finish, however for the broadcast samples without vibration, no additional vibration was provided after the application of aggregate to the surface. For the broadcast samples, aggregate was broadcasted to excess of the point at which the binder was completely covered in aggregate and no longer visible. Three samples for each surface type were constructed.

A total of 13 unique surface methods were constructed: Resin-Based, OD Vibrate, SSD Vibrate, OD Broadcast, SSD Broadcast, VE-15, VE-25, SE-25, SE-50, SE-125, SE-200, No Retarder with Wash, and No Retarder. For the intermixed samples using surface retarders, the retarder was

applied using a pump spritzer to completely coat the surface in a nearly even layer immediately after the surface was placed and vibrated to an even finished surface. After the prescribed cure time of 12 hours plus or minus approximately 30 minutes, the samples were pressure washed at using a 3400 psi, 2.5 gallon per minute pressure washer with a 40-degree spray nozzle attachment to remove the retarded surface.

During construction of vibrated broadcast samples the vibration method used induced some edge effects on the samples and some surface irregularities. Therefore, all the UHPC-based broadcast samples (OD vibrate, SSD vibrate, OD Broadcast and SSD broadcast) were reconstructed using larger pavers which were cut into three pieces that were of sufficient size for BPT friction and texture testing, and these pieces served as the individual samples for that application method.

All samples were open air cured in laboratory conditions. After initial texture measurements the samples were subjected to aggressive rubbing by a wood board to remove any remaining loosely bonded aggregate like methods described by other researchers which is referred to herein as initial conditioning [29,30].

6.3.1.4. LTS Methods

The texture of the HFST samples were scanned using the AMES Laser Texture Scanner (LTS) 9400HD. A sample holding stage was utilized that enabled the LTS to be held securely over the samples.

For each paver, two scans were completed at an orientation of 180 degrees from each other. Each scan consisted of 20 high-resolution scanlines evenly spaced across the surface. Scans were conducted after brushing and after the initial conditioning. For the larger paver used for broadcast surface samples, the brushed condition was collected by scanning across five locations on the slabs prior to cutting into three samples.

6.3.1.5. BPT Methods

The friction of the wetted samples was tested using the British Pendulum Test (BPT) according to the methods in ASTM E303-23 using a TRL-55 rubber slider which was recommended by the BPT manufacturer for pavement surfaces. For each surface, the British Pendulum Number (BPN) was recorded as the average of five successive swings after two setting swings. The samples were rotated 180 degrees, and the test was conducted again.

6.3.2. Phase 2: Performance of UHPC-Based HFST

6.3.2.1. Aggregates

Three aggregate sources were considered in this study. Calcined bauxite as the reference and two aggregates previously assessed by the authors, a trap rock from North Carolina and a granite from Georgia [1]. The calcined bauxite was used at the as-received HFST gradation which met the South

Carolina Department of Transportation gradation standard of 100.0% passing the #4, 95.0-100.0% passing the #6 and 0.0-5.0% passing the #16 sieves for HFST aggregate[2]. A 200-gram sample of the calcined bauxite was sieved over the #4 sieve #6, #8, #12, #16, #30 and #50 sieves. The other aggregates were crushed (using a Bico Chipmunk jaw crusher), sieved, and mixed to achieve equivalent proportions passing the same sieves.

6.3.2.2. Substrate casting and preparation

Substrate slabs that were approximately 20 by 20 inches and approximately two to three inches thick were constructed. The slabs were constructed using two different mixtures however the substrate effects were not considered a major factor in this study as the testing of this study was only concerned with surface properties.

6.3.2.3. Surface Retarders

Two surface retarders were utilized, SE-125 and SE-200. Before application to the surface, the products were shaken in their original containers and enough to coat the surface was run through a disposable paint filter and transferred to a pump sprayer.

6.3.2.4. Mix Design

The same mix design as phase 1 was used except for a HRWR dose increase to 4.5% by mass of Cm. For the samples made from intermixing the coarse aggregate, a coarse aggregate to Cm ratio of 3.0 was used and was assumed in the design of the broadcast samples. Only OD condition aggregate was used. Because the mixes were proportioned by mass, when producing the UHPC for the samples with intermixed coarse aggregate (retarded surface samples), adjusting for densities and absorptions of the aggregates resulted in a different mix for each aggregate following the material ratios when batching for a total volume.

For each slab, the mix was batched to produce a final surface treatment thickness between five and eight mm thick. For mixes where the aggregate was broadcasted or vibrated in, the same aggregate content was assumed in the mix design but was not added in and was not adjusted for the different aggregates' absorption and densities since the aggregate quantity and effective absorption are unknown. Therefore, the mixes were the same across the aggregates but based on the calcined bauxite density and absorption.

When utilizing OD condition aggregate for broadcast methods the true UHPC water content is unknown because it is dependent on the amount of aggregate embedment and the amount of aggregate absorption that occurs. Because the use of vibration was shown to successfully aid embedment, the need for a high flow mix was reduced. Therefore, the mix design for the vibrated samples assumed no aggregate absorption would take place and therefore no additional mix water was accounted for in it. This mix produced a binder with a true water to cementitious materials ratio (w/Cm) of 0.2 (or lower depending on the broadcasted aggregate absorption of water from the mix). This variation is referred to in this study as the Lo-w/c mix. In contrast, because broadcasting without vibration requires higher flow for adequate embedment of aggregate, the mix

design for those samples assumed that the full aggregate content of the intermixed samples was included, and that full absorption would take place from the OD aggregate. This resulted in a mix design that was identical in proportions to the intermixed retarder samples using calcined bauxite. In the intermixed samples the mix is adjusted to add additional water to account for aggregate absorption, which is assumed to reach an equilibrium in the mixing, such that additional water is absorbed into the aggregate pore structure and the binder itself maintains the true designed w/cm of 0.20. When using that mix without adding the coarse aggregate into the mixing process, the resulting UHPC binder has an effect w/cm that is about 0.27 before adding the coarse aggregate, which presumably would be reduced once the aggregate is broadcasted, and absorption takes place. The true w/cm ratio would then be between 0.20 and 0.27. This variation is referred to as the Hi-w/c mix in this study. Finally, to determine if there is a middle ground between the two approaches a final mix was made that assumed the full aggregate content of the intermixed samples, but only assumed only 30 percent of course aggregate absorption occurs resulting in a w/cm ratio of about 0.22 before that coarse aggregate is added, this is referred to as the Mid-w/c mix, and was only used on a single broadcast sample with calcined bauxite aggregate. Other variations tested included using the Lo-w/c mix with calcined bauxite aggregate without vibration.

6.3.2.5. Surface casting procedures

Before application of the surface material, the substrates which were prepared to a near SSD condition. For the intermixed samples, the coarse aggregate and UHPC binder mix were spread across the sample and hand troweled to an even surface with external vibration used for consolidation. After the final trowel pass the set retarder was sprayed onto the surface to full coverage as evenly as possible.

The surface samples were pressure washed after 12-hours +/- approximately 30 minutes of curing in the lab. They were washed with a 3400 psi, 2.5 gallon per minute pressure washer with a 40-degree spray nozzle attachment to remove the retarded surface.

For the broadcast surfaces, the UHPC binder was applied to the substrate and made into to an even surface with a spatula and/or trowel. External vibration was used to provide adequate consolidation and even distribution. Once the surface was even and smooth the aggregate was broadcasted by hand. Similar procedures were followed for the vibration embedment samples, except that after aggregate was distributed to full coverage a vibrating trowel was used across the surface to aid with embedment. If after surface vibration excess UHPC binder was observed, then additional aggregate was added followed by additional vibration as deemed necessary for full coverage.

The samples were cured a minimum of approximately 24 hours before removing excess aggregate that was not embedded into the UHPC. The calcined bauxite aggregate that was recovered from the surfaces was also used to create a broadcast sample using the Hi-w/c mix to determine if any effects were observed on the performance of reusing recovered aggregate. Additionally, a sample was created using the calcined bauxite aggregate and the Hi-w/c mix but on a dry subbase. Finally, for reference, surfaces made with HFST epoxy resin were constructed on dry substrates.

After a minimum 28-day cure all of the samples were conditioned utilizing a wood board to aggressively rub the surface to remove a weakly bonded or loose aggregates based on methods described by other researchers [29,30]. A total of 19 surface variations were produced.

6.3.2.6. Polishing with the TWPD

Samples were polished using a Troxler National Center for Asphalt Technology (NCAT) Three Wheel Polishing Device (TWPD) shown in **Figure 6.1**. This device simulates traffic polishing by using a weighted carriage with three pneumatic tires that move in a circular pattern across pavement samples. The device is sized such that the footprint of trafficking matches that of the Dynamic Friction Tester (DFT) testing. The weights and carriage applied a load of approximately 201 pounds during trafficking operated at approximately 57.7 cycles per minute.



Figure 6.1: Three Wheel Polishing Device

5,000 cycles of polishing were conducted on all samples except for the Dry subbase Broadcast Calcined Bauxite Hi-w/c sample and samples that failed to reach a minimum DFT60 of 0.75 based on typical range for agency requirements [8]. The top performing mixes were polished up to 70,000 cycles.

6.3.2.7. LTS Macrotexture

The MPD macrotexture of the samples was collecting using the AMES LTS 9400HD device. After conditioning, scans were conducted across 5 locations on the slabs (slightly in from each corner and at the center). For each scan 20 high resolution scanlines were collected. MPD was generated using the AMES software using the ISO 13473-1 (2019) method. After TWPD polishing, effort was made to capture any changes in texture from the polishing. However, the LTS collects in straight lines across a rectangular scan area. Therefore, the scan area of the 20 scanlines was reduced to a 1-inch-wide band and a template was made to place the device in a location that would measure the texture roughly in the path of polishing. Four scans were conducted at 90 degrees from each around the path of polishing. Precise placing of the LTS was difficult, and it was likely

not perfectly centered in the middle of the wheel path. On a review data were removed for some samples, reducing to 3 scans to produce the mean value.

6.3.2.8. Hydrotimer

The Hydrotimer or outflow meter is an alternative macrotexture device that assesses water drainage. It measures the time it takes for set volume of water to drain through the macrotexture of the pavement surface that interacts with rubber ring at the bottom of the device. Five Hydrotimer readings were taken on each slab sample, one near each corner and one near the center of the slab (**Figure 6.2**). The outflow time is reported as the average of these five readings. The Hydrotimer was only used on samples before polishing.



Figure 6.2: Hydrotimer on a HFST Sample Slab

6.3.2.9. Dynamic Friction Tester (DFT)

Friction was assessed using the DFT. It measures the friction of three rubber sliders mounted on a rotating disk that are brought in contact with the pavement surface. It uses an attached water tank to apply a water film to the surface during measurement. The results are reported as a DFT number with the operating speed, e.g., DFT60 for a 60 kilometer per hour (kmph) test. The operating speed was set at 75 kmph, which records the friction at the lower speeds until the friction brings the rotation to a full stop. Therefore DFT60, DFT40, and DFT20 were recorded from each test. The water tank was elevated approximately 24 inches except for the Dry subbase Broadcast Calcined Bauxite Hi-w/c sample which measured at a lower water tank height (and operating speed of 80 kmph). The total height difference between the bottom of the tank and testing surface was slightly less than the 24 to 39 inches prescribed for a specified flow rate and water thickness. The differences in sample height relative to the tank height and some minor variations in slopes at test locations may have produced minor variation in the water film thickness or load applied but are not believed to significantly affect the results. Surfaces were pre-wetted either from use of the

Hydrotimer immediately before testing or being briefly sprayed and tilted momentarily to have any excess surface water runoff. The average of two repeat runs from the DFT are reported.

6.4. Results and Discussion

6.4.1. Phase 1: Evaluation of Application Methods

6.4.1.1. Aggregate Moisture Content

EDS testing of white deposits indicated that the composition was consistent with carbonated calcium hydroxide. This indicates that these were deposits of high-water content cement on the surface of the aggregates that were carbonated during its open-air curing.

6.4.1.2. Results of Friction Testing (BPT)

The results of BPT friction testing of the samples are shown in **Figure 6.3**. The figure shows that all of the surfaces were able to produce a high level of friction exceeding a BPN of 83 with the exception of the sample with no retarder or washing applied which was constructed as a reference point and not designed as a friction surface. Error bars represent standard deviation. According to the Western Transportation Institute, for HFSTs the lower range of friction starts at BPN of 65 with the higher end of BPN in the high 90's [39]. Based on this, all the application methods were able to achieve adequate friction to be eligible as HFST. This is not a surprising result as all the samples used the calcined bauxite aggregate which has been proven as the premier friction aggregate for HFST applications. Because the BPN is considered a measure of the microtexture component of friction and the microtexture is a function of the aggregate surfaces it is expected that if the aggregate was adequately exposed in the surface samples, a high BPN should result [9]. The surface application methods are rank-ordered from highest to lowest in **APPENDIX B**: Supporting Tables and Figures. The order reveals an interesting finding that all the broadcast methods performed better than the retarder methods, with the resin-based system performing best overall. The higher friction resulting from broadcasting compared to the retarder methods is likely due to differences in macrotexture and differences in microtexture exposure. The macrotexture roughly corresponds to embedment depth for broadcasting and exposed depth for the retarder samples.

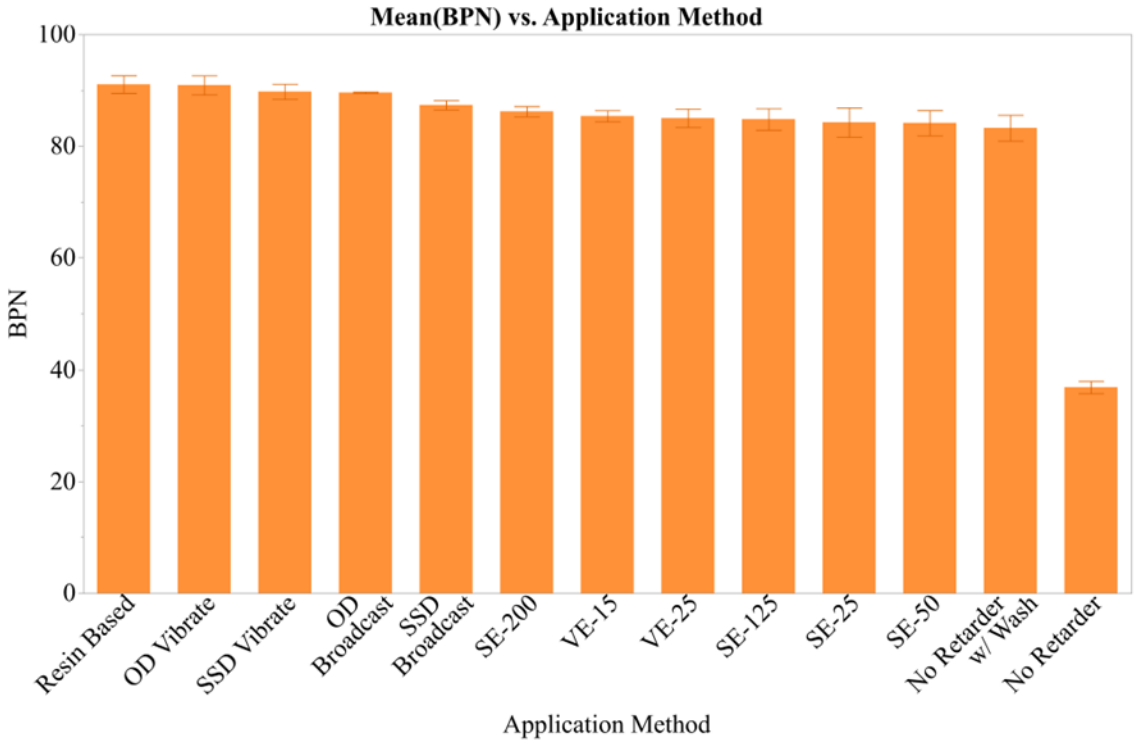


Figure 6.3: BPN of Sample Surfaces

6.4.1.3. Macrotexture and Effect of Retarder Grade

1.5 mm was established as the minimum target MPD. MPD was also used to assess the ranked performance of the varying grades of the SE line of retarders. The retarder manufactures present the effects of increasing product grades as depth of etch or exposure depth to which the measured MPD was compared. However, it should be noted that the retarder manufacturers do not report their depth as MPD, so it is not a direct comparison of the same exact parameter. **Figure 6.4** shows the results of measured MPD compared to the advertised depth. A clear reduction in depth is observed for the UHPC surface samples compared to advertised depth. Additionally, the slope of the relationship between grade and exposure depth is also lower. This reduction in retarder effective depth is likely a function of the very low water content of the UHPC mix.

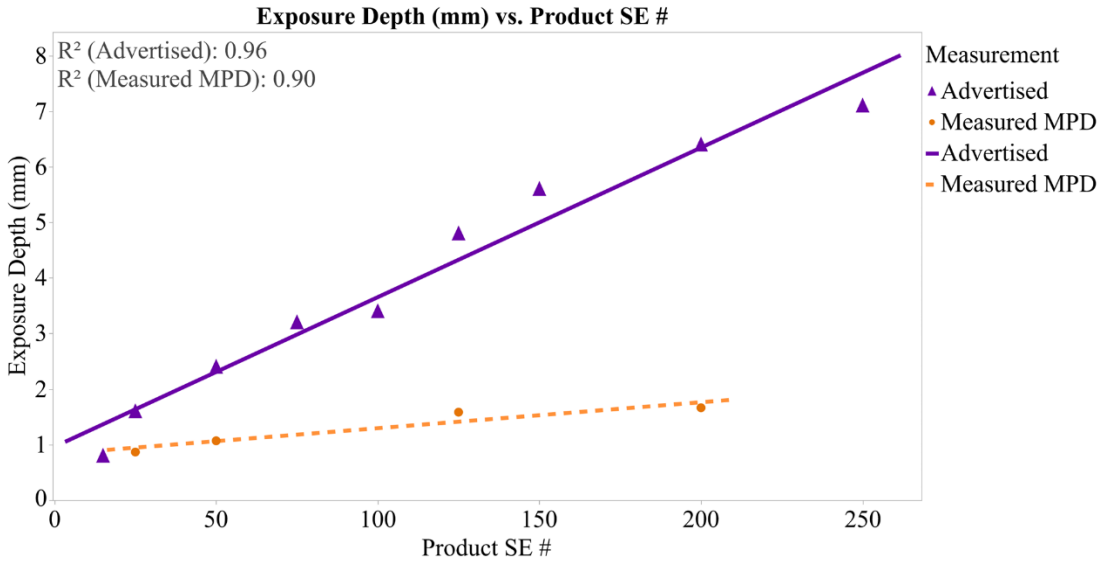


Figure 6.4: Retarder Grade Effect on Exposure Depth

Based on the MPD results the resin-based surface, the two highest grade retarders (SE-125 and SE-200) and broadcasted OD and SSD without vibration surfaces all met the minimum target MPD of 1.5 mm as shown in **Figure 6.5**, where error bars represent standard deviation. Additionally, while the vibrated OD and SSD samples were just below the 1.5 mm threshold, they were also not statistically significantly different that the un-vibrated broadcast samples as they were all connected by letter C in the Tukey's HSD comparison shown in **Table 6.1**. Furthermore, the acceptable range of MPD for HFSTs goes down to 1.0 mm depending on the agency requirements and the BPN of those samples exceeded that of the SE-125 and SE-200 [8]. Therefore, all the broadcast samples and high-grade retarded surfaces are considered a potentially viable alternative to resins based on the primary factors considered in this study of BPN and MPD. The lower grade retarders did not have a significantly different MPD than just washing the surface at 12-hours without the use of a surface retarder.

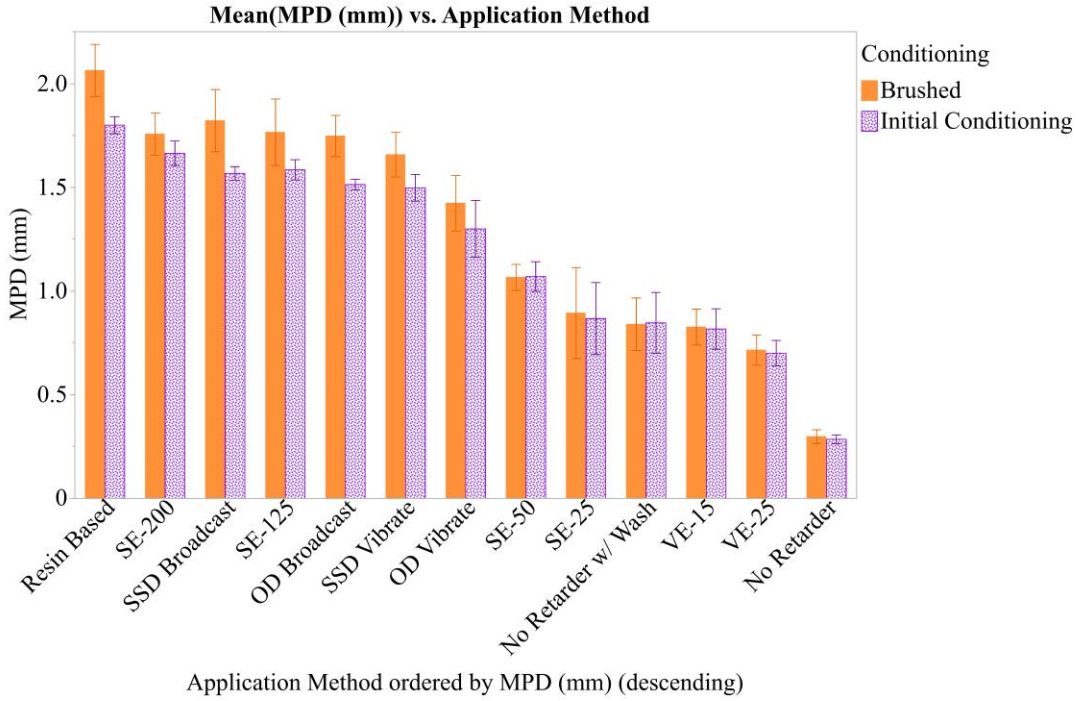


Figure 6.5: MPD of Surface Samples

Table 6.1: Conditioned Samples Tukey's HSD of MPD

Application Method								Least Sq Mean
Resin-Based	A							1.7993
SE-200	A	B						1.6637
SE-125	A	B						1.5843
SSD Broadcast	A	B	C					1.5668
OD Broadcast		B	C					1.5130
SSD Vibrate		B	C					1.4973
OD Vibrate			C	D				1.2995
SE-50				D	E			1.0695
SE-25					E	F		0.8672
No Retarder w/ Wash					E	F		0.8462
VE-15					E	F		0.8170
VE-25						F		0.7002
No Retarder							G	0.2850

6.4.2. Phase 2: Performance of UHPC-Based HFST

6.4.2.1. Initial Surface Performance

The macrotexture (MPD and outflow time) and DFT friction were evaluated across all samples after conditioning to evaluate performance. DFT60 of 0.75 and MPD of 1.5 mm were used as minimum threshold criteria. All the retarded samples using alternative aggregates (other than calcined bauxite), and the Broadcast Calcined Bauxite with Lo-w/c sample failed to reach the minimum friction and were not included in further testing. Additionally, the retarded samples using granite aggregate, the SE-125 Trap Rock, Broadcast Calcined Bauxite Lo-w/c, and Dry subbase Broadcast Calcined Bauxite Hi-w/c samples all failed to meet the minimum MPD, although the Dry subbase Broadcast Calcined Bauxite Hi-w/c samples was very close (average MPD of 1.499). Notably the Broadcast Calcined Bauxite Lo-w/c sample had very poor aggregate embedment and

the lowest overall initial DFT60 friction. Additionally, the abrasive force of the DFT test was able remove most of the aggregate from the testing path as shown in **Figure 6.6**.

(a)



(b)



(c)



Figure 6.6: Aggregate embedment and loss on Broadcast Calcined Bauxite Lo-w/c sample (a) after brushing, (b) after conditioning, (c) after DFT testing

The remaining samples were subjected to 5,000 cycles of the TWPD, and friction and texture were measured again. The samples that failed to meet the same thresholds were removed from further

testing. The broadcast Hi-w/c and resin-based samples using the granite and trap rock all failed to meet the minimum friction, the broadcast Hi-w/c samples using the granite and trap rock also failed to meet the minimum MPD as seen in **Figure 6.7** and **Figure 6.8**. This indicated a clear differentiation in performance among the aggregates. Because of the coinciding precipitous drop-off in friction performance after 5,000 TWPD cycles on the vibrated samples using the trap rock and granite, they were also removed from further testing, although they were still above the threshold at DFT60 of 0.8 and 0.78, respectively. Although the Broadcast Calcined Bauxite Mid-w/c sample dropped below the minim MPD of 1.5 mm, it was tested to 70,000 cycles.

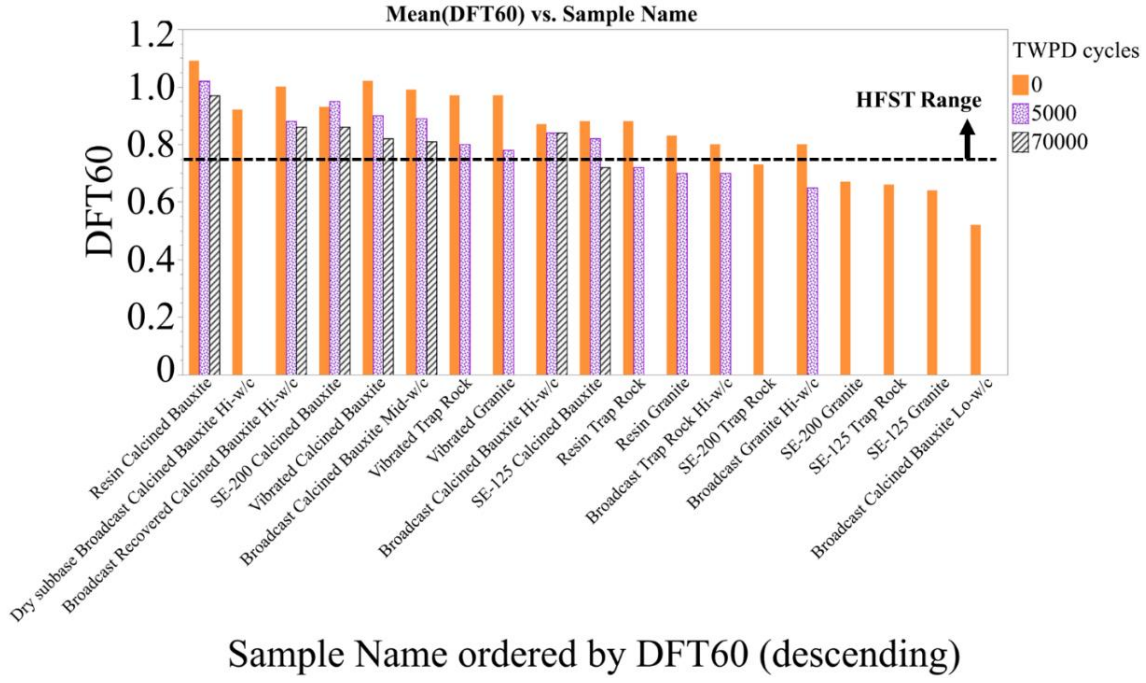


Figure 6.7: Average DFT 60 of Samples

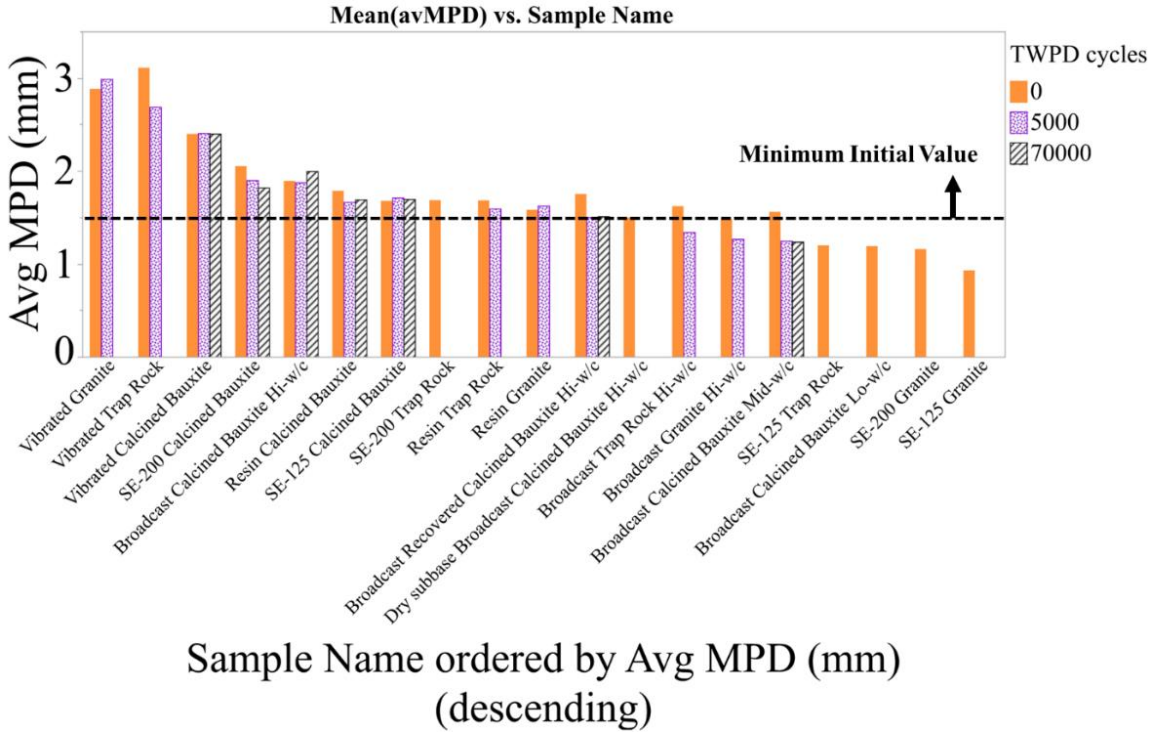


Figure 6.8: Average MPD of Samples

6.4.2.2. Comparison of Methods and Aggregate

Unpolished sample data sorted by the method used overlaid by the aggregate type is shown in **Figure 6.9**, **Figure 6.10**, **Figure 6.11**, **Figure 6.12**, and **Figure 6.13**. The data in these figures did not include any of the additional calcined bauxite variations therefore each bar represents a single sample where the Calcined Bauxite slabs were constructed in the same manner as the other aggregates in that group. Additionally, error bars (representative of one standard deviation from the mean) are shown for texture measurements to indicated differences in variance. The data indicate that the primary factor for macrotexture appears to the method used, with the use of vibration clearly producing higher levels. Interestingly, an unintended consequence of vibration appeared to be the introduction of additional texture at longer wavelengths than the aggregate. Presumably, the vibration mobilized the binder causing it to travel though the interaggregate spaces. The method of adding additional aggregate in construction as paste moved to the surface likely contributed to the effect as well. The effect is shown on the Vibrated Trap Rock sample, prior to conditioning depicted in **Figure 6.16**. Based on these results vibration not only produced higher texture (and shorter outflow time) (**Figure 6.9** and **Figure 6.10**) but also appeared to improve the friction at high speed where DFT60 was greatly improved with vibration (**Figure 6.13**) compared to broadcast samples. However, the difference was less pronounced at lower speed (**Figure 6.11** and **Figure 6.12**).

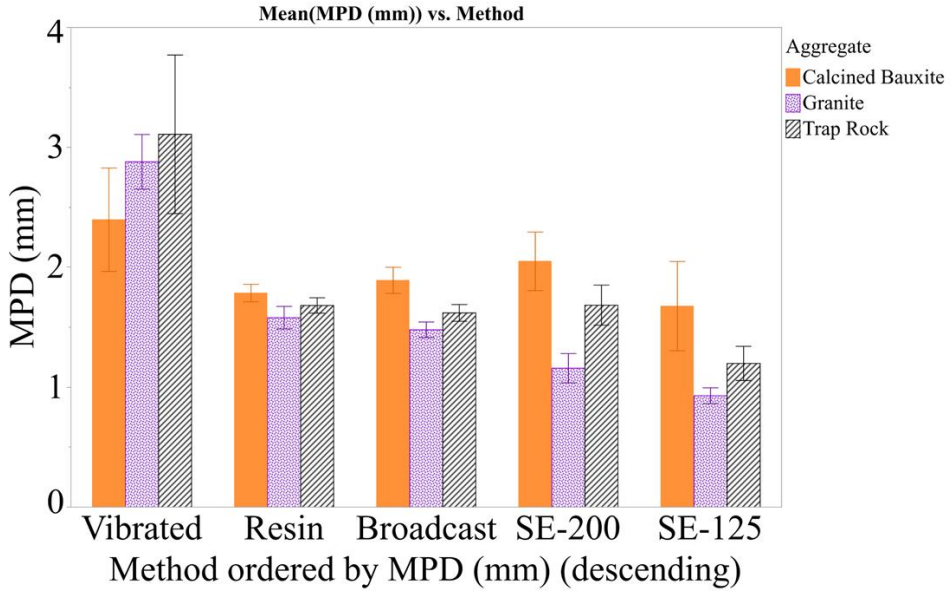


Figure 6.9: MPD by Application Method and Aggregate

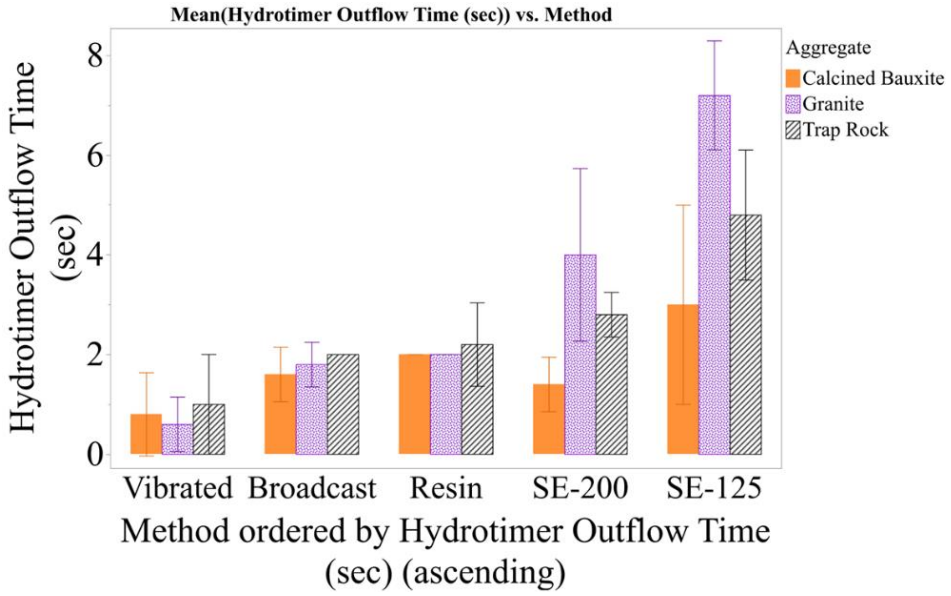


Figure 6.10: Hydrotimer Outflow Time by Application Method and Aggregate

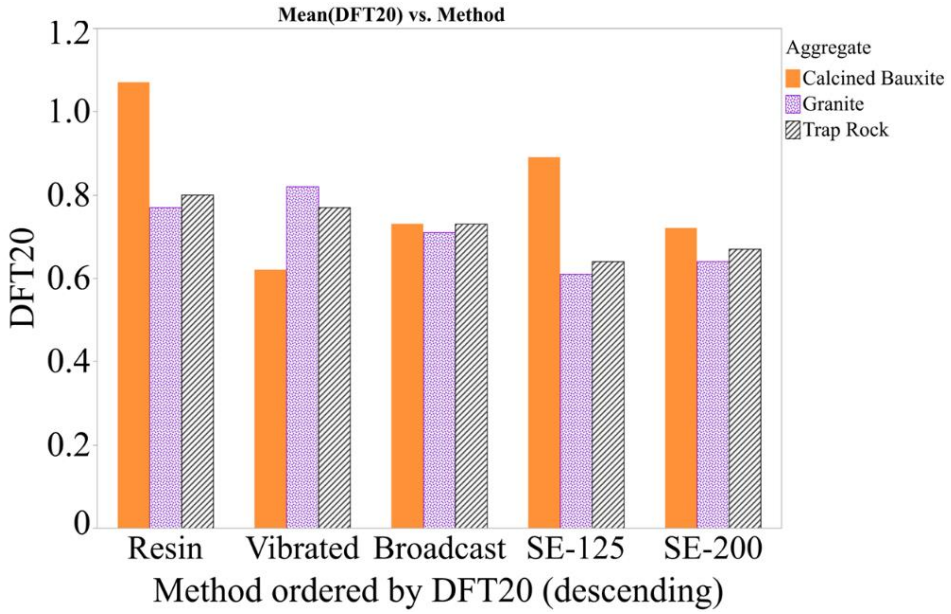


Figure 6.11: DFT20 by Application Method and Aggregate

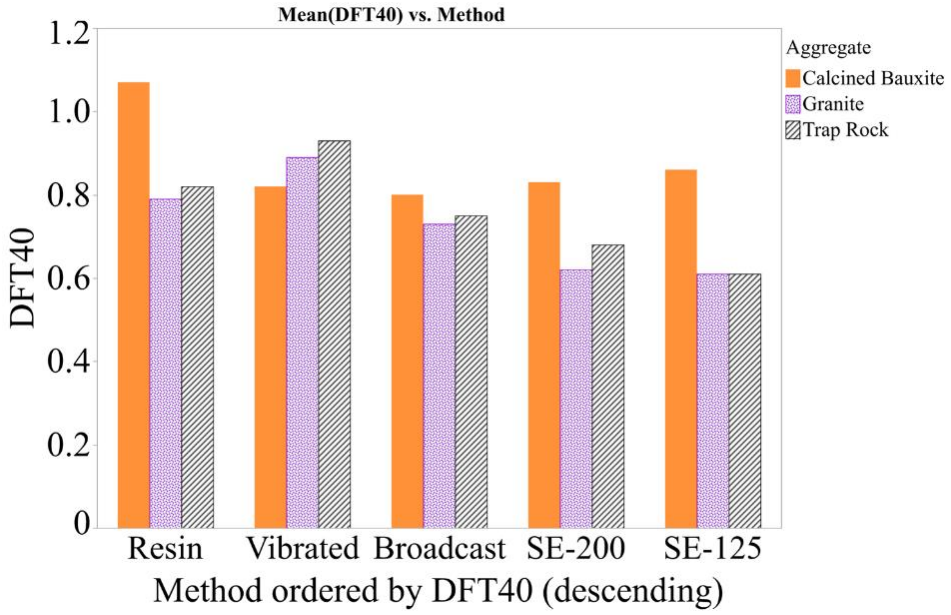


Figure 6.12: DFT40 by Application Method and Aggregate

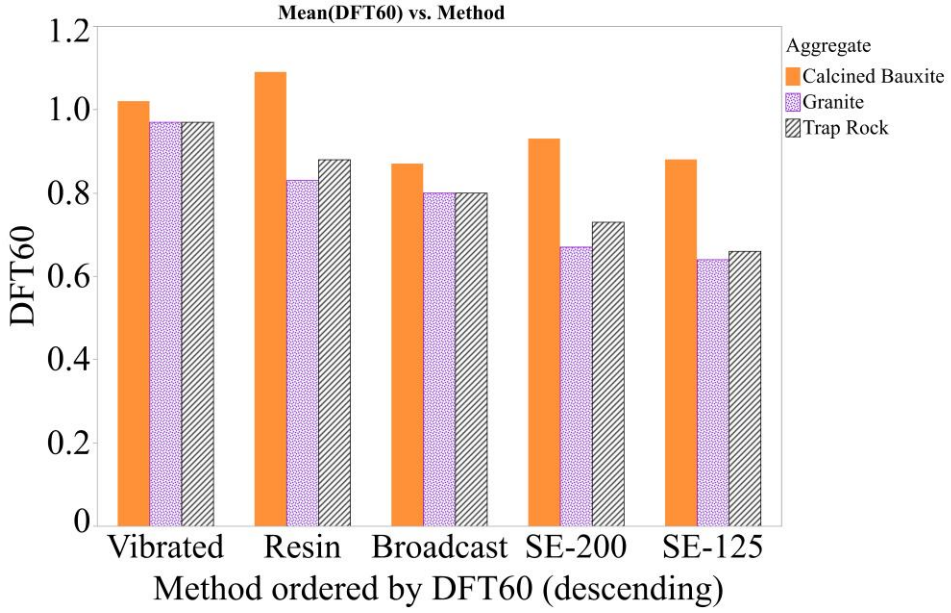


Figure 6.13: DFT60 by Application Method and Aggregate

This appears to be due to the tendency for the macrotexture component of texture to contribute more to friction at higher speeds and improve drainage of water film at the surface [1]. The linear

regression and ANOVA residual normal quantile plot illustrating the relationship between drainage from the outflow meter and the measured MPD is shown in Error! Reference source not found.. The outflow times indicated that all the samples provided between medium and low dynamic hydroplaning potential based on Air Force Civil Engineer Center values used for airfields, with the retarded samples have longer times related to their lower texture [2]. The interactions among speed, friction and macrotexture are illustrated by the relationship between the DFT measurements at 20, 40 and 60, and the measured MPD for these samples, where the strength of the relationship increases with increasing speed as shown in the linear regressions and ANOVA residual normal quantile plots in **Figure 6.15**.

outperformed the other aggregates in friction and macrotexture across similar methods except for the vibrated methods, where the vibration induced effects appeared to exert stronger influence on the measured properties. Still the findings at zero and 5000 cycles were sufficient to determine that while the trap rock and granite aggregates were able to provide adequate texture and friction initially, the ability to maintain HFST quality properties was greatly diminished under polishing. Therefore, these would represent a risk for long-term safety if used in an HFST.

A final observation is from the variance in the texture measurements indicated by the standard deviation bars shown in **Figure 6.9** and **Figure 6.10**. The results indicate that the methods using UHPC resulted in textures that were more variable than those of the resin-based surfaces. This is supported by visual observations across the surfaces of variations due to factors such as vibration, retarding and washing process, and hand broadcasting, and that the resin surfaces appeared more consistent across the surfaces.

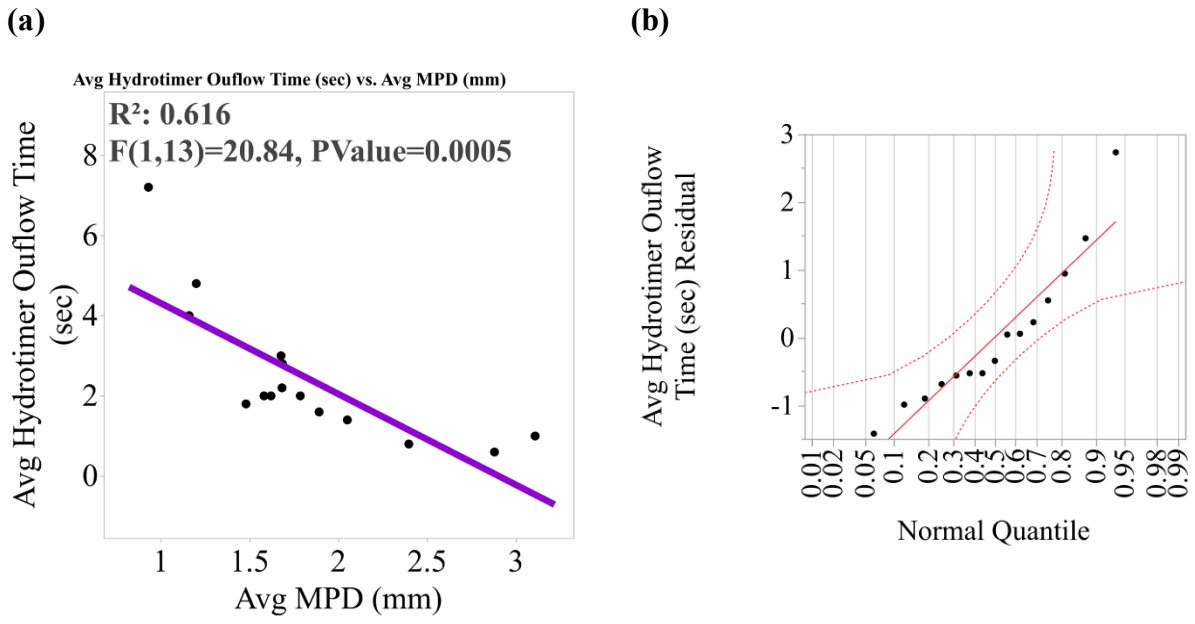


Figure 6.14: MPD effect on Outflow Time (a) linear regression, (b) normal quantile plot

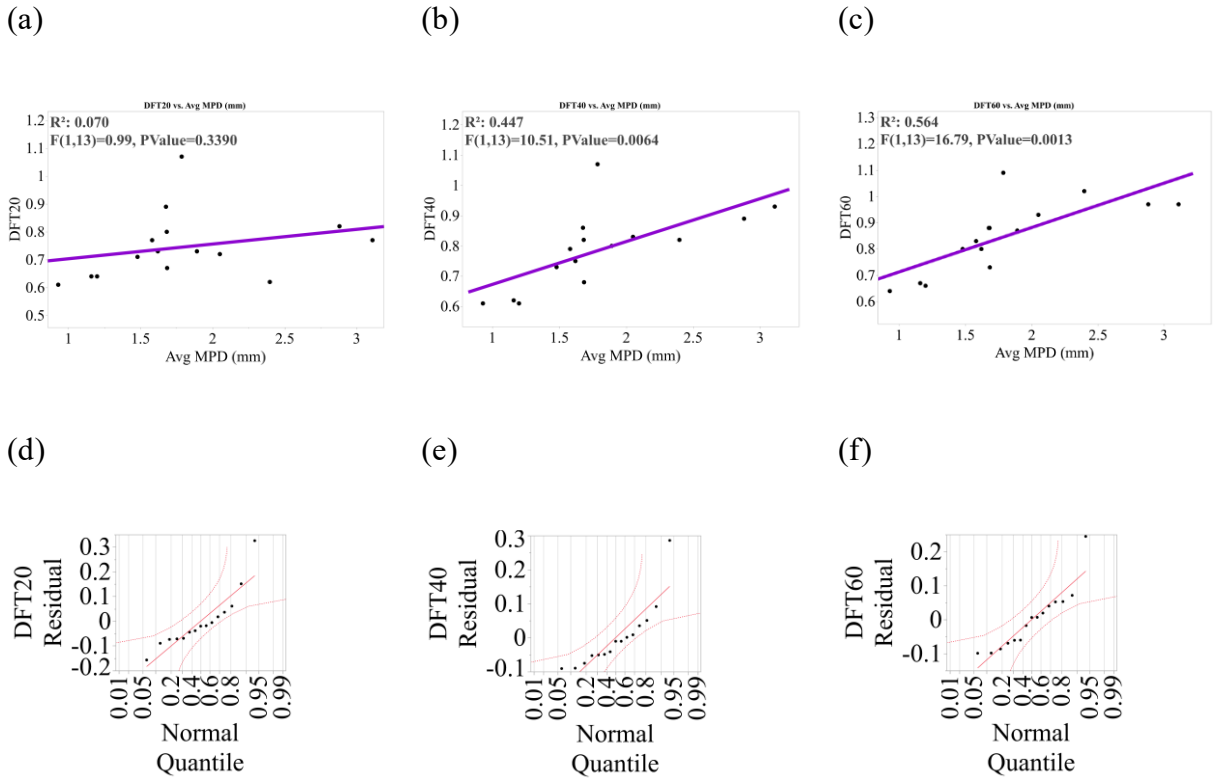


Figure 6.15: MPD Effect on Friction (a) DFT20 regression, (b) DFT40 regression, (c) DFT60 regression, (d) DFT20 Normal Quantile Plot, (e) DFT40 Normal Quantile Plot, (f) DFT60 Normal Quantile Plot

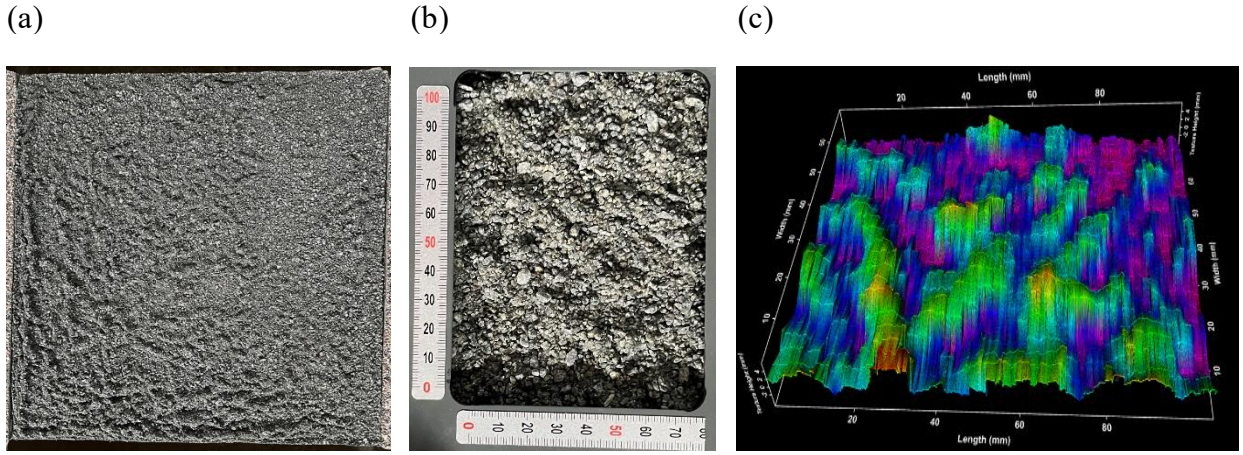


Figure 6.16: Vibration Induced Texture on Vibrate Trap Rock Sample (a) whole slab, (b) zoomed into selected area (c) LTS scan profiles (scales in mm)

It should be noted that the regressions presented are not intended as highly accurate predictive models, and are limited by the quantity of data, and variance and normality assumption requirements that may not be ideally met. However, they are presented to show the strength of relationship among the variables presented.

6.4.2.3. Effects of Water

The effects of water content were assessed from the unpolished sample data that included the UHPC-based sample variations of only the calcined bauxite aggregate. Therefore, each bar in the following figures represents a single sample which includes some of the previously presented variations, as well as the low w/c without vibration sample, the mid-w/c sample, the sample with recovered aggregate, and the dry substrate variation. The differences in DFT60 and MPD are shown in **Figure 6.17** And **Figure 6.18**.

No apparent negative effects were observed for the use of recovered calcined bauxite, however the laboratory techniques utilized for aggregate recovery are not representative of field conditions and therefore no conclusions about recovered aggregate should be drawn from this finding. The sample does however illustrate the variance in results across Hi-w/c samples and is included for comparative purposes. . No large disparity was observed for the dry substrate. The mid-w/c sample resulted in lower macrotexture than the high-w/c and vibrated lo-w/c, and while the mid-w/c provided higher friction than the hi-w/c initially, it decreased more under polishing. The low w/c without vibration performed worse overall and did not meet an HFST level of performance. However, it is noteworthy that just the addition of vibration to the low-w/c mix resulted in one of the top performing surfaces. One other observation was that the broadcast calcined bauxite Hi-w/c sample was relocated before being set, and some sloshing occurred which may have affected the final surface. This is a possible explanation of the lower observed friction compared to samples with the dry substrate and recovered aggregate which used the same mix w/c. Alternatively, the range among those three samples could simply be reflective of the inherent variability of these methods.

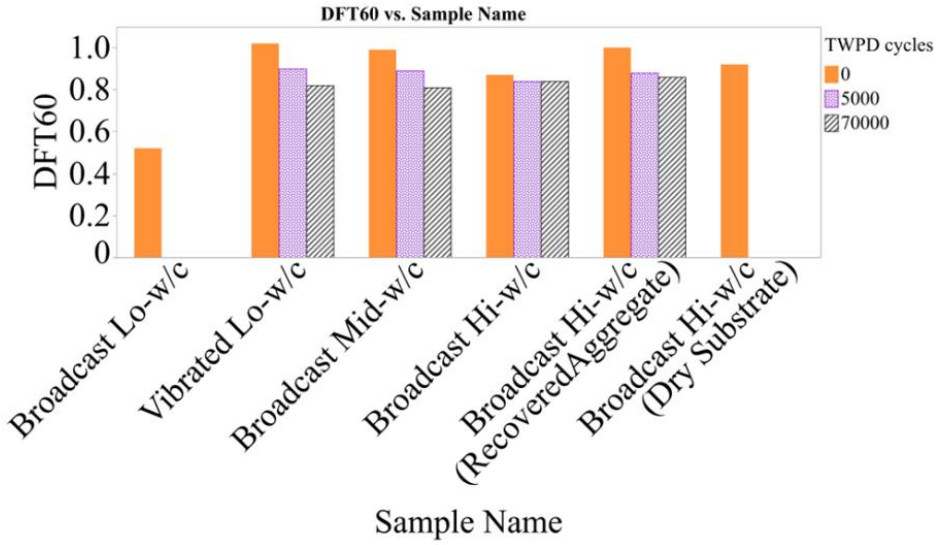


Figure 6.17: DFT60 of Calcined Bauxite Surfaces

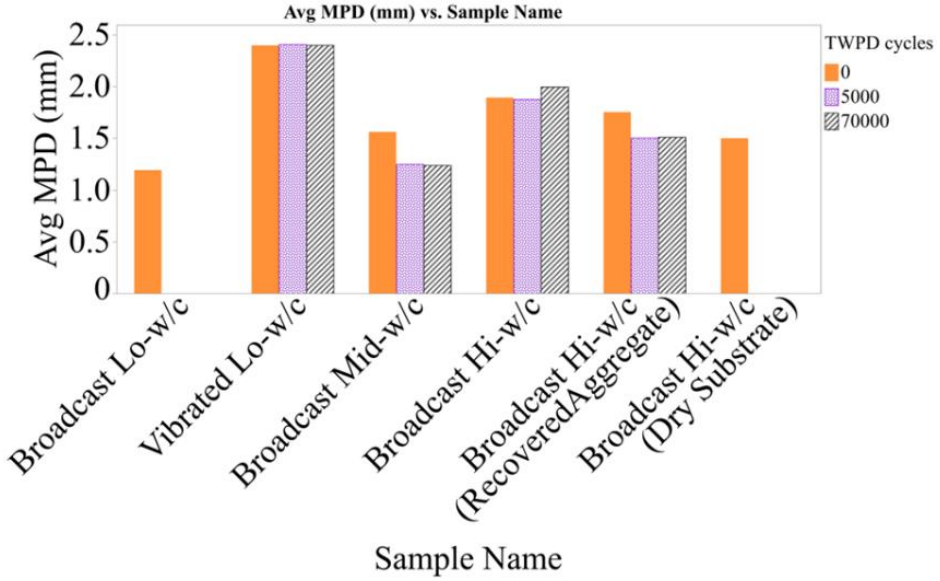


Figure 6.18: MPD of Calcined Bauxite Surfaces

6.4.2.4. Top Performers

The effect of TWPD cycles on the seven top performing methods DFT60 and MPD are shown in **Figure 6.19** and **Figure 6.20**, respectively. After 70,000 cycles all the samples maintained DFT60 above 0.75 except for the SE-125 calcined bauxite sample which dropped to 0.72. The increase in DFT60 after 5,000 cycles for the SE-200 sample is not easily explainable but could be due to polishing by removing excess paste from the surface or that the first measurement was under representative of the true friction. Six of the samples maintained MPD above 1.5 mm, while the

Broadcast Calcined Bauxite Mid-w/c sample dropped to 1.248 mm after 5,000 cycles and remained steady to 1.238 mm after 70,000 cycles. The MPD increases observed for some of the samples are difficult to reconcile, but likely due to the inherent variations in the texture, the different areas measured at unpolished and polished conditions and the difficulty of precisely placing the LTS to measure the same profile. While vibration was able to provide high levels of macrotexture, the resin-based HFST remained the premier performer in high-speed friction and provided a more uniform surface. None of the alterative aggregates were able to match the performance of calcined bauxite.

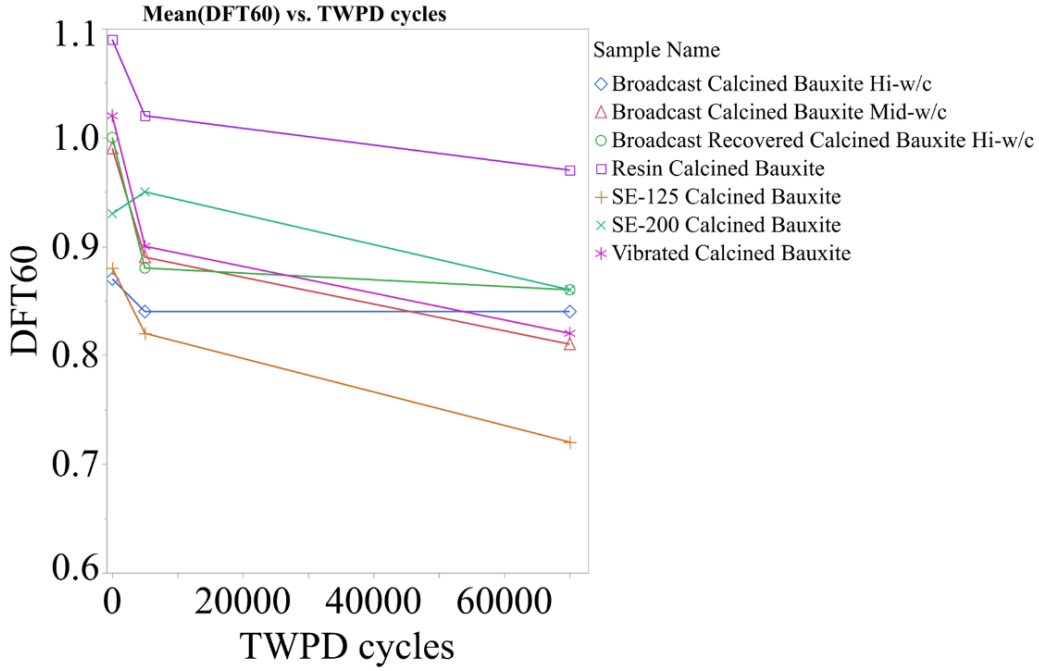


Figure 6.19: TWPD Cycles Effect on DFT60

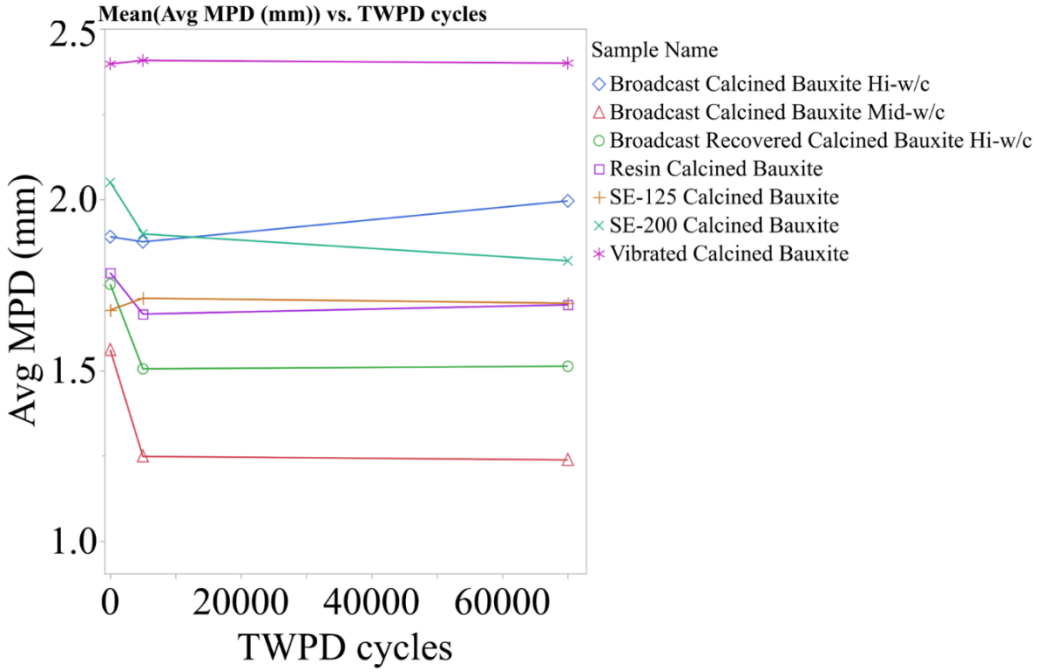


Figure 6.20: TWPD Cycles Effect on MPD

6.4.2.5. Error and Variability

During the study, some operational issues and variations were encountered which could have introduced some variability into the study but are not believed to greatly affect the overall findings of the study. Pressure washing was observed to be subject to potential operator bias along with BPT operation.

Other potential sources of additional variability include the possibility of unrepresentative aggregate samples used in testing (sample splitting was not conducted on aggregate samples), minor differences in gradation from the sieving, crushing and remixing operations or any other differences due to researcher induced effects, error, oversight, and equipment operation or standard test variations across the testing not described herein. Additional details are provided in one of this report's author's dissertation [90]. Statistical analysis and several figures in this chapter were generated using JMP pro-16.

6.5. Conclusions

6.5.1. Phase 1: Evaluation of Application Methods

Testing results on white deposits found on the surface of broadcast samples were consistent with carbonated calcium hydroxide (calcium carbonate), indicating excess aggregate moisture was intermixing with the UHPC binder and depositing high water content cement on the surface creating potential weak areas. Therefore, OD aggregate is recommended for UHPC-based HFSTs.

In assessing the various application methods, the resin-based surface provided the highest BPN friction. However, all methods were able to produce a high level of friction over a BPN of 83, exceeding the western transportation institute stated HFSTs lower range of BPN of 65, except for unwashed sample [39].

The use of UHPC was found to greatly decrease the effective depth of etch of surface retarders compared to the manufacturer's advertised depth. This is presumed to be due to the low water content of the binder. However, utilizing higher grades of retarders adequate macrotexture was achieved.

Although vibrated OD and SSD broadcast samples failed to reach the target 1.5 mm MPD threshold, they were also not statistically significantly different that the un-vibrated broadcast samples according to the Tukey's HSD results and the acceptable range of MPD for HFSTs go down to 1.0 mm [8]. Furthermore, the BPN of the vibrated samples exceeded that of all the samples except the resin-based surface. Therefore, all the broadcast samples and high-grade retarded surfaces are considered a potentially viable alternative to resins. There was not a significant difference in MPD between the washed surface with no retarder used and some of the lower grade retarders.

6.5.2. Phase 2: Performance of UHPC-Based HFST

Aggregates were able to effectively embed under self-weight when the UHPC mix had sufficient flow. Under the lowest water content, aggregate was not able to effectively embed in the binder under self-weight, however this was able to be overcome with the addition of vibration to the surface which resulted in a surface with adequate embedment and additional surface texture effects. Alternative aggregates to calcined bauxite did not perform acceptably under polishing.

The resin-based system with calcined bauxite aggregate (the traditional HFST makeup) produced the best friction performance at high speed and maintained it after polishing. Additionally, the resin-based surfaces provided a more consistent surface. However, UHPC-based methods were able to provide sufficient friction and texture. The texture and friction were maintained after polishing such that the surfaces produced could be considered viable HFSTs.

When considering the laboratory methods utilized and the challenges presented by them a full-scale application of these materials would require a method that is reproducible and minimizes operator errors as much as possible. While broadcast methods are possible, they could produce challenges with consistent and reliable embedment. The use of surface retarders is proven as a general method in the production of EACP, and adaptation of existing methods and technologies for EACP could provide the most feasible solution for near-term scaled production of UHPC-based HFSTs.

CHAPTER 7: CONCLUSIONS AND RECOMMENDATIONS

7.1. Introduction

Maintaining safe roadways and reducing crashes is of vital importance to transportation agencies. In crash prone areas the implementation of HFSTs has been a proven mitigation strategy but comes at high material costs. Two opportunities exist to reduce that cost, alternative aggregates, and alternative binders, both of which were assessed in this research. The calcined bauxite aggregates typically used in HFSTs are expensive compared to traditional aggregate materials. The current pricing for 2024 is approximately $750 per ton for calcined bauxite. Standard local aggregates could greatly reduce that cost if they can provide adequate performance. Aggregate sources local to the southeastern united states were evaluated for this purpose. Current pricing for 2024 for epoxy resins typically used in HFST range from around $400-500 for a 4-gallon application, which equates to an approximate range of $3.74 to $4.67 per square foot at the prescribed 60 mils thickness. Alternatively, a 2013 FHWA study showed nonproprietary UHPC material costs without steel fiber at around $500 per cubic yard [11]. Even if adjusted for inflation to 2024 using the Bureau of Labor Statistics CPI Inflation calculator, it would be about $671.28 [12]. This would give a unit cost of $0.52 per square foot at 0.25 inches.

7.2. Experimental Findings

7.2.1. Aggregate Conclusions

The work described in chapter four developed a novel technique for measuring the microtexture of aggregate samples for use in HFST applications. In conjunction with micro-deval and Los Angeles abrasion tests, the texture, friction and the effects of gradation and abrasion on these aggregate characteristics were studied across four alternative aggregates and in comparison, to calcined bauxite. Calcined bauxite outperformed the other aggregate in the testing, however two of the alternatives showed potential as suitable HFST aggregates, a North Carolina trap rock, and a Georgia granite. These aggregates were integrated into sample HFST surfaces utilizing UHPC-based binders as well as traditional epoxy resin. While the aggregates were able to provide high initial friction and adequate macrotexture, the friction dropped under polishing compared to calcined bauxite samples which were able to maintain high levels of friction after polishing. The use of the alternative aggregates tested cannot be recommended for long-term friction performance.

7.2.2. UHPC Mix Design Conclusions

In assessing the potential for UHPC-based HFSTs a study of mix design was conducted to determine if the UHPC could meet performance criteria for its intended use. The results indicated bond strength, compressive strength, and flowability could match or exceed guidelines set in place for equivalent systems. However, the performance of epoxy HFST binders on asphalt overlays greatly exceeds that of the UHPC especially for the compatibility of the coefficient of thermal expansion and pull-off bond strength. When intermixing calcined bauxite to the UHPC an increased compressive strength and abrasion resistance was observed, but bond strength was

negatively affected. Additionally, the inclusion of calcined bauxite reduced the workability which indicates the need for external vibration, compaction, or other methods to aid with placement at full scale.

Evaluation of the content of calcined bauxite in the UHPC showed that while a calcined bauxite to cementitious material ratio CB/CM of 2.5 provided the highest density, it did not offer the highest compressive strength, bond strength, or abrasion resistance. Instead, CB/CM of 2.0, which provided an elevated packing had the highest compressive strength at 16.7 ksi at 28-days. Bond strength testing showed lower CB mixes provided better bonds (especially at earlier age). Additionally, the shrinkage of these UHPCs increased with increased binder content. The results indicate a trade-off in calcined bauxite content benefits (higher compressive strength and reduced shrinkage) and the reduced bond strength and workability. CB/CM of 1.5 – 2.0 is the preferred ratio based on the testing results. Ultimately the work showed that UHPC can provide the mechanical properties necessary to be used as an HFST binder.

Finally, testing on the impact of including steel and glass fibers found an increase in compressive strength and decrease in early age shrinkage. However, due to the high cost of fibers and decrease in workability associated with their inclusion they are not recommended for use in HFSTs. However, if after field trial testing cracking proves a concern for UHPC-based HFSTs viability the inclusion of fibers may serve to reduce crack widths in service and improve viability. Furthermore, additional testing should investigate the tensile strain capacity of UHPC with fibers to quantify the increase in ductility

7.2.3. UHPC-Based HFST Performance Conclusions

The studies conducted revealed several key findings related to UHPC-based HFSTs. The coarse aggregate to cementitious material ratio should not exceed 3.0 by mass (which was also made clear by the mix design study). For intermixing coarse aggregate into UHPC the use of washing or surface retarding is required to reveal the aggregate microtexture necessary for high friction. When broadcasting the aggregate, the use of vibration resulted in better aggregate embedment into the binder, therefore without vibration, getting adequate aggregate embedment for broadcasting the aggregate required a high flow mix.

Excess aggregate moisture can result in pockets of high-water content cement within the binder, therefore only oven dry aggregate is recommended for UHPC-based HFSTs. Resin-based systems provided superior performance to that of UHPC-based systems. However, the UHPC-based systems utilizing gravity embedment, vibration embedment and intermixing with surface retarding all were able to produce acceptable levels of friction and texture and maintain the performance under polishing such that they can be categorized as HFSTs. Overall, as proof of concept, this research showed that UHPC can be used as an HFST binder using calcined bauxite coarse aggregate, achieving the main objective of developing and assessing the performance of a UHPC-based HFST. This makes the use of such systems worthy of further research and larger scale testing a reasonable next step.

7.3. Future Research Recommendations

There is an opportunity to further develop the microtexture methods utilized in this study. Alternative methods in data processing could improve the results. Additionally, other aggregate sources than those tested in this research could be evaluated for potential in HFSTs. The use of fibers, shrinkage mitigation techniques, and effects of substrate moisture on the performance of the mix designs should be further investigated. The surfaces produced with UHPC binders provided proof of concept for UHPC-based HFSTs. However, many other factors related to the performance and feasibility of these at full scale should be studied. Additionally, the effects of temperature, humidity, sun exposure, wind speed or other environmental factors on the performance of UHPC-based HFSTs should be evaluated. The effects observed with vibration are worthy of further study to evaluate the different effects of the applied mass, frequency, amplitude, and area of the applied vibration. Finally, the proper equipment for full scale paving should be assessed to adapt lab methods to standard or custom paving operations equipment.

CHAPTER 8: REFERENCES

[1] Bieber C. The Most Dangerous States For Drivers. Forbes 2023.

[2] Coppinger K, Keen M, Gissel J, Rainville L. High Friction Surface Treatments Final Report. FHWA Report 2021.

[3] Merritt D, Lyon C, Persaud B, Torres H. Developing Crash-Modification Factors for High-Friction Surface Treatments. FHWA Report 2020.

[4] Wilson B, Wang KC, Li JQ, Yang G. Recommendations Report for High Friction Surface Treatments: Candidate Sites, Materials, and Construction. 2020.

[5] Wilson B, Mukhopadhyay A. Alternative Aggregates and Materials for High Friction Surface Treatments. Final Report 2016.

[6] Federal Highway Administration. Pavement Comparative Analysis Technical Report Comprehensive Truck Size and Weight Limits Study. FHWA 2015.

[7] Atkinson J, Clark J, Ercisli S. High Friction Surface Treatment Curve Selection and Installation Guide. FHWA Report 2016.

[8] Merritt D, Himes S, Porter RJ. High Friction Surface Treatment Site Selection and Installation Guide. FHWA Report 2021.

[9] Hall JW, Smith KL, Titus-Glover L, Wambold JC, Yager TJ, Rado Z. Guide for pavement friction. Final Report for NCHRP Project 2009;1:43.

[10] Vulcan Materials Company. Vulcan Reports Fourth Quarter and Full Year 2022 Results. 2023.

[11] Graybeal BA. Development of non-proprietary ultra-high performance concrete for use in the highway bridge sector: TechBrief. 2013.

[12] Bureau of Labor and Statistics. CPI Inflation Calculator. 2024.

[13] Tsai YJ, Wang Z, Pranav C, Yu PL, Knezevich RW. Critical Assessment of HFST's Long-Term Performance in Georgia Under Different Roadway Conditions. 2022.

[14] Naaman AE, Wille K. The path to ultra-high performance fiber reinforced concrete (UHP-FRC): five decades of progress. Proceedings of Hipermat 2012:3–15.

[15] Graybeal B. Ultra-high performance concrete. 2011.

[16] Eide MB, Hisdal J. Ultra-high performance fibre reinforced concrete (UHPFRC)–State of the art: FA 2 Competitive constructions: SP 2.2 Ductile high strength concrete. 2012.

[17] Andresen A, Wambold JC. Friction fundamentals, concepts and methodology. 1999.

[18] Blau PJ. Amontons' laws of friction. Encyclopedia of Tribology.Springer, Boston 2013:71.

[19] PIARC. Term of the Road Dictionary: microtexture. PIARC 2022.

[20] PIARC. Term of the Road Dictionary: megatexture. PIARC 2022.

[21] PIARC. Term of the Road Dictionary: macrotexture. PIARC 2022.

[22] Veneziano D, Vilwock-Witte N. Safety Opportunities in High Friction Surfacing. ATSSA Report 2013.

[23] Zhao H, Wei F, Wang C, Li S, Shan J. Determination of Friction Performance of High Friction Surface Treatment Based on Alternative Macrotexture Metric. Materials 2021;14.

[24] Federal Highway Administration. Case Study: South Carolina US 25-Greenville County. FHWA 2015.

[25] Li S, Noureldin S, Zhu K, Jiang Y. Pavement surface microtexture: Testing, characterization, and frictional interpretation. In: Anonymous Pavement Performance: Current Trends, Advances, and Challenges: ASTM International; 2012.

[26] Zuniga-Garcia N, Prozzi JA. Contribution of Micro-and Macro-Texture for Predicting Friction on Pavement Surfaces. 2016.

[27] Serigos PA, Buddhavarapu P, Gorman GM, Hong F, Prozzi JA. The contribution of micro-and macro-texture to the skid resistance of flexible pavement. 2016.

[28] Flintsch GW, de León Izeppi E, Bongioanni V, Katicha SW, Meager K, Fernando E et al. Protocols for network-level macrotexture measurement. , 2021.

[29] Heitzman M, Moore J. Evaluation of laboratory friction performance of aggregates for high friction surface treatments. NCAT Report 2017:17–01.

[30] Heitzman M, Turner P, Greer M. High Friction Surface Treatment Alternative Aggregates Study. NCAT Report 2015.

[31] Bartlett JW, Frost C. Reliability, repeatability and reproducibility: analysis of measurement errors in continuous variables. Ultrasound in obstetrics & gynecology 2008;31.

[32] Rangaraju PR, Edlinski J. Comparative evaluation of micro-deval abrasion test with other toughness/abrasion resistance and soundness tests. J Mater Civ Eng 2008;20:343–51.

[33] Kuzmanić T, Lebar K, Mikoš M. Comparison of different-energy-level abrasion in Los Angeles and micro-Deval apparatuses using mass loss and rounding of sediment particles. Applied Sciences 2023;13:6102.

[34] Kamani M, Ajalloeian R. Investigation of the changes in aggregate morphology during different aggregate abrasion/degradation tests using image analysis. Constr Build Mater 2022;314:125614.

[35] Quintanilla ID. Multi-scale study of the degradation of railway ballast. 2018.

[36] Nålsund R. Railway ballast characteristics, selection criterion and performance. 2014.

[37] Zuniga-Garcia N, Prozzi JA. High-definition field texture measurements for predicting pavement friction. Transp Res Rec 2019;2673:246–60.

[38] El-Ashwah AS, Broaddus K, Abdelrahman M. Predicting the friction coefficient of high-friction surface treatment application aggregates using the aggregates' characteristics. J Mater Civ Eng 2023;35:04023089.

[39] Coulter ZC. Safety Opportunities in High Friction Surfacing. Transportation Research Record 2013.

[40] Teng, Valipour, Khayat. Design and performance of low shrinkage UHPC for thin bonded bridge deck overlay. Cement and Concrete Composites 2021;118.

[41] Farzad, Shafieifar, Azizinamini. Experimental and numerical study on bond strength between conventional concrete and Ultra High-Performance Concrete (UHPC). Engineering Structures 2019;186:297.

[42] Wu P, Wu C, Liu Z, Hao H. Investigation of shear performance of UHPC by direct shear tests. Engineering Structures 2019;183:780.

[43] Kusumawardaningsih Y, Fehling E, Ismail M, Aboubakr AAM. Tensile Strength Behavior of UHPC and UHPFRC. Procedia Engineering 2015;125:1081.

[44] Li, Wang, Chen, Wu, Han, Hou et al. Design and application of UHPC with high abrasion resistance. Construction and Building Materials 2021;309.

[45] Feng S, Xiao H, Liu M, Zhang F, Lu M. Shear behaviour of interface between normal-strength concrete and UHPC: Experiment and predictive model. Construction and Building Materials 2022;342.

[46] Haber, Munoz, De La Varga, Graybeal. Bond characterization of UHPC overlays for concrete bridge decks: Laboratory and field testing. Construction and Building Materials 2018;190:1056.

[47] Sritharan. Design of UHPC Structural Members: Lessons Learned and ASTM Test Requirements. Advances in Civil Engineering Materials 2015;4:113.

[48] Kim HS, Chin WJ, Cho JR, Kim YJ, Yoon H. An Experimental Study on the Behavior of Shear Keys According to the Curing Time of UHPC. ENG 2015;07:212.

[49] Hung, El-Tawil, Chao. A Review of Developments and Challenges for UHPC in Structural Engineering: Behavior, Analysis, and Design. J Struct Eng 2021;147.

[50] Yu, Spiesz, Brouwers. Development of an eco-friendly Ultra-High Performance Concrete (UHPC) with efficient cement and mineral admixtures uses. Cement and Concrete Composites 2014;55:383.

[51] Liu K, Yin T, Fan D, Wang J, Yu R. Multiple effects of particle size distribution modulus (q) and maximum aggregate size (Dmax) on the characteristics of Ultra-High Performance concrete (UHPC): Experiments and modeling. Cement and Concrete Composites 2022;133.

[52] Wang X, Yu R, Song Q, Shui Z, Liu Z, Wu S et al. Optimized design of ultra-high performance concrete (UHPC) with a high wet packing density. Cement and Concrete Research 2019;126.

[53] PCA. Soil-Cement Laboratory Handbook. Report 1992.

[54] Dingqiang F, Rui Y, Zhonghe S, Chunfeng W, Jinnan W, Qiqi S. A novel approach for developing a green Ultra-High Performance Concrete (UHPC) with advanced particles packing meso-structure. Construction and Building Materials 2020;265.

[55] Dingqiang F, Yu R, Kangning L, Junhui T, Zhonghe S, Chunfeng W et al. Optimized design of steel fibres reinforced ultra-high performance concrete (UHPC) composites: Towards to dense structure and efficient fibre application. Construction and Building Materials 2020;273.

[56] Chen, Gu, Heitzman, Powell, Kowalski. Influences of alternative friction aggregates on texture and friction characteristics of high friction surface treatment. Construction and Building Materials 2021;314.

[57] Yu, Xiong, Li, Cong, Shah, Jiang. Laboratory Evaluation of Critical Properties and Attributes of Calcined Bauxite and Steel Slag Aggregates for Pavement Friction Surfacing. J Mater Civ Eng 2019;31.

[58] Hossain M. Performance of Local Aggregate in High Friction Surface Treatment. Master's Thesis 2016.

[59] De Larrard F, Sedran T. High and ultra-High performance concrete in pavement : tools for the road eternity.

[60] De Larrard F, Sedran T, Petit J, Blanchard J, Auffret P, Charlicart S et al. Grooved Fibre-Reinforced ultra-High Performance Concrete: A New Material For Pavement Long-Lasting Wearing Course. Symposium on UHPFRC 2013.

[61] Hiremath PN, Yaragal SC. Influence of mixing method, speed and duration on the fresh and hardened properties of Reactive Powder Concrete. Construction and Building Materials 2017;141:271.

[62] Wu, Khayat, Shi. Changes in rheology and mechanical properties of ultra-high performance concrete with silica fume content. Cement and Concrete Research 2019;123.

[63] Feng, Xiao, Li. Influence of interfacial parameters and testing methods on UHPC–NSC bond strength: Slant shear vs. direct tensile testing. Cement and Concrete Composites 2022;131.

[64] Lyons K. Evaluation of Rubber Modified Porous Asphalt Mixtures. Master's Thesis 2012.

[65] SCDOT. Supplemental Specification: High Friction Surface Treatment. SCDOT Supplemental Specification 2015.

[66] Wang R, Gao X, Huang H, Han G. Influence of rheological properties of cement mortar on steel fiber distribution in UHPC. Construction and Building Materials 2017;144:65.

[67] Gu X, Tan H, He X, Zhang J, Li M, Su Y et al. Nano C-S-H seeds prepared from ground granulated blast-furnace slag-carbide slag and its application in Portland cement. Construction and Building Materials 2022;329.

[68] Su Y, Luo B, Luo Z, Huang H, Li J, Wang D. Effect of Accelerators on the Workability, Strength, and Microstructure of Ultra-High-Performance Concrete. Materials 2021;15.

[69] Yu J, Cong P, Wu S. Laboratory investigation of the properties of asphalt modified with epoxy resin. J of Applied Polymer Sci 2009;113:3557.

[70] Liu Y, Wei Y, Asce M. Internal Curing by Porous Calcined Bauxite Aggregate in Ultrahigh-Performance Concrete.

[71] Lim, Hong. Slant Shear Test for Determining the Interfacial Shear Strength of Concrete Strengthened with Ultra-High Performance Fiber Reinforced Concrete. Journal of the Korea Concrete Institute 2016;28:637.

[72] Steph LM, Durham S, Liu R. Performance of Thin Bonded Epoxy Overlays on Asphalt and Concrete Bridge Deck Surfaces. CDOT Report 2014.

[73] Pranav C, Tsai Y(. High Friction Surface Treatment Deterioration Analysis and Characteristics Study. Transportation Research Record 2021;2675:370.

[74] AASHTO. AASHTO MP 41-13: Standard Practice for High Friction Surface Treatment for Asphalt and Concrete Pavements. AASHTO Standard Practice 2013.

[75] Tran NP, Gunasekara C, Law DW, Houshyar S, Setunge S, Cwirzen A. A critical review on drying shrinkage mitigation strategies in cement-based materials. Journal of Building Engineering 2021;38.

[76] Frosch R, Fowler D, Nawy E, Hansen W, Brander M, Haynes H et al. Control of Cracking in Concrete Structures. ACI Report 2017.

[77] Bissonnette B, Pierre P, Pigeon M. Influence of key parameters on drying shrinkage of cementitious materials. 1999.

[78] Roziere E, Cortas R, Loukili A. Tensile behaviour of early age concrete: New methods of investigation. Cement and Concrete Composites 2014;55:153.

[79] Dai J, Huang B, Shah SP. Recent Advances in Strain-Hardening UHPC with Synthetic Fibers. J Compos Sci 2021;5.

[80] Sabih G, Rahman T, Tarefder RA. Quantifying the impact of coefficient of thermal expansion of overlay concrete on unbonded concrete overlay performance. Heliyon 2018;4.

[81] Zhu W, Wei J, Li F, Zhang T, Chen Y, Hu J et al. Understanding restraint effect of coarse aggregate on the drying shrinkage of self-compacting concrete. Construction and Building Materials 2016;114:458.

[82] Fung WWS, Kwan AKH. Effect of particle interlock on flow of aggregate through opening. Powder Technology 2013;253:198.

[83] Nežerka V, Bílý P, Hrbek V, Fládr J. Impact of silica fume, fly ash, and metakaolin on the thickness and strength of the ITZ in concrete. Cement and Concrete Composites 2019;103:252.

[84] Holt E, Leivo M. Cracking risks associated with early age shrinkage. Cement and Concrete Composites 2004;26:521.

[85] Kronliif A, Leivo M, Sipari P. Experimental Study on the Basic Phenomena of Shrinkage and Cracking of Fresh Mortar. 1995.

[86] American Concrete Institute. 239R-18: Ultra-High Performance Concrete: An Emerging Technology Report. 2018.

[87] Sivakumar A, Santhanam M. Mechanical properties of high strength concrete reinforced with metallic and non-metallic fibres. Cement and Concrete Composites 2007;29:603.

[88] Sivakumar VR, Kavitha OR, Prince Arulraj G, Srisanthi VG. An experimental study on combined effects of glass fiber and Metakaolin on the rheological, mechanical, and durability properties of self-compacting concrete. Applied Clay Science 2017;147:123.

[89] Meng W, Khayat KH. Effect of Hybrid Fibers on Fresh Properties, Mechanical Properties, and Autogenous Shrinkage of Cost-Effective UHPC. Journal of materials in civil engineering 2018;30.

[90] Maeger KF. Ultra High-Performance Concrete as a High Friction Surface Treatment for Pavements and Bridges. ProQuest Dissertations and Theses 2024.

[91] Lee J, Shields T. Treatment guidelines for pavement preservation. 2010.

[92] Shuler S. Manual for emulsion-based chip seals for pavement preservation. : Transportation Research Board, 2011.

[93] Li S, Noureldin S, Jiang Y, Sun Y. Evaluation of pavement surface friction treatments. 2011.

[94] Yamada A. Asphalt seal coat treatments. Transportation Research Record 1999.

[95] Wu Z. Performance evaluation of various rehabilitation and preservation treatments. 2010.

[96] NCAT. Evaluation of Rejuvenating Fog Seals. Auburn University 2019.

[97] Wang H, Wang Z. Evaluation of pavement surface friction subject to various pavement preservation treatments. Constr Build Mater 2013;48:194–202.

[98] Merritt DK, Lyon C, Persaud B. Evaluation of pavement safety performance. 2015.

[99] Abaza OA, Chowdhury TD, Arafat M. Comparative analysis of skid resistance for different roadway surface treatments. Am.J.Eng.Appl.Sci 2017;10:890–9.

[100] Howard IL. Chip and scrub seal field test results for Hwy 17 and Hwy 35. 2009.

[101] Putman BJ, Danish B, Lyons KR, Nekkanti H, Repik TS. Evaluation of Open Graded Friction Courses: Construction, Maintenance, and Performance Phase II. 2021.

[102] King W, Kabir S, Cooper SB, Abadie C. Evaluation of open graded friction course (OGFC) mixtures. 2013.

[103] Johnston CJ. Maximizing the lifespan of open-graded friction course on South Carolina highways. South Carolina State Documents Depository 2019.

[104] Wu Z, King B. Development of surface friction guidelines for LADOTD. 2012.

[105] Gao L, de Fortier Smit A, Prozzi JA, Buddhavarapu P, Murphy M, Song L. Milled pavement texturing to optimize skid improvements. Constr Build Mater 2015;101:602–10.

[106] Jones K, Lane Jr OJ. Shotblasting to Improve Frictional Properties. 1992.

[107] Plati C, Georgouli K, Papadimitriou F, Loizos A. Performance of shotblasting as a pavement preservation technique. 2014.

[108] Sarkar MTA, Gu F, Heitzman M, Powell B. Influence of shotblasting treatment on asphalt pavement performance. International Journal of Pavement Engineering 2022;23:4831–44.

[109] Snyder MB. Pavement surface characteristics: a synthesis and guide. , 2006.

[110] Neuman TR, Pfefer R, Slack K, Hardy KK, Council F, McGee H et al. Volume 6: A guide for addressing run-off-road collisions, NCHRP Report 500. Transportation Research Board of the National Academies, Washington, DC 2003;8:9.

[111] Wibowo H, Sritharan S. Use of ultra-high-performance concrete for bridge deck overlays. 2018.

[112] Hoerner TE, Smith KD, Larson RM, Swanlund ME. Current practice of portland cement concrete pavement texturing. Transp Res Rec 2003;1860:178–86.

[113] Federal Highway Administration (FHWA). High Performance Concrete Pavements: Project Summary. FHWA 2006.

[114] Dąbrowski M, Glinicki MA, Gibas K, Antolik A, Dziedzic K. Influence of surface retarders on texture profile and durability of upper layer of exposed aggregate concrete pavement. 2019.

[115] Rith M, Kim YK, Lee SW. Characterization of long-term skid resistance in exposed aggregate concrete pavement. Constr Build Mater 2020;256:119423.

[116] Shen P, Chen W, Lu L, Geng H, Li Q. Effect of aggregate exposing and curing agent on the performance of exposed aggregate concrete. Constr Build Mater 2017;156:675–83.

APPENDIX A: OTHER PAVEMENT SURFACE TREATMENTS

There are numerous pavement surface treatment options available to agencies to repair and rehabilitate roadways. While not all of them are designed to address friction, in some cases the friction may be improved. The following section summarizes many of the options available, the expected level of friction and some data available on crash reduction.

A.1.1 Chip Seal with and without Fog Seal

A chip seal (sometimes called seal coat) consists of a layer of asphalt emulsion sprayed onto a pavement surface upon which a layer of aggregates (typically 0.25 to 0.5 inch diameter) is placed [91,92]. The aggregate layer is then rolled using pneumatic tires to imbed the aggregate in the asphalt and excess aggregate is removed. Chip seals are a wearing course that serves the purpose of sealing cracks and preventing intrusion of water into sub layers of pavement [92]. Improved friction is seen as a potential benefit of chip seals; however it requires an optimal application of the asphalt binder, too little and aggregate loss may occur, too much and flushing can occur which greatly reduces friction [92]. Sometimes a chip seal application may be followed with a fog seal (a coat of asphalt emulsion) treatment to increase asphalt content and the contrast (higher visibility) for markings, however this could reduce the friction gained by the chip seal especially if the application rate is too high [91,92]. A 2011 study sponsored by Indiana DOT demonstrated that new chip seals greatly improved the friction (ribbed tire, locked wheel skid tester friction number, FN40R) by 16 to 43 percent producing FN between 50 and 70 with friction decreasing over time [93]. This study also observed that a fog seal after chip seal reduced the friction 20 to 33 percent, but friction was regained after around 6 months as the coat was worn off the surface of the aggregates under traffic. A FHWA study showed some mixed results of chip seal effects on crash reduction, but overall, a net benefit in crash reduction especially in wet conditions [30]. Chip seals have an approximate service life as low as four to six years and up to six to seven years [92,94].

A.1.2 Fog Seal

A fog seal is the application of asphalt and water emulsion to the surface of a pavement [95]. Fog seals are used to correct raveling and cracking of pavement due to the aging effects from exposure to ultraviolet light which cause asphalt pavements to become brittle. Additionally, the sealing effect of a fog seal can prevent further deterioration that comes with water intrusion [91]. As with the chip seal and fog seal combination treatments, fog seals as a lone treatment method result in lower friction and it is recommended that only pavements with at least a FN of 30 (smooth wheel) be fog-sealed and result in a FN of at least 20 after treatment (locked wheel smooth tire) [91]. Evaluation of three applications of fog seal in Indiana showed a 50 percent or more reduction in friction followed by a return to the friction levels before treatment after about 18 months [93]. Service life of fog seals ranges from one to three years [94].

A.1.3 Rejuvenating Seal

Rejuvenating seals also called rejuvenating fog seals are a subset of a fog seal application wherein a chemical rejuvenator is added to improve the flexibility of the asphalt binder of the existing pavement [96]. A study in Indiana showed a significant decrease in friction of more than 40 percent (locked wheel, FN) after application with an increase observed over 30 days that failed to reach the original friction level at 18 percent and 35 percent lower after 24 months in the two tested areas [93].

A.1.4 Slurry Seal

A Slurry seal is a mixture of asphalt emulsion, "fine aggregate, mineral filler," and water along with additives that is applied in a thin layer using spreader box in order to treat raveling and minor cracks in ageing pavements. A study of Long Term Pavement Performance (LTPP) data showed slurry seals demonstrated improved friction compared to the control section and were ranked highest in friction performance among other treatments including chip seal, thin overlays and crack seals [97]. A FHWA study showed a benefit to crash reduction in wet conditions and a statistically insignificant reduction in dry condition crashes [98]. Service life of slurry seals ranges from four to six years [94].

A.1.5 Cape Seal

A cape seal is chip seal covered with a slurry seal after the chip seal cures with the goal to limit aggregate raveling that can occur in chip seals alone [98]. A study in Alaska compared BPT results among cape seal, fog seal, sand seal chip seal, High friction and glass seal treatments in field and lab samples [99]. This study showed that the cape seal provided similar mean friction to that of the slurry seals but had greater variation between lab and field testing compared to the other surface treatments. This study apparently referred to BPT results as skid numbers and compared results to typical skid number guidelines. Cape seals may extend the pavement life from six to eight years [94].

A.1.6 Scrub Seal

Scrub seals are very similar to chip seals with the exception that the asphalt emulsion is scrubbed into the substrate surface to penetrate cracks thereby enabling the treatment to be applied to pavements with severe cracking but are structurally sufficient [98]. It could be assumed that frictional performance would not vary greatly compared to chip seals [98]. A comparative study in Mississippi found no significant difference in skid numbers between chip seal and scrub seal treatments [100]. Scrub seals have an estimated service life of four to six years [94].

A.1.7 Microsurfacing

Microsurfacing is a thin overlay of "cationic polymer-modified asphalt emulsions, mineral aggregate, mineral filler, water, and other additives as needed" that serves to prevent raveling and oxidation, repair ruts up to 1.25 inches, improve the profile and increase friction [91]." While

similar to a slurry seal (as it is a slurry mixture applied in a similar manner by spreader box behind a slurry truck) it is noted to be distinct from a slurry seal due to the polymer modifiers in the asphalt emulsion which result in increased flexibility [98]. An Indiana study showed that shortly after placement of microsurfacing test sections showed significant variability in friction likely because of curing [93]. This study also showed that friction increased in the six months following application, peaked at 12 months producing FN of 40 to 60 and then decreased over time afterward. A FHWA study showed mixed results of microsurfacing effects on crashes with some areas showing increases and other decreases in crash events after microsurfacing treatments [98]. Microsurfacing can increase the pavement services life between six and eight years [94].

A.1.8 Ultra-thin Bonded Wearing Course (UTBWC)

UTBWC also sometimes abbreviated UBWC refers to a very thin layer of asphalt pavement (specific definition of thickness ranges vary by source with 0.5 to 0.75 inches described by Merritt et al. or 0.7 to 1.0 inch described by Lee and Shields [91,98]. It is constructed by utilizing aggregate in polymer modified asphalt which is immediately preceded by an asphalt emulsion (in one pass) which serves as the bonding mechanism [91,98]. These treatments can be applied to both asphalt and portland cement concrete pavements in generally good structural condition, while serving to correct minor surface distresses [98]. A FHWA study demonstrated a small reduction in wet weather crashes and no effect on dry crashes when UTBWC's were applied to freeways and for two-lane roads a significant reduction in wet crashes and smaller reduction in dry crashes [98].

A study in Indiana showed that across applications in four locations the freshly placed UTBWC provided sufficient skid resistance and macrotexture with a locked wheel FN range of 48 to 63 and MPD from 0.95 to 0.99 mm [93]. This study also showed that friction tended to peak at 6 months (presumably from wearing off excess binder on the surface), while long term friction decreased in varying magnitude depending on the aggregate gradation and abrasion resistance. In one case the study showed that friction decreased 34% after only 33 months which was attributed to polishing of the aggregate.

A.1.9 Thin Asphalt Overlays

Thin asphalt overlays are often referred to as thin HMA (hot mix asphalt) or sometimes mill and fill which refers to milling of the existing surface to a prescribed depth prior to placement of the thin overlay which is usually included in the application of a thin overlay [98]. The depth of the overlay can vary, but 1.5 to 2 inches in a single lift is typical [98]. FHWA research showed that thin HMA overlays did reduce wet crashes where they were applied on freeways and multilane roads, but with no effect observed for dry crashes [98]. Alternatively, the study showed a large increase in both dry and wet crashes on two-lane roads [98]. The FHWA study postulated that the decreases in crashes were possibly related to improvement of rutting and flushing and the increases in crashes related to increased speed due to smooth ride quality of new pavement or edge effects where no paved shoulders existed [98].

A study in Indiana assessed friction of thin (4.75mm) dense-graded HMA overlays across 4 locations [93]. The results indicated that freshly placed treatments could provide locked wheel skid

friction FN40S, between 35 and 52 that rapidly decreased over time under traffic showing a 25% reduction in six months and up to 48% reduction after 12 months [93]. After 12 to 18 months the FN was between 20 and 30 [93]. Furthermore, the macrotexture was low with MPD between 0.20 mm and 0.25 mm [93]. The thinness of the layer in this study required a smaller gradation of aggregate, therefore the effective macrotexture is limited [93]. This study should not be used as an indicator of all thin overlays as a 4.75mm dense-graded application is not representative of the typical overlay.

A.1.10 Open Graded Friction Course (OGFC)

OGFC is considered a subcategory of thin HMA overlays that is notable for its use of an open gradation aggregate (that is a gradation that is primarily comprised of larger sizes and contains only a smaller fraction of smaller sizes). The term PFC (Porous friction course) is sometimes used synonymously with OGFC, however, typically OGFC has a 10 to 15% air content while PFCs have greater than 18% (Cooley et al. 2009 as cited by Putman et al. [101]). The large open graded nature allows for high macrotexture on the surface improving drainage and reducing splash and spray [102]. This makes them ideal for areas with high rainfall; however they can perform poorly in locations with freeze-thaw cycles. OGFC are designed for a 10-year service life [103].

A FHWA study showed there was an increase in dry road crashes for multi-lane and two-lane roads with negligible effect on wet-road crashes where OGFCs were applied [98]. This study also showed that for freeways there was a decrease in wet crashes with no effect on dry crashes.

A study in Louisiana summarized in this paragraph assessed various aggregates across four application types, two Superpave mixes, stone matrix asphalt and OGFC [104]. The results indicated that OGFC demonstrated higher levels of macrotexture compared to the other applications and the highest friction values from IFI F(60) was an OGFC sample [104].

Another Louisiana study showed that OGFC lead to significant reduction in wet crashes and a comparison to SMA and Superpave roads demonstrated that the OGFC had higher locked wheel skid tester (smooth tire at 50 mph) friction with the OGFC FN ranging from 36.4 to 49.8, while the other HMA section ranged from 31.7 to 38.4 [102].

A.1.11 Profile Milling

Milling refers to the removal of material using milling teeth on a rotating head. This is distinct from grinding as the action of grinding is a cutting action, milling is more akin to an impact method [98]. Generally milling produces a texture that is too rough for practical purposes and is therefore commonly followed by an overlay treatment. However, there are applications in which milling can be used as a surface treatment by itself in order to correct profile issues in improve texture and ride quality [91]. Micro-milling is a subset of milling that is more suited as a friction treatment and is characterized by tighter teeth spacing and more bites per milling drum resulting in a finer texture [105]. Gao et al. demonstrated that milling can improve the friction (locked wheel, smooth tire at

50 mph skid number, SN) and that finer drums produced higher friction. However, their study also showed that the friction reduced precipitously and extrapolated that SN would fall below 20 after 2 years on HMA pavements [105].

A.1.12 Shotblasting

Shotblasting is a technique that uses steel balls (also called shot) that are shot onto a pavement surface at a high velocity resulting in the breaking of pieces of the surface and pitting. This has been used as both a surface preparation before a surface treatment or overlay on both asphalt and PCC pavements. As a surface preparation it can provide a range of macro and microtexture resulting in ICRI concrete surface profiles (CSP) ranging from 2-9 on its prescribed 1-10 scale. Numerous studies have shown that shotblasting can improve the friction and macrotexture of pavements at an efficient cost. Some studies have shown that the long-term frictional performance may not be sufficient [106,107]. However, more recently an NCAT study showed that shotblasting improved friction, and while there was a decrease under traffic loading, even after 3.1 million ESALs the surfaces still provided a minimum safety level of friction (defined as at least a 30 locked wheel SN at 40 mph with ribbed tire), and that the macrotexture was not greatly disrupted by traffic loading [108].

A.1.13 Diamond Grinding (PCC)

Diamond grinding is similar in concept to profile milling but applied to PCC pavements and that cuts in contrast to the impact or ripping effect that characterizes milling [109]. It is distinguished by the use of "closely spaced diamond saw blades mounted side-by-side on a rotating Shaft" that are used to remove the surface at a depth typically between 0.1 and 0.8 inches [109]. It can be performed on newly placed pavements or used as a preservation or restoration technique. Through several studies it has been demonstrated that diamond griding can improve friction by creating macrotexture and exposing aggregate microtexture in order to reduce accidents while also reducing unwanted noise from tire-pavement interaction [109]. FHWA's study across several states showed that diamond grinding led to a significant reduction in dry and wet crashes [98].

A.1.14 Grooving (PCC)

Grooving uses the same diamond saw blade technology as diamond grinding but at a wider spacing (typically 0.75iches on center) with the goal of producing a finished surface that is akin to longitudinal tining [109]. It primary improves the macrotexture component of friction and enables greater drainage of surface water reducing water film thickness. This leads to the safety benefits of grooving largely affecting wet conditions, while dry conditions may be affected to a lesser extent based on literature review presented by FHWA and NCHRP Report 500 [98,110].

A.1.15 Next Generation Concrete Surface (NGCS)

NGCS refers to an optimized approach to PCC pavement surfacing that combines diamond grinding and grooving to get the benefits of both [98]. While primarily designed with a noise reduction goal, friction is also greatly improved along with ride quality.

A.1.16 (Ultra) Thin White Topping

Whitetopping is a PCC overlay onto an asphalt concrete surface. Assuming a good bond between the asphalt substrate and PCC overlay allows for a composite action that enables the benefit of the overlay to be realized through a relatively thin layer (generally, thin whitetopping (TWT) is between and 4 and 8 inches thick and ultra-thin whitetopping UTWT is 4 or less inches thick of PCC). While not designed specifically to address friction issues, the methods for improving or creating friction in traditional PCC surfaces should apply to whitetopping if they do not affect the structural performance.

A.1.17 UHPC Overlay

UHPC as an overlay is a relatively new method. The high-performance properties of UHPC allow very thin layers to be utilized (1 to 2 inches). UHPC saw its first North American use as a bridge overlay in 2016 in Iowa [111]. Evaluation showed that UHPC can provide equivalent or better performance to that of latex modified concrete overlays.

There is minimal research available on utilizing UHPC to address frictional properties of pavement surfaces in the United States. A European study developed a High-Performance Cementitious Material (HPCM) which consisted of a thin layer (eight mm) steel fiber reinforced UHPC mortar with three-to-seven-millimeter calcined bauxite chippings embedded [60]. This study had difficulty controlling the calcined bauxite embedment at larger scale, therefore several adjustments were made including: increasing water-to-cement ratio, decreasing silica fume content, adjusting mixer type, increasing UHPC mortar thickness to up to 20 mm, increasing aggregate size up to 10 mm, increasing the amount of chippings and using a vibratory screed to help embedment of the aggregate [59]. However, due to the difficulty of embedment and noise generated by the surface the study adjusted the design to include grooving instead of embedded chippings [60]. The ultimate coefficient of friction for the grooved solution was higher than traditional asphalt but still significantly lower than that produced using the calcined bauxite chippings [60].

A.1.18 Exposed Aggregate Concrete Pavement

Exposed aggregate concrete pavements consists of a PCC surface that has had the aggregate exposed by the use of washing and brushing of the fresh concrete, or use of surface retarding to remove the unset material from the surface later (Descornet et al. as cited by Hoerner et al. [112]). A skid resistance near that of transversely tined pavements can be expected for exposed aggregate concrete [112]. While it has been employed in Europe, it has had limited use in the United States [112]. However, there was an exposed aggregate concrete (referred to as the "European" pavement section) produced on I-75 in Michigan in 1993 along with a standard pavement for comparison,

and the comparison revealed that the standard pavement provided higher friction than the exposed aggregate concrete [113].

A study in Poland assessed the use of surface retarders to produce exposed aggregate concrete or (EAC) [114]. They found that increasing the quantity of surface retarder beyond recommended dose did not increase texture, but using a deeper penetrating grade of retarder did result in increased texture depth. Rith et al. compared performance of EACP to transverse and longitudinal tined surfaces and found that the initial friction of transverse tining was highest followed by EACP then longitudinal tining, however under simulated traffic wear the EACP maintained the highest level of friction showing a lower loss under the trafficking cycles [115].

Shen et al. assessed the effects of exposing and curing agents on performance of properties and showed that exposing the aggregate results in a small reduction of compressive strength compared to normal concrete but can be improved with the application of curing agents [116]. Shen et al. also showed that EAC performed better in abrasion resistance than normal concrete due to the absence of a weak layer of surface mortar and therefor was dependent on the exposed aggregates performance, and the performance was slightly improved through use of a curing agent. Furthermore, Shen et al.'s permeability testing indicated that the aggregate exposure was increasing porosity and deteriorating the surface microstructure which again could be improved by use of a curing agent.

A.2 Summary of Surface Treatments

A summary of the review of the literature presented on pavement surface treatments is presented in

Table A.1. This is not an all-inclusive list, and some assumptions were made with gaps in available information acknowledged.

Table A.1: Summary of Friction and Safety of Pavement Surface Treatments

Surface Treatment	Pavement Type	Friction (Effect)	Initial Friction value	Safety Effects	Durability Information
HFST	Resin on PCC or ACC	+	FN40R: >65 DFT60: 0.75-0.9 BPT: 65-100+ MPD: 1.9 mm	decrease stop distance 25-30% decrease wet crashes up to 86%	service life7-12 years, friction decreases over time with MPD down to 1.1 mm
Chip Seal	AC	+	FN40R: 50-70 MPD: >1.0 mm	some mixed results, overall net reduction in wet crashes	service life 4-7 years
Fog Seal	AC	-	FN: as low as 20	up to 50% reduction in friction	Friction returns to prior levels after 18 months, service life 1-3 years
Rejuvenating Seal	AC	-	Low	40% reduction, improves to 0-35% reduction over time	Friction returns between 4 days and 2 years
Slurry Seal	AC	+	FN40R: > 50+ MPD: 0.3 to 0.6 mm	reduction in wet weather crashes	service life 4-6 years
Cape Seal	AC	+	Results in similar mean friction to that of slurry seals		service life 6-8 years
Scrub Seal	AC	+	Results in similar mean friction to that of chip seals		service life 4-6 years
Micro-surfacing	AC	+	FN: 40-60, highly variable MPD: 0.5 to 1.0 mm	mixed results	service life 6-8 years
Ultra-thin Bonded Wearing Course (UTBWC)	AC	+/-	FN: 48-63 MPD: 0.95->1.0mm	small reduction in wet weather crashes	Friction peaks after 6 months (wearing of binder); long term decrease in friction based on gradation
Thin Asphalt Overlay	AC	+/-	FN40S: 35-52 MPD: 0.4 to 0.6 mm (dense grad) >1.0 mm (SMA)	mixed results	After 12 months FN40S down to 20-30

Open Graded Friction Course (OGFC)	AC	+/-	FN50S: 31.7 -38.4 increase in macrotexture more pronounced than friction MPD 1.5-3.0 mm	mixed results	service life of 10 years
Surface Treatment	**Pavement Type**	**Friction (Effect)**	**Initial Friction value**	**Safety Effects**	**Durability Information**
Profile Milling	AC	+	FN50S: >50 MPD: >2.0 mm	limited data	loss of friction modeled at -20 FN after 2 years
Shotblasting	AC and PCC	+	FN40R: 30-50 DFT20: up to 0.6 MPD: ~0.9-2.7 mm	limited data	FN40R > 30 after 3.1 million ESALs MPD maintained fairly steady
Diamond Grinding	PCC	+	exposes aggregate and improves macrotexture MPD: 0.7-1.2mm	significant reduction in dry and wet crashes	limited by life of the pavement
Grooving	PCC	+	primarily improves macrotexture MPD: 0.9-1.4mm	crash reduction mostly limited to wet conditions	limited by life of the pavement
Next Generation Concrete Surfaces	PCC	+	Improves macro and microtexture MPD: up to 1.4 mm	limited data	limited by life of the pavement
Ultra-thin white topping	PCC on AC	+	Based on grooving/grinding employed up to 1.4 mm	limited data	limited by life of the pavement
UHPC Overlay	PCC on PCC or AC	+	comparable to surfacing on PCC (grinding/grooving) up to 1.4 mm	limited data	limited by life of the pavement

UHPC-based HFST	PCC on PCC or AC	+	large scale applications not employed due to difficulty with aggregate embedment		
EACP	PCC	+	Comparable to tined surfaces	limited data for US	limited data for US

APPENDIX B: SUPPORTING TABLES AND FIGURES

Table B.1 Chemical and Mineralogical Composition of Aggregates

		Granite-1	Granite-2	Calcined Bauxite	Slag	Trap Rock
Al_2O_3	%	13.25	15.38	85.64	11.19	17.55
SiO_2	%	67.72	56.77	5.95	9.96	46.58
Na_2O	%	3.81	3.93	0.280	0.356	2.17
MgO	%	2.01	4.06	0.209	13.96	10.25
P_2O_5	%	0.233	0.250	0.283	0.369	0.093
K_2O	%	3.17	1.24	0.217	0.044	0.255
CaO	%	2.24	6.11	0.760	32.75	11.06
TiO_2	%	0.484	0.786	3.50	0.464	0.448
MnO	%	0.093	0.155	0.005	2.38	0.153
Fe_2O_3	%	5.72	9.92	3.00	27.53	10.83
V_2O_5	%	0.022	0.035	0.059	0.081	0.030
Sum Of Major Oxides	%	98.75	98.64	99.90	99.08	99.43
LOI	%	1.25	1.36	0.10	0.92	0.57
Primary Crystal Phases		Predominantly quartz (SiO_2), minor phases of feldspar and micas	Predominantly quartz (SiO_2), with other mineral compounds from degradation of feldspars	Predominantly aluminum oxide (Al_2O_3) with some aluminum silicate	Predominantly wustite (FeO), larnite (Ca_2SiO_4) and magnesium ditanium (III) oxide. An amorphous phase was also present.	Predominantly anorthite, Sodian (Ca, Na)(Si, $Al)_4O_8$
Nearest AASHTO M43 Gradation		#89	#78	HFST	#6	#9

as Received						

Table B.2: Effects of Gradation ANOVA Results

Response Variable	ANOVA Test	Effect Test	By Aggregate	Prob>F (P-value)	Model Adj R^2
Micro-MPD	Factorial	Aggregate		<.0001*	0.91
		Gradation		<.0001*	
		Aggregate*Gradation		<.0001*	
	One-way	Gradation	Granite-1	0.0003*	0.69
		Gradation	Granite-2	<.0001*	0.82
		Gradation	Calcined Bauxite	<.0001*	0.89
		Gradation	Slag	<.0001*	0.95
		Gradation	Trap Rock	<.0001*	0.94
Micro-RMS	Factorial	Aggregate		<.0001*	0.92
		Gradation		<.0001*	
		Aggregate*Gradation		<.0001*	
	One-way	Gradation	Granite-1	0.0001*	0.75
		Gradation	Granite-2	<.0001*	0.84
		Gradation	Calcined Bauxite	<.0001*	0.86
		Gradation	Slag	<.0001*	0.95
		Gradation	Trap Rock	<.0001*	0.94
Micro-Ra	Factorial	Aggregate		<.0001*	0.92
		Gradation		<.0001*	
		Aggregate*Gradation		<.0001*	
	One-way	Gradation	Granite-1	0.0002*	0.71
		Gradation	Granite-2	<.0001*	0.82
		Gradation	Calcined Bauxite	<.0001*	0.88
		Gradation	Slag	<.0001*	0.95

		Gradation	Trap Rock	<.0001*	0.95
Micro-Rku	Factorial	Aggregate		<.0001*	0.95
		Gradation		<.0001*	
		Aggregate*Gradation		<.0001*	
	One-way	Gradation	Granite-1	<.0001*	0.90
		Gradation	Granite-2	<.0001*	0.92
		Gradation	Calcined Bauxite	0.0866	0.22
		Gradation	Slag	<.0001*	0.93
		Gradation	Trap Rock	0.3394	0.03
Micro-Rsk	Factorial	Aggregate		<.0001*	0.55
		Gradation		0.2628	
		Aggregate*Gradation		0.1190	
	One-way	Gradation	Granite-1	0.4664	-0.03
		Gradation	Granite-2	0.5568	-0.06
		Gradation	Calcined Bauxite	0.1203	0.18
		Gradation	Slag	0.7651	-0.12
		Gradation	Trap Rock	0.3246	0.03
PSD Slope	Factorial	Aggregate		<.0001*	0.31
		Gradation		0.2372	
		Aggregate*Gradation		0.0876	
	One-way	Gradation	Granite-1	0.9104	-0.15
		Gradation	Granite-2	0.1975	0.11
		Gradation	Calcined Bauxite	0.3128	0.04
		Gradation	Slag	0.0518	0.29
		Gradation	Trap Rock	0.2371	0.08

PSD Intercept	Factorial	Aggregate		<.0001*	0.94
		Gradation		<.0001*	
		Aggregate*Gradation		<.0001*	
	One-way	Gradation	Granite-1	<.0001*	0.87
		Gradation	Granite-2	<.0001*	0.78
		Gradation	Calcined Bauxite	<.0001*	0.84
		Gradation	Slag	<.0001*	0.96
		Gradation	Trap Rock	0.7504	-0.11

Table B.3: Comparison Surface and Bulk Sample Rank order and Connecting Letters

		Bulk Aggregate							Sample Surface								
		Aggregate	Connecting Letters					Least Sq Mean	Aggregate	Connecting Letters			Least Sq Mean	Difference (Surface - Bulk Value of same aggregate)	Rank Order Maintained ?	Difference within Cr = 0.0045
Micro-MPD	As Received	Trap Rock	A					0.0444	Trap Rock	A			0.0485	0.0042	Yes	Yes
		Calcined Bauxite		B				0.0419	Calcined Bauxite	A	B		0.0425	0.0005	Yes	Yes
		Granite 1			C			0.0343	Granite 1		B		0.0390	0.0047	Yes	No
		Granite 2				D		0.0316	Granite 2			C	0.0282	-0.0034	Yes	Yes
		Slag					E	0.0279	Slag			C	0.0278	-0.0002	Yes	Yes
		Aggregate	Connecting Letters					Least Sq Mean	Aggregate	Connecting Letters			Least Sq Mean	Difference (Surface - Bulk Value of same aggregate)	Rank Order Maintained	Difference within Cr = 0.0421
Micro-Rsk	As Received	Slag	A					0.0089	Slag	A			0.0424	0.0335	Yes	Yes
		Calcined Bauxite	A					-0.0035	Calcined Bauxite	A	B		0.0136	0.0171	Yes	Yes
		Trap Rock		B				-0.0423	Trap Rock	A	B		-0.0112	0.0311	Yes	Yes
		Granite 2		B				-0.0498	Granite 1		B		-0.0228	0.0273	No	Yes
		Granite 1		B				-0.0501	Granite 2		B		-0.0290	0.0208	No	Yes
	P4R8	Slag	A					0.0023	Slag	A			0.0687	0.0664	Yes	No
		Trap Rock		B				-0.0278	Calcined Bauxite	A	B		0.0188	0.0591	No	No
		Calcined Bauxite		B				-0.0403	Granite 2		B		0.0032	0.0478	No	No
		Granite 2		B				-0.0446	Trap Rock		B		-0.0287	-0.0009	No	Yes

Table B.4: Effects of Abrasion ANOVA Results

Abrasion	Gradation	Parameter	Effect Test	Estimate (Slope)	Prob>|t| (P-value)	Prob>F (P-value)	R^2 Adj
Micro-Deval Abrasion Test	As Received	Micro-MPD	Abrasion	-2.13E-05	<.0001	<.0001	0.94
			Aggregate			<.0001	
			Aggregate*Abrasion			0.1301	
		Micro-RMS	Abrasion	-9.77E-06	<.0001	<.0001	0.95
			Aggregate			<.0001	
			Aggregate*Abrasion			0.2335	
		Micro-Ra	Abrasion	-7.54E-06	<.0001	<.0001	0.95
			Aggregate			<.0001	
			Aggregate*Abrasion			0.2768	
		Micro-Rku	Abrasion	1.80E-04	0.1899	0.1899	0.97
			Aggregate			<.0001	
			Aggregate*Abrasion			0.0012	
		Micro-Rsk	Abrasion	-3.30E-04	<.0001	<.0001	0.83
			Aggregate			<.0001	
			Aggregate*Abrasion			0.0008	
		PSD Slope	Abrasion	1.67E-04	<.0001	<.0001	0.48
			Aggregate			<.0001	
			Aggregate*Abrasion			0.0009	
		PSD Intercept	Abrasion	-2.92E-04	0.0004	0.0004	0.96
			Aggregate			<.0001	
			Aggregate*Abrasion			0.2749	
	P4R16	Micro-MPD	Abrasion	-2.79E-05	<.0001	<.0001	0.77
			Aggregate			<.0001	

			Aggregate*Abrasion			<.0001	
		Micro-RMS	Abrasion	-1.32E-05	<.0001	<.0001	0.78
			Aggregate			<.0001	
			Aggregate*Abrasion			<.0001	
		Micro-Ra	Abrasion	-9.43E-06	<.0001	<.0001	0.82
			Aggregate			<.0001	
			Aggregate*Abrasion			<.0001	
		Micro-Rku	Abrasion	-5.02E-04	0.0009	0.0009	0.93
			Aggregate			<.0001	
			Aggregate*Abrasion			0.0622	
		Micro-Rsk	Abrasion	-4.90E-04	<.0001	<.0001	0.81
			Aggregate			<.0001	
			Aggregate*Abrasion			0.0437	
		PSD Slope	Abrasion	2.45E-04	<.0001	<.0001	0.52
			Aggregate			<.0001	
			Aggregate*Abrasion			0.0217	
		PSD Intercept	Abrasion	-1.86E-04	0.0183	0.0183	0.77
			Aggregate			<.0001	
			Aggregate*Abrasion			0.0059	
Los Angeles Abrasion Test	P4R8	Micro-MPD	Abrasion	8.46E-07	0.3655	0.3655	0.68
			Aggregate			<.0001	
			Aggregate*Abrasion			<.0001	
		Micro-RMS	Abrasion	6.10E-07	0.1929	0.1929	0.70
			Aggregate			<.0001	
			Aggregate*Abrasion			<.0001	
		Micro-Ra	Abrasion	4.17E-07	0.2258	0.2258	0.76

			Aggregate			<.0001	
			Aggregate*Abrasion			<.0001	
		Micro-Rku	Abrasion	1.02E-04	0.0239	0.0239	0.90
			Aggregate			<.0001	
			Aggregate*Abrasion			0.0423	
		Micro-Rsk	Abrasion	-2.80E-05	0.0095	0.0095	0.59
			Aggregate			<.0001	
			Aggregate*Abrasion			0.672	
		PSD Slope	Abrasion	1.86E-05	0.0045	0.0045	0.11
			Aggregate			0.6774	
			Aggregate*Abrasion			0.4773	
		PSD Intercept	Abrasion	-6.85E-05	<.0001	<.0001	0.78
			Aggregate			<.0001	
			Aggregate*Abrasion			0.0014	

Table B.5: Effect of Abrasion on Aggregate Friction

Change in Average BPN with Abrasion and Effects Test P-Value (Prob>|t|)								
	LAA (500 Rev) of P4R8				MD (120 Min) of P4R16			
Aggregate	Before	After	% change	P-Value	Before	After	% change	P-Value
Calcined Bauxite	77.3	78.3	1.3	0.7384	80.7	71.7	-11.2	<0.0001
Granite 1	78.9	81.2	2.9	0.3697	74.8	68	-9.1	0.0181
Granite 2	85	73.4	-13.6	<0.0001	81.7	64.4	-21.2	<0.0001

Slag	82.8	75.6	-8.7	0.0021	87.3	62.2	-28.8	<0.0001
Trap Rock	79.7	76	-4.6	0.0301	73.7	71	-3.7	0.2858

Table B.6: Regression of Texture Parameters Effect on BPN

	Parameter	Linear Model	Prob >F (P-Value)	R^2
Linear Model	Micro-MPD	BPN = 33.593475 + 935.32369*Micro-MPD	<.0001	0.71
	Micro-RMS	BPN = 33.606193 + 1850.5386*Micro-RMS	<.0001	0.70
	Micro-Ra	BPN = 32.722618 + 2466.4665*Micro-Ra	<.0001	0.70
	Micro-Rku	BPN = -3.774977 + 21.465368*Micro-Rku	<.0001	0.56
	MicroRsk	BPN = 70.813532 - 11.872018*Micro-Rsk	0.8443	0.00
	MPD	BPN = 49.903058 + 12.176565*MPD	<.0001	0.44
	RMS	BPN = 49.132584 + 24.632054*RMS	<.0001	0.43
	Ra	BPN = 45.801268 + 33.532391*Ra	<.0001	0.40
	Rku	BPN = 67.407259 + 6.4248321*Rku	0.0216	0.15
	Rsk	BPN = 68.791553 - 5.9675371*Rsk	0.6226	0.01
	PSD Slope	BPN = 5.9926239 + 34.097492*PSD Slope	0.0002	0.35
	PSD Intercept	BPN = 93.322726 + 12.071265*PSD Intercept	<.0001	0.76
	Parameter	Logarithmic Model	Prob>F (P-Value)	R^2
Logarithmic Model	Micro-MPD	BPN = 158.69126 + 26.371792*ln(Micro-MPD)	<.0001	0.81
	Micro-RMS	BPN = 175.5283 + 26.071924*ln(Micro-RMS)	<.0001	0.81

	Micro-Ra	BPN = 187.17821 + 27.240714*ln(Micro-Ra)	<.0001	0.81
	Micro-Rku	BPN = -16.86056 + 71.186493*ln(Micro-Rku)	<.0001	0.60
	Micro-Rsk	N/A Due to negative values		
	MPD	BPN = 68.640355 + 10.912832*ln(MPD)	<.0001	0.59
	RMS	BPN = 75.874223 + 12.307095*ln(RMS)	<.0001	0.60
	Ra	BPN = 77.411307 + 14.465309*ln(Ra)	<.0001	0.40
	Rku	BPN = 31.270948 + 32.190556*ln(Rku+3)	0.0014	0.28
	Rsk	N/A Due to negative values		
	PSD Slope	BPN = 40.231926 + 48.896108*ln(PSD Slope)	<.0001	0.42
	PSD Intercept	BPN = 84.087203 - 27.207967*ln(PSD Intercept*[-1])	<.0001	0.68